NOTE TO USERS

DISSERTATION

IMPLICATION OF ATMOSPHERE AND CLOUD STATE UNCERTAINTIES ON THE GLOBAL RETRIEVAL OF ICE CLOUD MICROPHYSICAL PROPERTIES

Submitted by

Steven James Cooper

Department of Atmospheric Science

In partial fulfillment of the requirements

For the Degree of Doctor of Philosophy

Colorado State University

Fort Collins, Colorado

Fall 2004

COLORADO STATE UNIVERSITY

October 15, 2004

WE HEREBY RECOMMEND THAT THE DISSERTATION PREPARED UNDER OUR SUPERVISION BY STEVEN J. COOPER ENTITLED IMPLICATION OF ATMOSPHERE AND CLOUD STATE UNCERTAINTIES ON THE GLOBAL RETRIEVAL OF ICE CLOUD MICROPHYSICAL PROPERTIES BE ACCEPTED AS FULFILLING IN PART REQUIREMENTS FOR THE DEGREE OF DOCTOR OF PHILOSOPHY.

Committee on Graduate Work

C. Kummerow

R. Johnson

V. Chandrasekar

Advisor, G.L. Stephens

Department Head, S. Rutledge

ABSTRACT OF DISSERTATION

IMPLICATION OF ATMOSPHERE AND CLOUD STATE UNCERTAINTIES ON THE GLOBAL RETRIEVAL OF ICE CLOUD MICROPHYSICAL PROPERTIES

Cirrus clouds play an important yet poorly determined role in the Earth's climate system and its various feedback mechanisms. As such, a significant amount of work has been accomplished not only in understanding the fundamental physics of the ice cloud problem but also in using this knowledge to infer cirrus cloud microphysical properties from satellite- based observations. A virtual plethora of retrieval schemes based upon known spectral sensitivities of top of the atmosphere radiance to ice cloud microphysical properties are found throughout the literature. Each of these different retrieval schemes, however, is susceptible to its own unique set of potential errors resulting from the inversion assumptions used in mapping between radiance and retrieval space. Since the deviations of these assumptions from truth behave in a spectrally un- predictable manner, it is likely that retrieval schemes using different wavelengths will give highly dissimilar retrieval results. This dissertation work re- examines the ice cloud retrieval problem in context of these often- neglected inversion uncertainties and examines their implications for the global retrieval of ice cloud microphysical properties.

The optimal combination of MODIS measurements for an ice cloud microphysical property retrieval scheme constrained by CloudSat cloud boundary information was determined through application of a formal information content analysis.

Channel selection for the retrieval depends not only on the sensitivity of the measurements to changes in retrieved cloud properties but also to the combined uncertainty in the measurements from the instrument itself and from such inversion assumptions as ice crystal habit, particle size distribution, and atmospheric profile. Quantification of these uncertainties was made possible only by the recent development of optical properties at the MODIS wavelengths for a variety of realistic, non- spherical ice crystals. The results show that that channels that maximize retrieval information are strongly dependent upon the state of the atmosphere, meaning that there is no ideal combination of two or three channels that will always ensure an accurate retrieval. We therefore suggest a five- channel retrieval scheme consisting of a combination of error-weighted visible, near- infrared, and infrared channels chosen to use the inherent sensitivities in each of these spectral regions to ensure high retrieval information content across expected cloud and atmospheric conditions. The performance of the five- channel retrieval scheme was assessed in terms of both synthetic studies and real- world CRYSTAL-FACE data. Uncertainties in retrieved ice water path and effective radius are large and state dependent, with typical random errors near 40 to 50 percent. The large uncertainties found using this relatively complex retrieval scheme need consideration when examining the utility of absolute numbers or small trends found in existing cloud products that are often based on much simpler retrieval techniques.

Steven James Cooper
Atmospheric Science Department
Colorado State University
Fort Collins, CO 80523
Fall 2004

Contents

List of Tables

List of Figures

Chapter 1

Introduction

> I suffer from the fact that I'm surrounded by people with deformed brains, with such self- assured, ready- made theories that it's folly to write anything for them; there's no way of getting through to them at all.
>
> - Count Leo Tolstoy

Cirrus clouds play an important role in regulating climate (Liou, 1986). They directly influence the radiative budget by increasing the amount of shortwave and decreasing the amount of longwave radiation emitted to space. These competing radiative effects will impact climate variability through a variety of possible feedback mechanisms involving convection, sea surface temperature, water vapor, and large-scale dynamics. The sign or magnitude of these forcings, however, is poorly understood due to uncertainties in both cloud distribution and microphysics (Stephens and Webster, 1981; Stephens et al., 1990), so subsequently the role of these clouds in the climate feedback mechanisms and global warming scenarios is still poorly determined (Lindzen, 2001; Fu, 2002).

Measuring the global distribution of cirrus cloud microphysical properties therefore has been a concern of many satellite missions. As such, a significant amount of work

has been done in both understanding the underlying physics of the ice cloud problem and using this knowledge in inferring cirrus cloud properties from satellite- based measurements (Inoue (1985); Prabhakara et al. (1988); Nakajima and King (1990); King et al. (1992)). In this work, we do not question the usefulness of these past efforts or their validity for their specific applications but instead offer a re-examination of the ice cloud retrieval problem in context of recent developments in the understanding of ice cloud physics. This dissertation explores our ability to retrieve ice cloud properties based on a realistic examination of the fundamental physics of the problem. In other words, the idea was to take a step backwards to our core knowledge in attempt to assess our confidence in retrieved cloud properties given the practical constraints of our current observational platforms. The motivation for this work springs from a simple curiosity of the real world. If the reader is not inherently interested in ice clouds, it is hoped that he at least can appreciate the importance of gaining a more realistic characterization of these clouds as input for the many speculative, climate processes studies currently found in the literature.

1. Uncertainties in Retrieval Approach

Ice cloud retrievals depend on an accurate, *a priori* understanding of both ice crystal optical properties and the state of the atmosphere. For an inversion from a given set of radiance measurements, the assumption of these properties in mapping between retrieval and observation space will lead to significant error when inconsistent with the real atmosphere.

Figure 1.1 adapted from Cooper et al. (2003) shows theoretical arches for the split-window approach to retrieving cloud properties. The split- window technique relies on differences in radiative properties for cloud particles at two wavelengths in the window region to estimate cloud optical depth and effective radius from satellite- observed brightness temperatures. Cloud optical depth is determined by the 10.8 μm brightness

temperature; effective radius is determined by the difference in 10.8 μm and 12.0 μm brightness temperatures once optical depth is known. An inherent short- coming of this approach is that retrieved parameters are heavily dependent upon assumed cloud temperature. For given 10.8 μm and 12.0 μm brightness temperatures, a different effective radius and optical depth are found for each cloud temperature assumption in Figure 1.1. The use of visible and near- infrared channels to retrieve cloud optical properties suffers from similar difficulties, as suggested by the Nakajima and King (1990) type retrieval approach shown in Figure 1.2. This technique relies on the the conservative scattering properties of the visible channel to estimate cloud optical depth and the non- conservative scattering properties of the near- infrared channel to estimate effective radius once optical depth is known. The inherent problem of this approach is not uncertainty in cloud temperature but uncertainty in cloud optical properties. Figure 1.2 shows that for given 0.65 and 2.11 μm reflectance functions, the retrieved parameters depend heavily on the *a priori* assumption of crystal habit through their differing radiative properties.

Although variations of the Nakajima and King and split- window retrieval approaches are the most commonly applied, a virtual plethora of retrieval approaches based on the many different combinations of wavelengths listed in Table 1.1 are found throughout the literature (e.g. Liou et al. (1990); Stone et al. (1990); Wielicki et al. (1990); Minnis et al. (1993); Ou et al. (1993); Gao and Kaufman (1995)). Each of these retrieval schemes exploits known sensitivities to estimate cloud properties from observed radiances but also suffer from its own potential sources of error as discussed above which may fundamentally limit its utility depending upon the state of the atmosphere. Since these uncertainties are nearly always neglected in current retrieval schemes, each of these retrieval techniques must assume that they have made the correct assumptions and that retrieved cloud properties are therefore accurate, an unlikely scenario as exhibited in Figures 1.1 and Nakajima and King (1990). The studies presented in this dissertation will explicitly account for these uncertainties and examine their implications for the retrieval of ice cloud microphysical properties. In addition to crystal habit and cloud temperature,

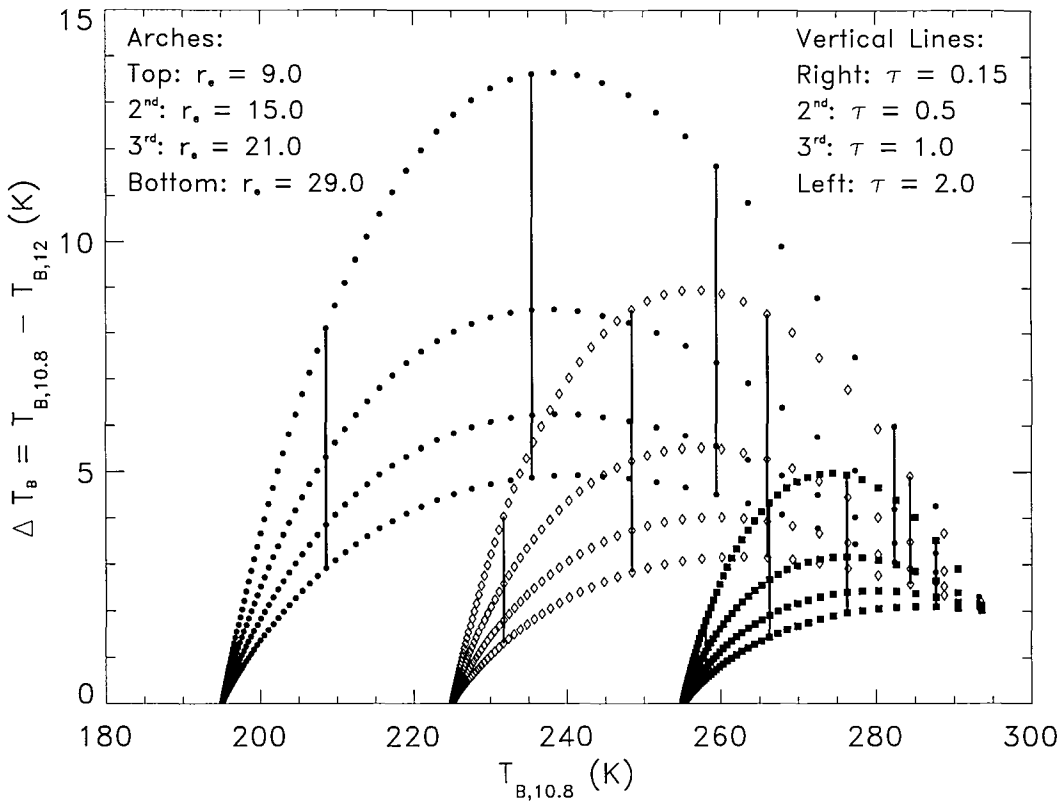

Figure 1.1: Relationship between ΔT_B and $T_{B,10.8}$ for a number of cirrus clouds with optical depths ranging from 0 to 4 and effective radii ranging from 9 to 29 μm. Clouds with emitting temperatures of 195 K (filled circles), 225 K (open diamonds), and 255 K (filled squares) are modeled.

other possible retrieval uncertainties result from assumptions of cloud particle size distribution, cloud 3-D scattering effects, surface type, and atmospheric temperature and humidity profiles. To limit the scope of this dissertation, certain assumptions such as single- layer clouds overlying an ocean surface and the absence of 3-D scattering effects necessarily were made.

An additional concern for the large number of retrieval schemes developed is that these different retrievals do not necessarily return the same cloud properties, e.g. Figure 5.30 shows markedly different estimates of ice water path (IWP) for each the split-window and Nakajima and King retrieval schemes for a cirrus cloud case from the Cirrus

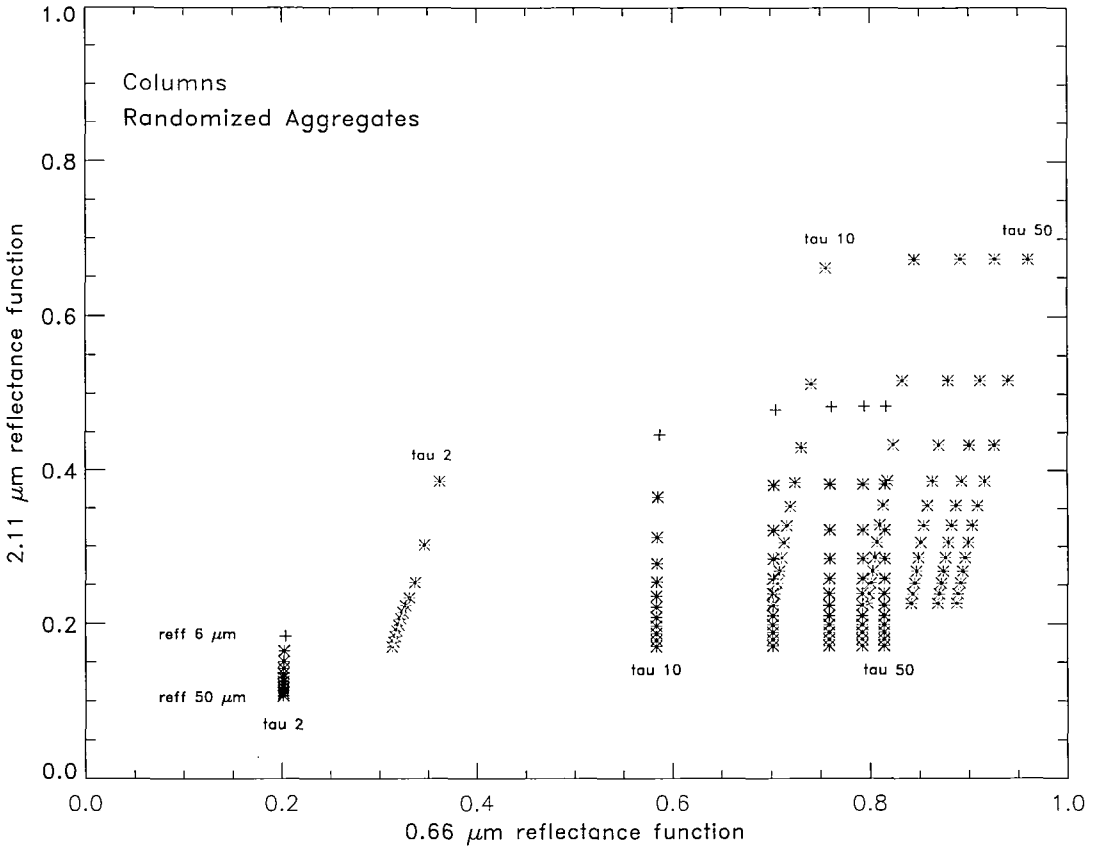

Figure 1.2: Relationship between 0.66 μm and 2.11 μm reflectance functions for ice clouds composed of both a modified gamma distribution of randomized aggregates and an equivalent distribution of columns. Effective radius range from 6 to 50 μm and optical depths from 2 to 50.

Regional Study of Tropical Anvils and Cirrus Layers - Florida Area Cirrus Experiment (CRYSTAL-FACE). Large discrepancies in retrieved cloud products from these different retrieval schemes not only raise doubts about the true value of these cloud properties but also may make comparisons of cloud products between measurement campaigns with different retrieval assumptions somewhat useless. This dissertation will therefore use an underlying knowledge of the fundamental physics of the ice cloud problem to outline a unified approach to ice cloud retrievals that are consistent with each of the above techniques.

MODIS channel	wavelength	MODIS channel	wavelength
1	0.62-0.67	27	6.53-6.90
2	0.84-0.88	29	8.40-8.70
5	1.23-1.35	31	10.78-11.28
6	1.63-1.65	32	11.77-12.27
7	2.10-2.15	33	13.18-13.49
19	0.91-0.96	34	13.48-13.78
20	3.66-3.84	35	13.78-14.08
23	4.02-4.08	36	14.08-14.38
26	1.36-1.39		

Table 1.1: MODIS channels evaluated for ice cloud retrieval scheme.

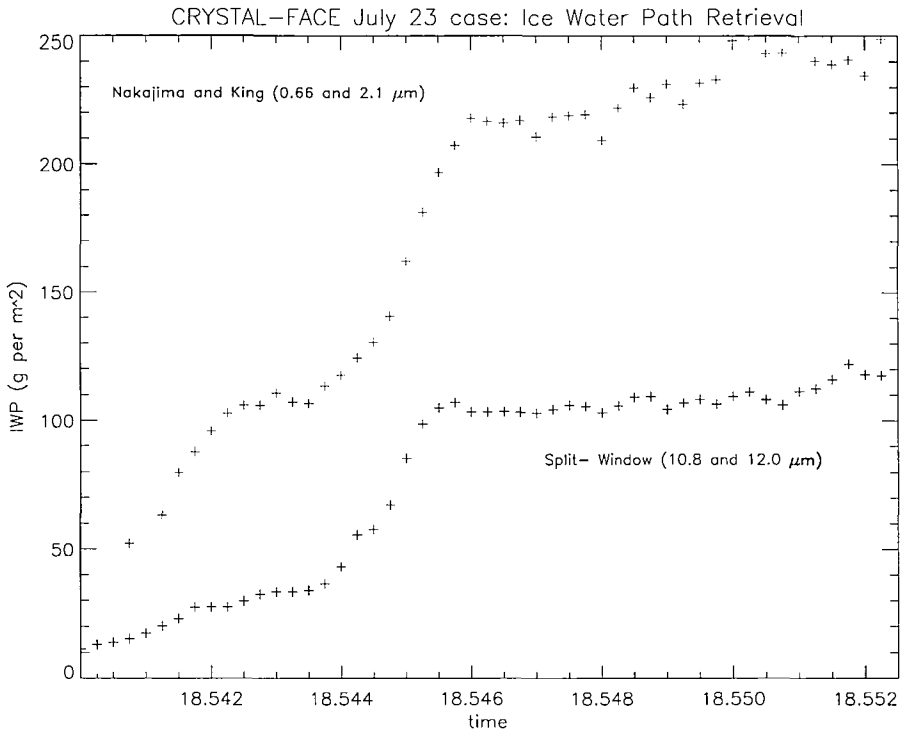

Figure 1.3: Retrieved IWP for CRYSTAL-FACE cirrus cloud case using each the Nakajima and King and split- window approaches.

2. The Research Plan of Attack

These attempts to address the neglected uncertainty and consistency issues in ice cloud retrievals will capitalize on the recent development of optical properties at the Moderate Resolution Imaging Spectroradiometer (MODIS) wavelengths for a number of realistic crystal habits (Yang et al. (2000); Baran et al. (2001); Yang et al. (2003)). Optical properties for each columns, plates, bullets, dendrites, and a variety of polycrystal aggregates were utilized to determine the variability in retrieval results based on selection of habit. The explicit consideration of the above uncertainties in the estimation of cloud properties will be achieved through implementation of the optimal- estimation based retrieval framework (Rodgers (1976); Marks and Rodgers (1993)). This technique relies upon a rigorous characterization of uncertainties in each measurements, forward model assumptions, and *a priori* guess to estimate a most likely solution of cloud properties for a

given set of radiance measurements. The approach has additional advantages over a simple inversion approach in that it provides a flexible framework to combine information from multiple sensors and also a set of built- in diagnostic tools which quantify retrieval uncertainties. The complexities of both the optimal- estimation retrieval approach and the realistic phase functions used to represent realistic ice crystals in the forward model, however, result in a heavy computational expense which currently prohibits the application of such a retrieval on a global scale. The studies presented in this dissertation therefore are primarily of a theoretical nature, where it is hoped that insights gleaned from these studies will ultimately result in improved algorithms for better characterizing the distribution and microphysical properties of these clouds and their impacts on climate.

Chapter 2 describes in detail the adding and doubling radiative transfer forward model and the optimal- estimation based retrieval technique used for the studies presented in the remaining chapters. Special attention is given to the physical assumptions used to realistically represent the ice clouds in the forward model.

Chapter 3 begins our investigation of the impacts of uncertainties on the retrieval of ice cloud properties using the instruments aboard the NASA Afternoon A-Train constellation of satellites as a practical constraint. This chapter casts the split-window cirrus cloud retrieval technique in an optimal estimation framework to examine uncertainties in the retrieval of cirrus cloud optical depth and effective radius as a function of uncertainty in cloud emitting temperature. The incorporation of cloud boundary information from either the CloudSat Cloud Profiling Radar or the CALIPSO lidar to constrain the window- region measurements from MODIS is found to substantially reduce the errors inherent to this approach. Regardless of co-incident cloud boundary information, however, retrieval errors are found to be large and heavily dependent upon forward model uncertainties from such forward model assumptions as ice crystal habit. Although originally meant to stand alone, the results and insights gained from this work eventually led to the the final dissertation topic and format.

Chapter 4 exploits the methodology developed in the split- window paper to examine the potential utility of the MODIS cloud retrieval channels listed in Table 1.1. The results of rigorous sensitivity and uncertainty analyses at each of these channels are incorporated into a formal information content study to select those channels that contain the most information for a retrieval scheme designed in terms of ice water path and effective radius. It is found that the ideal combination of channels is heavily dependent upon the state of the atmosphere, meaning that the use of traditional bi- spectral schemes that only employ one or two of these spectral regions, such as the Nakajima and King and split- window approaches, cannot always ensure an accurate estimate of cloud properties for all retrievals. We therefore suggest a five channel retrieval scheme that would consist of a combination of error- weighted visible, near- infrared, and infrared channels chosen to use the inherent sensitivities in each of these regions to ensure high information content regardless of the state of the atmosphere. Application of this scheme to the global retrieval of ice cloud properties would allow consistency of retrieved cloud products with all available measurements and would provide a uniform means to compare cloud products from different measurement campaigns.

Chapter 5 re-examines the relatively abstract concept of relative information content in the more practical terms of retrieval performance. The five- channel retrieval scheme is assessed in context of numerical 'synthetic' experiments and, perhaps more importantly, real- world measurements from the CRYSTAL-FACE experiment. The synthetic studies suggest that the five- channel approach does indeed perform better than the traditional bi- spectral retrieval techniques for all states of the atmosphere. Regardless of relative retrieval performance, however, the base physical uncertainties suggest substantial errors in retrieved properties, often nearly to a factor of two. Such inherently large uncertainties for a near ideal observation system consisting of both MODIS and CloudSat measurements suggest a strong note of caution in the literal interpretation of exact values or small trends found in existing cloud climate products based on simpler inversion schemes. Application of the five- channel retrieval approach to CRYSTAL-

FACE data agrees well with expectations and implies that this technique may work at an operational level. Potential limitations of the approach both in terms of the optimal-estimation framework and real- world difficulties for an operational, global retrieval are discussed.

Chapter 6 presents conclusions and recommendations for future work.

Chapter 2

On the Forward and Inverse Problems

1. Introduction

The purpose of this dissertation is a re- examination of the ice cloud retrieval problem based upon a realistic assessment of the fundamental uncertainties associated with estimating ice cloud properties from satellite- based measurements. As discussed in the previous chapter, these uncertainties arise from the practical application of both the forward and inverse problems in mapping between radiance and physical space. The forward problem describes the manner in which top of the atmosphere radiances are determined from an assumed set of cloud and atmospheric properties. The inverse problem describes the reverse technique in which cloud microphysical properties are estimated from a set of radiance measurements. The purpose of this chapter then is to describe the forward and inverse techniques used for these ice cloud studies in hope of facilitating a better understanding of the work presented in the following three chapters. The forward model theory, validation, and physical assumptions used for the information content analysis of Chapter 4 and the retrieval applications of Chapter 5 are described in Section 2.2. It should be noted that the infrared radiative transfer model used in Chapter 3 will be ignored here as its simplicity allows a complete description in that chapter. The optimal- estimation technique used to invert satellite- observed radiances to estimate

cloud properties is described in Section 2.3. The knowledgeable reader will be well acquainted with most of the methods presented in this chapter. It is recommended, however, that the reader at least review sub-section 2.2.c to gain an understanding not only of the base physical assumptions used to represent ice clouds in the forward model but also the manner in which these assumptions are altered to gain an estimate of forward model uncertainty.

2. Forward Problem

This section describes the Cooper doubling and adding radiative transfer model (COOPDART) used for both the information content analysis of Chapter 4 and for the retrieval applications of Chapter 5. Although the adding and doubling technique is well- established in the literature, its theory is documented briefly in sub-section 2.2.a, primarily to highlight the physical input required to model ice clouds in this technique. Those looking for more detail than presented here should turn to Miller (2000) or Christi and Gabriel (2003) for wonderful discussions of the development of the adding and doubling approach used here or, alternately, refer to Appendix A for the actual COOPDART code in its entirety. In sub-section 2.2.b, radiative transfer calculations from COOPDART are compared to those of RADIANT Christi and Gabriel (2003) and van de Hulst (1980) to show that the method was implemented correctly. Since the application of any radiative transfer model is only valid when used in conjunction with realistic model inputs, the base physical assumptions used to represent ice clouds in COOPDART for these studies are detailed in sub-section 2.2.c.

a. Solution to the Radiative Transfer Equation

A radiative transfer model need account for the basic fundamental radiative processes of absorption, scattering, and emission. A simple integral form of the radiative transfer equation can be written as,

$$\begin{aligned}
\mu \frac{dI}{dz}(z,\mu,\phi) &= -\sigma_{ext}(z)\, I(z,\mu,\phi) \\
&+ \frac{\sigma_{sca}(z)}{4\pi} \int_0^{2\pi} \int_{-1}^{1} P\left(z,\mu,\phi,\mu',\phi'\right) I\left(z,\mu',\phi'\right) d\mu' d\phi' \\
&+ \frac{F_\odot}{4\pi} \sigma_{sca}(z)\, P(z,\mu,\phi,\mu_\odot,\phi_\odot)\, e^{-\sigma_{ext}(z_T-z)/\mu_\odot} \\
&+ \sigma_{abs}(z)\, B(T) \qquad (2.1)
\end{aligned}$$

where a wavelength dependence is understood and the above terms are as follows:

- I - radiance
- z - altitude
- μ - cosine of observation zenith angle
- ϕ - observation azimuthal angle
- σ_{ext} - extinction coefficient
- σ_{sca} - scattering coefficient
- σ_{abs} - absorption coefficient
- P - scattering phase function
- $F_\odot$ - solar flux
- $B(T)$ - Planck blackbody function

Each of the terms on the right-hand side of Equation 3.6 can be defined in context of absorption, scattering, and emission. The first term represents extinction or loss of photons due to the combination of scattering and absorption from such atmospheric media as clouds, hydro-meteors, aerosols, and gases. The second and third terms describe the

in- scattering of the diffuse and direct solar radiance fields, respectively, and thus represent a gain of photons. The final term characterizes Planck blackbody emission along the path of propagation and thus also details a gain. Although each of these terms are easy to understand physically, the integral of the second term prevents a simple analytic solution to the radiative transfer equation and therefore some numerical tricks will be needed to solve for radiance.

The usual approach is to discretize the integral form of the radiative transfer equation as in Equation 3.6 into a discrete number of streams which represent the continuous radiance field. Through application of an appropriate quadrature scheme, such as Gaussian or Lobatto, and proper manipulation of the scattering phase function, the solution to the integral radiative transfer equation is exact. The phase function, P, is first represented as a series of Legendre polynomials, as given by

$$P\left(cos\theta\right) = \sum_{l=0}^{N} \chi_l P_l cos\left(\theta\right) \tag{2.2}$$

where P_l is the l^{th} order Legendre polynomial, N is the number of polynomial terms needed to adequately describe the phase function, and χ_l is the l^{th} associated expansion coefficient, as defined by

$$\chi_l = \frac{2l+1}{2} \int_{-1}^{1} P\left(cos\theta\right) P_l\left(cos\theta\right) dcos\left(\theta\right) \tag{2.3}$$

In COOPDART, a slightly different form of the phase function based on re-normalized associated Legendre polynomials (Dave and Armstrong (1970)) is used to ensure mathematical stability and re-cast the phase function into discrete angles based on the selected quadrature scheme,

$$P\left(\mu, \phi, \mu^{'}, \phi^{'}\right) = \sum_{m=0}^{N} \sum_{l=m}^{N} \chi_l^m Y_l^m\left(\mu\right) Y_l^m\left(\mu^{'}\right) cosm\left(\phi^{'} - \phi\right) \tag{2.4}$$

where Y_l^m are re-normalized associated Legendre polynomials given by,

$$Y_l^m(\mu) = \left(\frac{(l-m)!}{(l+m)!}\right)^{\frac{1}{2}} P_l^m(\mu) \tag{2.5}$$

and where χ_l^m are modified expansion coefficients of degree m, as defined by

$$\chi_l^m = (2 - \delta_{0,m})\,\chi_l \tag{2.6}$$

The number of discrete streams, n, needed to adequately characterize the radiance field primarily depends upon the complexity of the scattering phase function, or more precisely, the number of polynomial terms, N, needed to properly represent the phase function. For the Lobatto quadrature scheme used in COOPDART to be exact, the necessary number of streams is $2n \geq N + 3$, where N is found objectively through satisfactory convergence of the radiance field. For the relatively complex phase functions needed to realistically model cirrus clouds in these studies, 48 streams will be employed, 24 each in the 'up' and 'down' hemispheres.

The radiance field itself is then decomposed into terms of a Fourier expansion,

$$I(z, \mu, \phi) = \sum_{m=0}^{M} I_m(z, \mu)\, cos\left[m(\phi - \phi_\odot)\right] \tag{2.7}$$

It should be noted that Equation 2.7 applies only to horizontally homogeneous atmospheres with the radiation field symmetric about $\phi_\odot$, meaning that the adding and doubling model presented here applies only to a plane- parallel atmospheres and may lead to substantial errors when 3-D scattering effects are important. Hopefully, such an assumption should be adequate for the relatively thin, homogeneous cirrus clouds which are the focus of these studies. Given the above assumptions and discretizations, the integral form of the radiative transfer equation is then written as a set of matrix equations, as following Christi and Gabriel (2003),

$$\begin{aligned}\frac{d^m I^{\pm}}{dz} &= \mp\sigma_{ext}\left(M^{-1}\right)\left({}^m I^{\pm}\right) \\ &\pm (1+\delta_{0m})\frac{\sigma_{sca}}{4}\left[\left(M^{-1}\right)\left({}^m P^{\pm}\right) C\left({}^m I^{+}\right) + \left(M^{-1}\right)\left({}^m P^{\mp}\right) C\left({}^m I^{-}\right)\right] \\ &\pm \frac{\sigma_{sca}}{4\pi} F_{\odot}\left(M^{-1}\right)\left({}^m P_{\odot}^{\mp}\right) e^{[-\sigma_{ext}(z_T - z)/\mu_{\odot}]} \\ &\pm \sigma_{abs}\left(M^{-1}\right)\left({}^m Y\right) B\left(T\right) \end{aligned} \tag{2.8}$$

where,

- $P^{\pm}$ - the phase function for forward (+) and backward (-) hemispheres for scattering of the diffuse radiation field
- $P_{\odot}^{\pm}$ - the phase function for forward (+) and backward (-) hemispheres for scattering of the direct solar beam
- M^{-1} - matrix of the reciprocals of the quadrature angles
- C- a matrix of quadrature weights
- ${}^m Y$ a vector of unity for m=0 and vector of zero otherwise

Equation 2.8 can be expressed much more succinctly in matrix form as,

$$\frac{d}{dz}\begin{bmatrix} {}^m I^{+} \\ {}^m I^{-} \end{bmatrix} = \begin{bmatrix} t^m & -r^m \\ r^m & -t^m \end{bmatrix}\begin{bmatrix} {}^m I^{+} \\ {}^m I^{-} \end{bmatrix} + \begin{bmatrix} {}^m \Sigma^{+} \\ -{}^m \Sigma^{-} \end{bmatrix} \tag{2.9}$$

where t^m, r^m, and Σ^m are the 'local' transmittance, reflectance, and source terms, respectively. These terms describe the radiative properties for an infinitesimal layer of optical depth, $\delta\tau$, and are of mathematical form,

$$t^m = -\sigma_{ext}\left(M^{-1}\right) + (1+\delta_{0m})\frac{\sigma_{sca}}{4\pi}\left[\left(M^{-1}\right)\left({}^m P^{+}\right) C\right] \tag{2.10}$$

$$r^m = -\left(1+\delta_{0m}\right)\frac{\sigma_{sca}}{4\pi}\left[\left(M^{-1}\right)\left({}^mP^-\right)C\right] \tag{2.11}$$

$${}^m\Sigma^{\pm} = \frac{\sigma_{sca}}{4\pi}F_{\odot}\left(M^{-1}\right)\left({}^mP^{\mp}_{\odot}\right)e^{\left[-\sigma_{ext}(z_T-z)/\mu_{\odot}\right]} + \sigma_{abs}\left(M^{-1}\right)\left({}^mY\right)B \tag{2.12}$$

It is only the rigorous determination of the terms in Equations 2.10 - 2.12 and their faithful representation in the forward model that allow a realistic simulation of radiances for our cirrus cloud studies. More specifically, the appropriate selection of scattering phase function, extinction coefficient, and single scatter albedo are critical for the validity of the information content and retrieval applications of the following chapters.

With the radiative transfer equation in relatively tractable form, the next step is to use interaction principle of radiative transfer (Chandrasekhar (1960)) and the inter- related techniques of adding and doubling to transform the local functions, as described in Equations 2.10 - 2.12, into 'global' radiative properties, from which exitant radiances can be modeled. Doubling is the process in which the local radiative properties for an infinitesimally small, atmospheric layer of optical depth, $\delta\tau$, are combined to produce the global radiative properties for a homogeneous, finite layer of optical depth, $\Delta\tau$, i.e. the local t, r, and Σ functions are converted to their global T, R, and S equivalents. These global properties are then combined through the adding process to determine total T, R, and S for an atmosphere consisting of any number of inhomogeneous layers.

These ideas are most easily understood graphically as in Figure 2.1. The interaction principle is founded on the idea that the fate of any photon in the layer (a,b) can be described completely in terms of the reflectance, transmittance, and source functions. Provided that the radiance boundary conditions, $I^-(a)$ and $I^+(b)$, are known, the exitant radiance are completely defined. Mathematically,

$$I^+(a) = T(b,a)\,I^+(b) + R(a,b)\,I^-(a) + S(b,a) \tag{2.13}$$

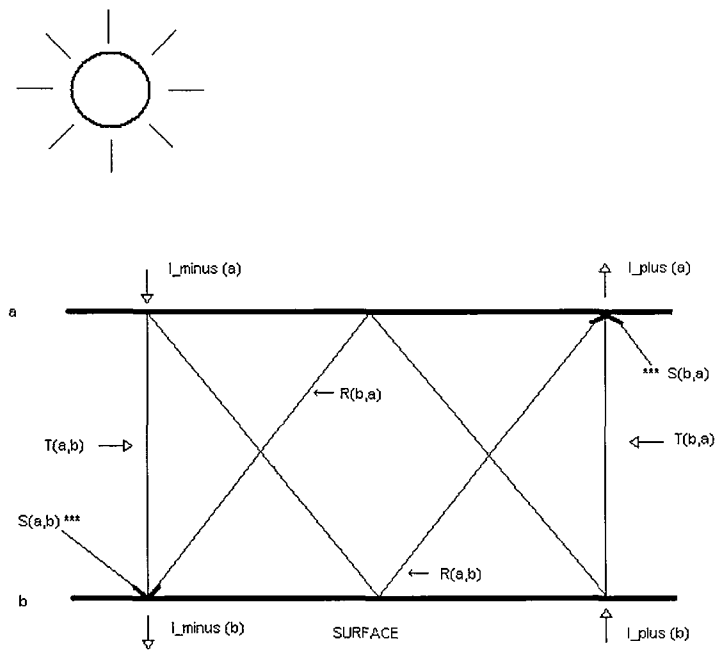

Figure 2.1: Representation of the transmittance, reflectance, and source functions for a single- layer atmosphere used to describe the interaction principle and inter- related topics of doubling and adding.

and

$$I^{-}(b) = T(a,b)\, I^{-}(a) + R(b,a)\, I^{+}(b) + S(a,b) \tag{2.14}$$

where $I^{-}(a)$ is incoming solar radiation

$$I^{-}(a) = \frac{\mu_{\odot} F_{\odot}}{\pi} = f_0 \tag{2.15}$$

and $I^{+}(b)$ is the combined radiance from reflectance and emission from the surface,

$$I^{+}(b) = R_g I^{-} + B_g(T) \tag{2.16}$$

where R_g is the reflectance function with albedo, a_g.

If Equations 2.15 - 2.16 are substituted into Equations 2.13 - 2.14, a rather complicated expression for both up-welling TOA and down-welling surface radiance is found in terms of the total atmosphere R, T, and S functions.

The precise mathematical forms for these R, T, and S arise from the adding process and are best determined by examination of the interaction principle but now for a two-layer atmosphere, as seen in Figure 2.2. The interaction principle for the two layers, (a,b) and (b,c), taken separately can be written as

$$I^{+}(a) = T(b,a)\, I^{+}(b) + R(a,b)\, I^{-}(a) + S(b,a) \tag{2.17}$$

$$I^{-}(b) = T(a,b)\, I^{-}(a) + R(b,a)\, I^{+}(b) + S(a,b) \tag{2.18}$$

$$I^{+}(b) = T(c,b)\, I^{+}(c) + R(b,c)\, I^{-}(b) + S(c,b) \tag{2.19}$$

$$I^{-}(c) = T(b,c)\, I^{-}(b) + R(c,b)\, I^{+}(c) + S(b,c) \tag{2.20}$$

Elimination of $I^{+}(b)$ and $I^{-}(b)$ from Equations 2.17 - 2.20 yields the following composition relationships for the transmittance, reflectance, and source functions for the combined layer (a,c). It should be noted that these functions are directionally dependent and are of form,

$$T(c,a) = T(b,a)\left[E - R(b,c)\, R(b,a)\right]^{-1} T(c,b) \tag{2.21}$$

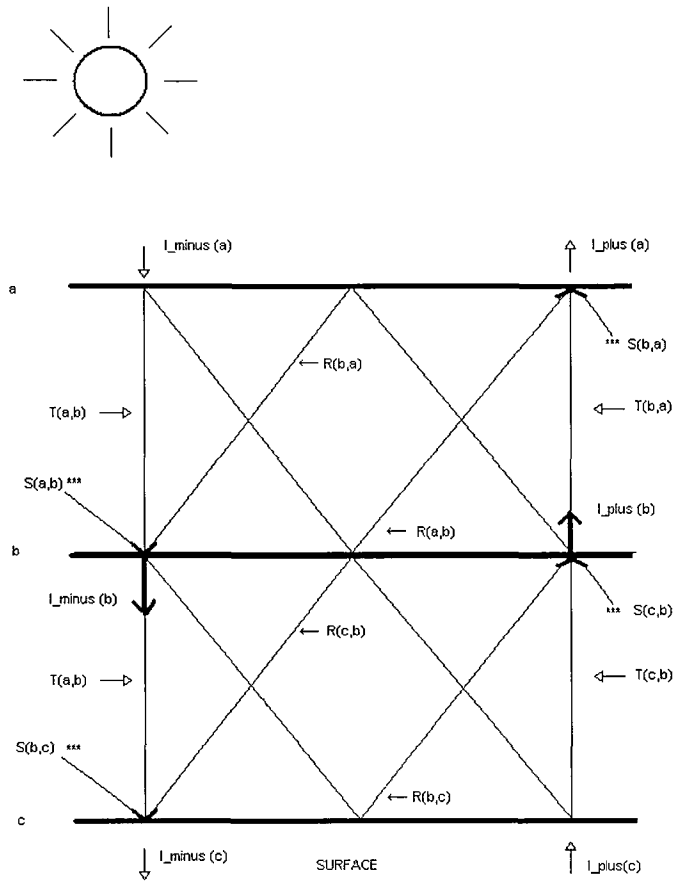

Figure 2.2: Representation of the transmittance, reflectance, and source functions for a multiple- layer atmosphere used to describe the interaction principle and inter- related topics of doubling and adding.

$$R(a,c) = T(b,a)\left[E - R(b,c)\,R(b,a)\right]^{-1} R(b,c)\,T(a,b) + R(a,b) \tag{2.22}$$

$$S(c,a) = T(b,a)\left[E - R(b,c)\,R(b,a)\right]^{-1}\left[R(b,c)\,S(a,b) + S(c,b)\right] + S(b,a) \tag{2.23}$$

$$T(a,c) = T(b,c)\left[E - R(b,a)\,R(b,c)\right]^{-1} T(a,b) \tag{2.24}$$

$$R(c,a) = T(b,c)\left[E - R(b,a)\,R(b,c)\right]^{-1} R(b,a)\,T(c,b) + R(c,b) \tag{2.25}$$

$$S(a,c) = T(b,c)\left[E - R(b,a)\,R(b,c)\right]^{-1}\left[R(b,a)\,S(c,b) + S(a,b)\right] + S(b,c) \tag{2.26}$$

These composition relationships allow the radiative properties of any arbitrary number of inhomogeneous, atmospheric layers to be added to produce the total atmosphere reflectance, transmittance, and source functions needed to model exitant radiances.

The precise mathematical form of the R, T, and S functions for each homogeneous layer arises from the process of doubling, which is just a form of adding with the minor change that each of the doubled layers is identical. Therefore, the same general composition relationships hold,

$$R_{n+1} = T_n\left[E - R_n R_n\right]^{-1} R_n T_n + R_n \tag{2.27}$$

$$T_{n+1} = T_n\left[E - R_n R_n\right]^{-1} T_n \tag{2.28}$$

The source terms are modified by an attenuation factor, e_n, which has value unity for a homogeneous emitting layer but exhibits exponential decay for solar wavelengths,

$$S_{n+1}^{-} = T_n\left[E - R_n R_n\right]^{-1}\left(e_n R_n S_n^{+} + S_n^{-}\right) + e_n S_n^{-} \tag{2.29}$$

$$S_{n+1}^{+} = T_n\left[E - R_n R_n\right]^{-1}\left(R_n S_n^{-} + e_n S_n^{+}\right) + S_n^{+} \tag{2.30}$$

$$e_{n,solar} = exp\left(-2^n \delta\tau/\mu_\odot\right) \tag{2.31}$$

A general form for the exitant radiances for the multiple- layer atmosphere of Figure 2.2 with internal sources above a reflecting surface is found in terms of the above composition relationships,

$$I^-(c) = \left[E - R(c,a)\, R_g\right]^{-1} \left[T(a,c)\, I^-(a) + R(c,a)\left[a_g f_0 e^{-\tau/\mu_0} + B_g(T)\right] + S(a,c)\right] \tag{2.32}$$

and

$$I^+(a) = T(c,a)\left[a_g\left(R_g I^-(c) + f_0 e^{-\tau/\mu_0}\right) + B_g(T)\right] + R(a,c)\, I^-(a) + S(c,a) \tag{2.33}$$

b. Forward Model Validation

Radiative transfer calculations from COOPDART were compared to those of both the RADIANT eigenmatrix solver of Christi and Gabriel (2003) and the flux tables of van de Hulst (1980) to ensure that the model was implemented correctly. Figure 2.3 shows sample radiative transfer calculations using 16 streams for each COOPDART and RADIANT for a cloud case with optical depth of 1.0 with a Henyey- Greenstein phase function with asymmetry parameter, g, equal to 0.8. Both upwelling TOA and downwelling surface radiances agree to approximately 5 decimal points for all quadrature angles. Similarly, Figure 2.4 shows the up and down fluxes as calculated by both COOPDART and van de Hulst (1980) as a function of single scatter albedo for a cloud of optical depth of 1.0 with a Henyey- Greenstein phase function with asymmetry parameter, g, equal to 0. Agreement in fluxes is good to approximately 4 decimal places. These results clearly

suggest that the core COOPDART adding and doubling routines are working correctly. Slight modifications of this code was required to address the cirrus cloud problem and is discussed in the following sub- section.

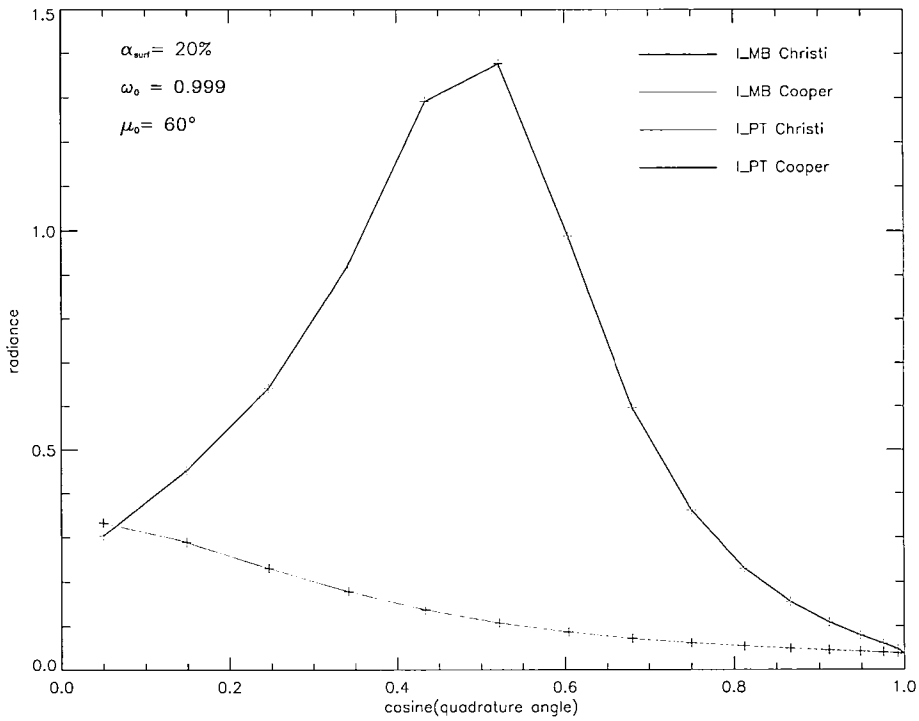

Figure 2.3: Comparison of TOA and surface radiances from COOPDART and the RADIANT eigenmatrix solver Christi and Gabriel (2003) for a cloud with optical depth of 1.0 and a Henyey- Greenstein phase function with asymmetry parameter, g, equal to 0.8.

c. Forward Model Assumptions

Application of any forward radiative transfer model, however elegant or computationally efficient, is only valid when used in conjunction with physically realistic model inputs. This sub-section therefore examines both the physical assumptions used in COOPDART and their impact on the mathematical form of the forward model, primarily focusing on the ice crystal habit and atmospheric absorption properties which need critical consideration for any ice cloud retrieval scheme. The presentation of these assumptions here

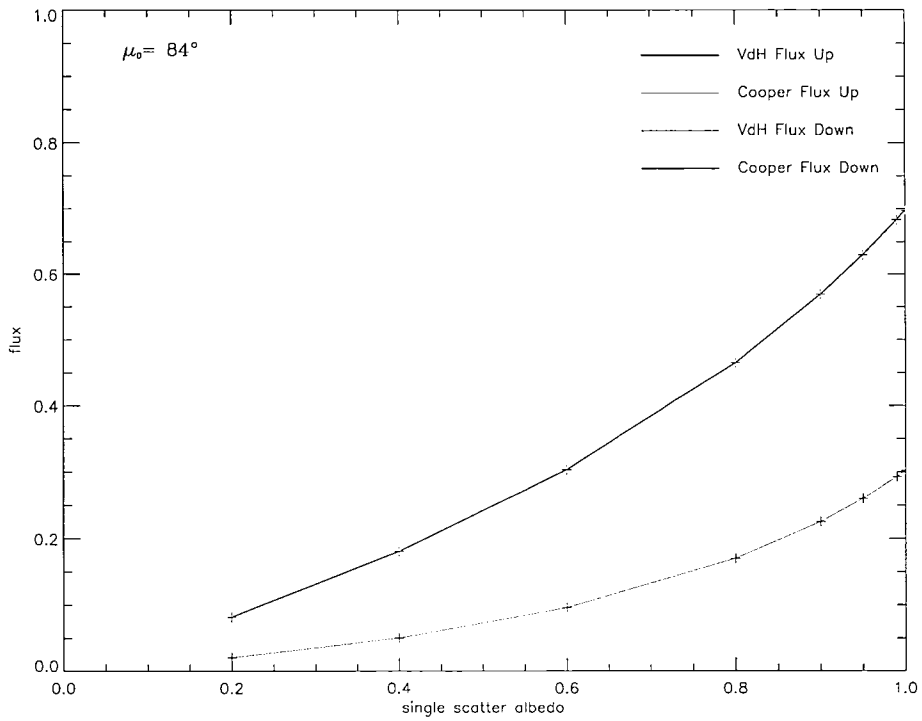

Figure 2.4: Comparison of TOA and surface fluxes from COOPDART and the van de Hulst (1980) for a cloud with optical depth of 1.0 and a Henyey- Greenstein phase function with asymmetry parameter, g, equal to 0.

is in much greater detail than will be found in the following chapters which were written in 'journal style' format. It is hoped the rigorous exploration of these topics here will not only facilitate a better understanding of these later chapters but also provide the completeness needed to replicate this work. Since much of the work in this dissertation involves examining the variability of forward model calculations resulting from different base assumptions, a brief discussion on equivalent crystal distributions is also included, i.e. how can a distribution of dendrites be equated quantitatively to a distribution of hexagonal columns?

Ice crystal habit Ice clouds may be composed of a variety of crystal types ranging from pristine hexagonal columns to nearly spherical aggregates, with each distinct habit having its own set of unique optical properties. The selection of a representative crystal

type for a forward model is therefore problematic and is, of course, the motivation for much of this dissertation. We will exploit the recent development of optical properties for a number of realistic crystal habits for the MODIS wavelengths listed Table 2.1 for 24 discrete particle sizes to produce a quantitative estimate of forward model uncertainty resulting from assumptions of crystal habit. Our base assumption for crystal habit in the information content and retrieval applications of Chapters 4 and 5 will be that of a randomly oriented randomized hexagonal aggregate (Baran et al. (2001)), as the theoretical single scattering properties for these aggregates combined with a modified Henyey- Greenstein phase function were found to better match observed radiances than the theoretical optical properties for more pristine crystal types (Baran et al. (2003)). To gain a measure of forward model variability about this base assumption, the optical properties for for each plates, bullets, dendrites, rough aggregates, smooth aggregates, and droxtals as calculated by Yang et al. (2000) were used.

Differences in the optical properties for these different crystal types can be significant. Figures 2.5 and 2.6 show the scattering phase functions for the Baran aggregates and Yang columns, respectively, in which the smooth Baran phase functions lack the complex secondary scattering features of the Yang hexagonal columns. It is these discrepancies, and similar others in single scatter albedo and extinction coefficient, that result in large differences in radiance as a function of crystal habit as discussed in Chapter 1 and as visualized in the Nakajima and King (1990) retrieval scheme shown in Figure 2.7.

Delta-M scaling The complex nature of the phase functions shown in Figures 2.5 and 2.6 raises several practical concerns for the radiative transfer calculations performed in these cirrus clouds studies. First, the accurate representation of the large forward scattering peaks observed in both crystal types would require such a large number of forward model streams and thus such large computational expense as to make these studies intractable. To get around this difficulty, a modified form of the Delta- M scal-

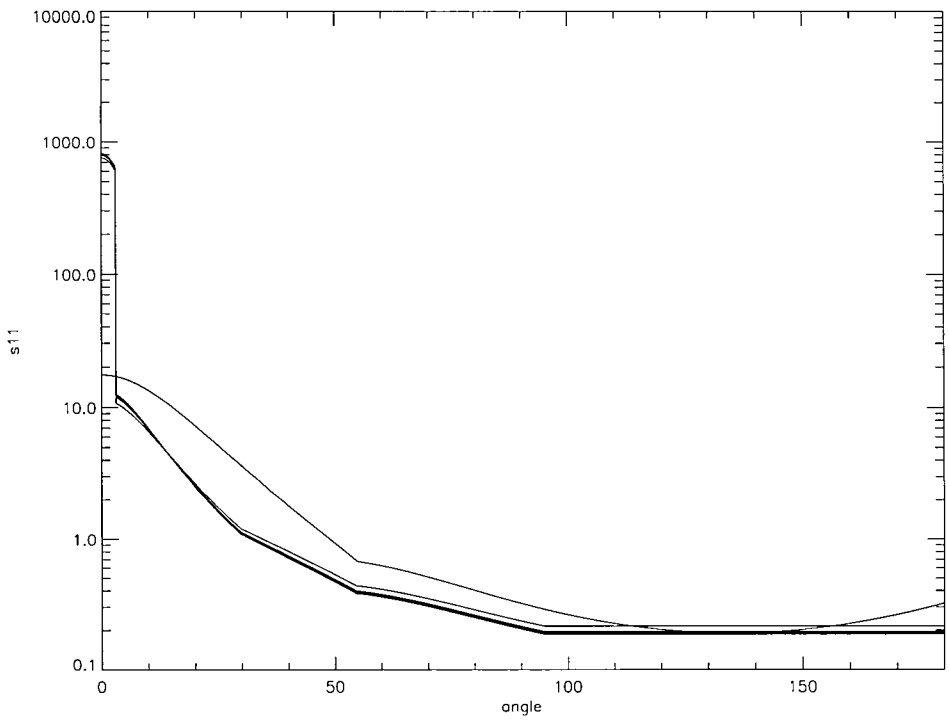

Figure 2.5: Phase function at 0.65 μm for randomly oriented randomized hexagonal aggregates (Baran et al. (2001)) with maximum crystal dimension ranging from 3.5 μm to 3500 μm.

ing technique (Wiscombe (1977)) recently developed by Mitrescu and Stephens (2004) was implemented. The idea is to truncate the large forward peak at some specified angle, e.g. 3 ° would be a reasonable choice for the aggregate of Figure 2.5, and then fit chi- expansion coefficients to the simpler, truncated phase function for use in the forward model. To account for the reduction in forward scattering, both the optical depth and single scatter albedo are re-normalized based upon the fractional energy, f, in the truncated portion of the forward peak. Mathematically, the new optical depth, $\tau^{'}$, and single scatter albedo, $\omega_0^{'}$, become

$$\tau^{'} = (1 - f\omega_0)\,\tau \tag{2.34}$$

and

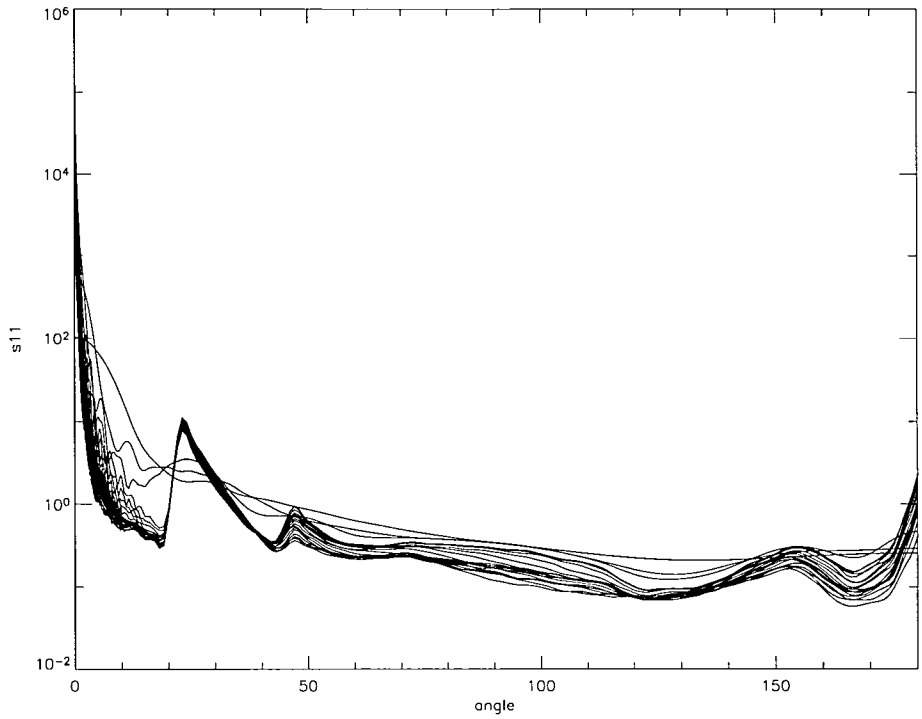

Figure 2.6: Phase function at 0.65 μm for hexagonal columns (Yang et al. (2000)) with maximum crystal dimension ranging from 3.5 μm to 3500 μm.

$$\omega_0^{'} = \frac{1-f}{1-f\omega_0}\omega_0 \tag{2.35}$$

Even with this technique, it is still not possible to fit a computationally reasonable number of streams to the complex secondary 22° and 46° halos associated with the hexagonal columns. Although these features are somewhat smoothed once the individual crystal particles are merged into distribution form as discussed below, additional smoothing of these maxima is required. Such modifications allow COOPDART to be run with a computationally feasible 48 streams for all crystal types while maintaining satisfactory convergence of the radiance field.

Ice crystal size distribution The ice crystal size distributions in the forward model were assumed to be of modified gamma form with variance parameter, ν, equal to 2,

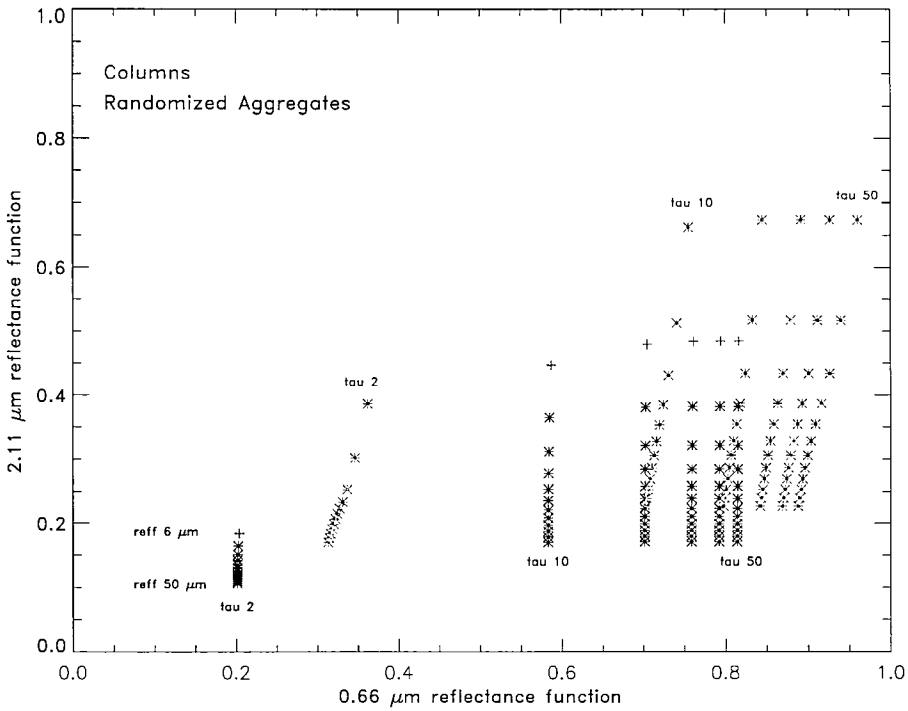

Figure 2.7: Relationship between 0.66 μm and 2.11 μm reflectance functions for ice clouds composed of both a modified gamma distribution of randomized aggregates and an equivalent distribution of columns. Effective radius range from 6 to 50 μm and optical depths from 2 to 50.

$$n(D) = N_0 \frac{1}{\Gamma(\nu)} \left(\frac{D}{D_n}\right)^{\nu-1} \frac{1}{D_n} e^{-D/D_n} \tag{2.36}$$

where $n(D)$ is the number of ice crystals of size D, N_0 is the number concentration, and D_n is the characteristic diameter (Stephens (1994)). By clever manipulation of the number concentration for each of the 24 discrete particle sizes from Baran and Yang, modified gamma distributions with effective radius ranging from 6 μm to 50 μm were created. Here, the relatively ambiguous effective radius, r_{eff}, is defined as

$$r_{eff} = \frac{3}{4} \frac{Vol}{A_P} \tag{2.37}$$

where Vol is total distribution volume and A_P is total distribution projected area. The

optical properties for the distribution as a whole come simply from merging the optical properties of each of the constituent particles. The following relationships were used to calculate the optical depth, single scatter albedo, and phase functions for the modified gamma distributions,

$$\tau = \sum_{i=1}^{NRAD} N_{0,i}\, c_{ext,i}\, dz \tag{2.38}$$

$$\omega_{0,total} = \frac{\sum_{i=1}^{NRAD} N_{0,i}\, c_{ext,i}\, \omega_{0,i}}{\sum_{i=1}^{NRAD} N_{0,i}\, c_{ext,i}} \tag{2.39}$$

and

$$P_{11,total} = \frac{\sum_{i=1}^{NRAD} N_{0,i}\, c_{ext,i}\, \omega_{0,i}\, P_{11,i}}{\sum_{i=1}^{NRAD} N_{0,i}\, c_{ext,i}\, \omega_{0,i}} \tag{2.40}$$

where NRAD is the number of discrete particle sizes used for the distribution, N_0 is number concentration, c_{ext} is the extinction cross-section, dz is cloud geometric thickness, and P_{11} is the first stokes vector.

Equivalent distributions and habits Much of the work in this dissertation involves examining the variability of forward model calculations resulting from different base assumptions. For most physical fields, such as atmospheric temperature profile or particle size distribution, our base assumption is replaced with an alternative in a very straightforward manner. For instance, the modified gamma distribution with variance parameter ν equal to two will is replaced by both a different modified gamma distribution with ν equal to three and a lognormal distribution,

$$n(D) = \frac{1}{D \ln\sigma_g (2\pi)^{0.5}} \exp\left[\frac{(\ln D - \ln D_g)^2}{2(\ln\sigma_g)^2}\right] \tag{2.41}$$

where D_g is the geometric mean diameter and σ_g is the geometric standard deviation (Reist (1994)).

The use of equivalent crystal habits in determining forward model variability is more problematic. The difficulty lies in equating a distribution of one crystal habit to a distribution of another crystal habit in a manner which is not arbitrary. The approach taken for this work comes from insights gleaned from the use of equal- area and equal- volume spheres, which traditionally have been used to represent non- spherical habits in computationally expensive GCM and radiative transfer calculations. This technique does not work well (Liou and Takano (1994)), in that the equal volume sphere has too little surface area as compared to an irregularly shaped crystal and therefore scatters too little whereas the equal area sphere has too much volume and thus absorbs too much. Recent work has suggested the use an equivalent sphere that has the same volume to area ratio as the irregular shaped crystal, such that volume and area is conserved by allowing the number concentration of the different crystal types to vary (Francis et al. (1994); Mitchell and Arnott (1994); Grenfell and Warren (1999); Yang et al. (2001)). Figure 2.8 displays an artificial conversion between columns, spheres, and dendrites in which each crystal type has a different volume and area but the same surface to area ratio. By varying the number of crystals for each habit, it is possible to conserve both volume and area for the equivalent distributions. This approach will be utilized in the uncertainty analyses of Chapter 3 and 4, Each of the individual randomized hexagonal aggregates in the modified gamma crystal size distribution will be converted to a set of equivalent crystals, say dendrites, that has the same volume and area of the aggregates. The optical properties for this equivalent distribution of dendrites will then be merged as above except for an additional term, N_s, that accounts for the conversion of number concentration between crystal types,

$$\tau = \sum_{i=1}^{NRAD} N_{s,i}\, N_{0,i}\, c_{ext,i}\, dz \tag{2.42}$$

$$\omega_{0,total} = \frac{\sum_{i=1}^{NRAD} N_{s,i}\, N_{0,i}\, c_{ext,i}\, \omega_{0,i}}{\sum_{i=1}^{NRAD} N_{s,i}\, N_{0,i}\, c_{ext,i}} \tag{2.43}$$

and

$$P_{11,total} = \frac{\sum_{i=1}^{NRAD} N_{s,i}\, N_{0,i}\, c_{ext,i}\, \omega_{0,i}\, P_{11,i}}{\sum_{i=1}^{NRAD} N_{s,i}\, N_{0,i}\, c_{ext,i}\, \omega_{0,i}} \tag{2.44}$$

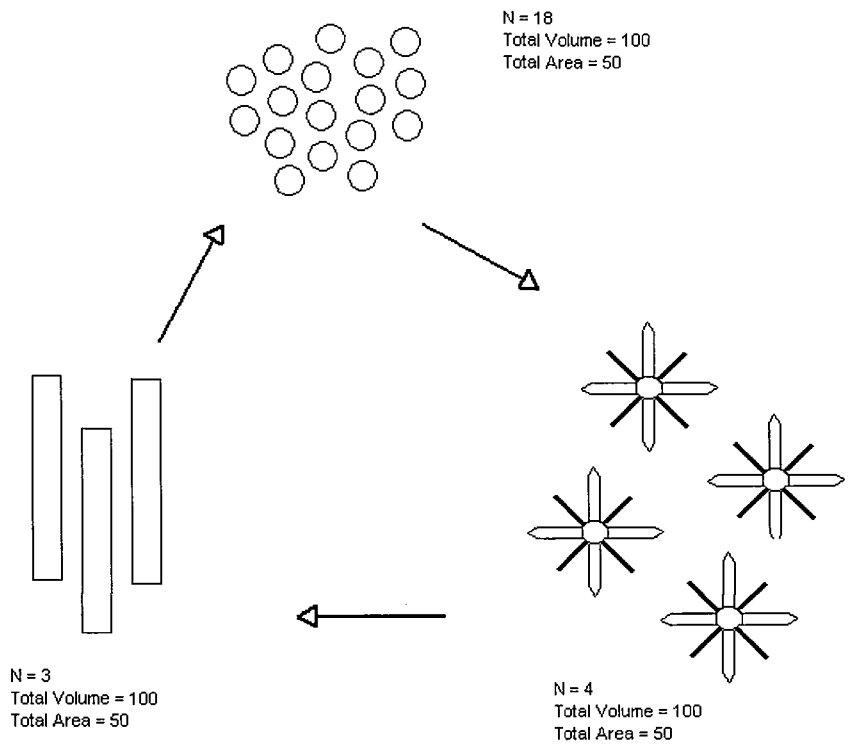

Figure 2.8: The technique used to determine equivalent size distributions for ice particles with different habits depends on conserving both distribution area and volume by varying the number concentration of the different shaped particles.

Atmospheric absorption Many of the traditional means to estimate cirrus cloud properties, such as the split- window technique (Inoue (1985); Prabhakara et al. (1988)), rely not only an *a priori* understanding of cloud optical properties but also on an *a priori* understanding of atmospheric absorption and emission. Atmospheric absorption in COOPDART is modeled using correlated- k distributions developed specifically for the MODIS wavebands (Kratz (1995)) listed in Table 2.1. The correlated- k approach

allows computationally efficient radiative transfer calculations by grouping individual line- by- line absorption characteristics into discrete bins of constant absorption properties. The first task is to identify the radiatively important gases for each MODIS channel, e.g. absorption in the 1.626- 1.653 μm band comes from each water vapor, carbon dioxide and methane. Each of these gases are then broken into fractional bandwidth bins with given absorption characteristics, which are directly related to optical depth through assumption of atmospheric profile. Since these optical depths have no precise location in spectral space, it is necessary to then perform a 'blurred' radiative transfer calculation using all permutations of the gaseous fractional bins. So for the 1.64 μm band in which each of the three absorbing gases are segregated into two distinct absorption bands, it would be necessary to perform eight fractionally- weighted, radiative transfer calculations to determine the radiance across the entire bandwidth. A perfect step- function detector response across the MODIS bandwidths is therefore presumed. Table 2.2 shows a comparison of top of the atmosphere brightness temperatures found from COOPDART with correlated-k absorption and from MODTRAN with line- by-line absorption assuming a McClatchey tropical atmosphere. Brightness temperatures agree well, with minor differences primarily due to slightly different assumptions of the importance of trace gases.

Other considerations In addition to the ice cloud optical and atmospheric properties discussed above, many other fields need be assumed for the COOPDART calculations. These fields, such as atmospheric temperature and humidity profiles, are generally straightforward and are adequately explained in the following chapters. It bears repeating, however, that each of these studies assumes an isotropic ocean surface for simplicity, where an albedo of 10 % is assumed for the visible and near- infrared channels and of 1 % for the emitting channels. The use of a surface with a greater or more variable albedo could change the results of this work.

MODIS channel	wavelength	MODIS channel	wavelength
1	0.62-0.67	27	6.53-6.90
2	0.84-0.88	29	8.40-8.70
5	1.23-1.35	31	10.78-11.28
6	1.63-1.65	32	11.77-12.27
7	2.10-2.15	33	13.18-13.49
19	0.91-0.96	34	13.48-13.78
20	3.66-3.84	35	13.78-14.08
23	4.02-4.08	36	14.08-14.38
26	1.36-1.39		

Table 2.1: MODIS channels used in forward model.

MODIS channel	wavelength (μm)	COOPDART T_b (K)	MODTRAN T_b (K)
27	6.7	241	239
29	8.5	292	291
31	11.0	294	294
32	12.0	293	292
33	13.3	262	260
34	13.6	276	274
35	13.9	248	250
36	14.2	230	230

Table 2.2: Comparison of COOPDART and MODTRAN.

3. Inverse Problem

This section describes the optimal- estimation retrieval framework (Rodgers (1976); Marks and Rodgers (1993)) used to estimate cloud properties for the split- window and MODIS schemes of Chapters 3 and 5. As seen in the introduction, simple inversion techniques in which cloud optical properties are linked directly to radiance through forward model assumptions may not always work well for ice clouds. For the infrared split- window problem, uncertainties in cloud temperature will cause huge errors in the absence of accurate cloud boundary information. Similarly, uncertainties in cloud optical properties resulting from the variability of crystal shape may cause significant biases when visible radiances are directly inverted to estimate cloud microphysical properties. The optimal- estimation framework provides a means to work around some of these difficulties. A brief review of this retrieval scheme is presented to allow a more precise understanding of the advantages of this approach for the complex ice cloud retrieval

problem.

Many recent studies have applied the optimal estimation technique to retrievals of ozone, water vapor, cloud properties, rainfall, and aerosols from a combination of lidar, radar, and passive measurements at visible, infrared, and microwave wavelengths (Engelen and Stephens (1997), Engelen and Stephens (1999), Miller et al. (2000), Austin and Stephens (2001), Stephens et al. (2001b), and L'Ecuyer and Stephens (2002)) . Many of the mathematical details of the approach can be found in these references but a short summary is provided here for completeness. Letting $\hat{\mathbf{x}}$ denote the vector of cloud properties to be retrieved, the optimal estimation technique consists of minimizing a combination of the variance between the set of observations, $\mathbf{y}$, and a corresponding set of simulated measurements, $F(\hat{\mathbf{x}})$, and that between $\hat{\mathbf{x}}$ and a suitable *a priori* guess, $\mathbf{x}_a$. Assuming Gaussian statistics, this is accomplished by minimizing the scalar cost function,

$$\begin{aligned} \Phi(\hat{\mathbf{x}}, \mathbf{y}, \mathbf{x}_a) &= (\mathbf{y} - F(\hat{\mathbf{x}}))^T \mathbf{S}_y^{-1} (\mathbf{y} - F(\hat{\mathbf{x}})) \\ &+ (\hat{\mathbf{x}} - \mathbf{x}_a)^T \mathbf{S}_a^{-1} (\hat{\mathbf{x}} - \mathbf{x}_a) \end{aligned} \tag{2.45}$$

with respect to $\mathbf{x}$. F denotes the physical model relating the cloud parameters to the observations called the "forward model", $\mathbf{S}_a$ is the *a priori* error covariance matrix, and $\mathbf{S}_y$ is the measurement error covariance matrix consisting of a combination of observation and the forward model uncertainties.

The values of $\hat{\mathbf{x}}$ for which Equation. (3.1) is minimum can be found by Newtonian iteration via

$$\hat{\mathbf{x}}^{i+1} - \hat{\mathbf{x}}^i = \mathbf{S}_x \left[\mathbf{K}_i^T \mathbf{S}_y^{-1} \left(\mathbf{y} - \mathrm{F}(\hat{\mathbf{x}}^i) \right) + \mathbf{S}_a^{-1} \left(\mathbf{x}_a - \hat{\mathbf{x}}^i \right) \right] \tag{2.46}$$

where

$$\mathbf{S}_x = \left(\mathbf{S}_a^{-1} + \mathbf{K}_i^T \mathbf{S}_y^{-1} \mathbf{K}_i \right)^{-1} \tag{2.47}$$

is the error covariance matrix of the estimated parameters accounting for uncertainties in the forward model, measurements, and *a priori* data. The Kernel or weighting function matrix, $\mathbf{K}$, is the Jacobian of the forward model with respect to the retrieval vector, with elements given by

$$K_{jk} = \frac{\partial F_j}{\partial x_k} \tag{2.48}$$

The iteration proceeds until such time as the covariance-weighted mean difference between successive estimates is much less than the number of independent variables in the retrieval vector, i.e.

$$\left(\hat{\mathbf{x}}^{i+1} - \hat{\mathbf{x}}^{i}\right) \mathbf{S}_y^{-1} \left(\hat{\mathbf{x}}^{i+1} - \hat{\mathbf{x}}^{i}\right) << N_x \tag{2.49}$$

The optimal estimation framework also includes several useful diagnostics that need consideration to determine the quality of the retrieval. The *a priori* matrix,

$$\mathbf{A} = \mathbf{S}_x \mathbf{K}_i^T \mathbf{S}_y^{-1} \mathbf{K}_i \tag{2.50}$$

measures the relative dependence of the retrieved parameters on the measurements and on the *a priori* assumptions. For an ideal retrieval, $\mathbf{A}$ will be the identity matrix indicating that the retrieved parameters were completely determined by the measurements. The chi- square diagnostic,

$$\chi^2 = \frac{\left[y - F\left(\hat{x}\right)\right]^2}{S_y} + \frac{\left(x_a - \hat{x}\right)^2}{S_a} \tag{2.51}$$

presented here in scalar form, is another useful diagnostic that shows how well retrieved parameters match our observations. This chi- square value roughly will be of order of magnitude of the number of degrees of freedom in the retrieval problem for a well-behaved retrieval.

The relatively complex retrieval approach outlined above has significant advantages over a simple inversion approach for the ice cloud problem given its inherent uncertainties. In fact, without this retrieval approach, the studies presented here and final

recommendations for re-casting the ice cloud retrieval would simply not be possible.

The flexible framework of the estimation approach provides a simple means to incorporate information from a variety of sensors into a given retrieval. This capacity will be used to combine information from both passive and active sensors into the ice cloud retrieval schemes of Chapters 3 and 5.

Another useful aspect of this approach is its explicit consideration of uncertainties, both in retrieval input and output. Proper characterization of the forward model and measurement covariance matrix allows a retrieval scheme to place emphasis on those measurements which contain the most information dependent upon the state of the atmosphere, an idea that will be revisited in the development of a unified five- channel ice cloud retrieval approach outlined in Chapters 4 and 5. The results of this inversion technique, however, are only valid when used in conjunction with physically realistic assumptions for the error covariance matrices, $\mathbf{S_y}$ and $\mathbf{S_a}$. Hence, a rigorous characterization of the forward model error covariance matrix is performed to ensure retrieved cloud properties which are based upon a realistic assessment of the physics of the ice cloud problem. Determination of $\mathbf{S_a}$ is less problematic as it simply comes from the expected climatological range of ice cloud properties. Use of these realistic uncertainties for $\mathbf{S_y}$ and $\mathbf{S_a}$ in this inversion technique will result in an honest assessment of uncertainties associated with our retrieved cloud properties, as defined in $\mathbf{S_x}$. Such a characterization will be useful not only in determining how precisely we can actual measure these fields given the constraint of our current observational platforms but also in providing a useful diagnostic for determining the relative merits of different retrieval approaches. Finally, the built- in error diagnostics such as the $\mathbf{A}$ matrix provide a quantitative means to evaluate the quality of each retrieval, an obvious improvement over the simple inversion techniques which simply return an answer.

Chapter 3

The Impact of Explicit Cloud Boundary Information on Ice Cloud Microphysical Property Retrievals from Infrared Radiances

1. Preface

The following chapter consists of a reproduction of the journal article, 'The Impact of Explicit Cloud Boundary Information on Ice Cloud Microphysical Property Retrievals from Infrared Radiances' by Steven J. Cooper, Tristan S. L'Ecuyer, and Graeme L. Stephens published in the *Journal of Geophysical Research* in 2003, 2002JD002611. It is left in near published format for consistency. This brief preface, therefore, is used simply to place the contents of this work in the overall logical structure of the dissertation.

The chapter begins our investigation of the impacts of uncertainties on the retrieval of ice cloud properties using the instruments aboard the NASA Afternoon A-Train constellation of satellites as a practical constraint. This chapter casts the split-window cirrus

cloud retrieval technique in an optimal estimation framework to examine uncertainties in the retrieval of cirrus cloud optical depth and effective radius as a function of uncertainty in cloud emitting temperature. The incorporation of cloud boundary information from either the CloudSat Cloud Profiling Radar or the CALIPSO lidar to constrain the window- region measurements from MODIS is found to substantially reduce the errors inherent to this approach. Regardless of co-incident cloud boundary information, however, retrieval errors are found to be large and heavily dependent upon not only on the characteristics of the observation platforms but also on the forward model uncertainties from such forward model assumptions as ice crystal habit. The methodologies and insights gleaned from this examination of the split- window problem were then applied to the much more challenging problem of selecting the ideal combination of measurements from the visible, near- infrared, and infrared spectral regions for an ice cloud microphysical property retrieval scheme as discussed in Chapter 4.

ABSTRACT

Cirrus clouds have a profound impact on the radiation balance of the Earth-atmosphere system. Accurate representation of their radiative properties is critical to understanding climate and predicting climate change. This paper casts the split-window cirrus cloud retrieval technique in an optimal estimation framework facilitating direct inclusion of explicit cloud boundary information from complementary sensors as well as providing a suite of diagnostic tools for evaluating the dominant sources of uncertainty in all retrieved quantities. Errors in retrieved microphysical properties are used to determine the resulting errors in the calculation of global scale radiative budgets.

Uncertainties in optical depth and effective radius are found to diminish from ~45 and ~80 %, respectively, in the absence of explicit cloud boundary information to ~15 and ~60 % when accurate radar- or lidar-based estimates are included. It is demonstrated that the improvements to cirrus cloud optical properties afforded by accurate cloud boundary information may lead to as much as a factor of three increase in the accuracy to which their impact on the Earth's radiative balance can be modeled. Co-located infrared radiances from the MODIS instrument aboard the Earth Observing System (EOS) Aqua satellite and cloud radar observations from the CloudSat satellite will soon allow the retrieval presented here to be integrated into an operational retrieval of the vertical distribution of cloud properties on a global scale.

2. Introduction

The Earth's weather and climate is driven by the exchange of energy between the sun, atmosphere, surface, and space. Cirrus clouds play a critical role in regulating this global energy balance through a combination of reflecting incoming solar radiation and absorbing and re-emitting terrestrial radiation (Liou (1986)). The relative magnitudes of these competing effects and their spatial and temporal variability is a crucial component modulating global atmospheric circulations, but the net effect of cirrus clouds on the global scale and associated climate feedbacks are, at present, still poorly understood. Inadequate knowledge of the vertical distribution of cirrus cloud microphysical properties on a global scale limits our ability to determine either the sign or the magnitude of their net radiative impact (Stephens and Webster (1981); Stephens et al. (1990)). As a result, significant uncertainties remain as to the net response and resulting feedback of cirrus clouds to global warming due to increasing CO_2 concentrations in the atmosphere (Sassen (2002)) and the role of cirrus clouds in the ocean-water vapor-convection feedback system (Pierrehumbert (1995); Lindzen et al. (2001); Fu et al. (2002)). Furthermore, the role of cirrus in dehydrating the lower stratosphere and the resulting effects on stratospheric chemistry are as yet undetermined. General circulation models (GCMs) may provide an invaluable tool for furthering our understanding of these and other processes in the cloud-radiation-climate system. Such models are involve highly parameterized approximations to real-world physical processes and require accurate global observations of cirrus cloud microphysical properties to constrain and validate their results.

Measuring the global distribution of cirrus cloud microphysical and optical properties has been a goal of numerous satellite missions such as the Television and Infrared Observations Satellite (TIROS) series, the Geostationary Operational Environmental Satellite (GOES) satellites, and the International Satellite Cloud Climatology Project (ISCCP) and continues to be a focal point for future endeavors including CloudSat and

Cloud-Aerosol Lidar and Infrared Pathfinder Satellite Observations (CALIPSO) projects recently funded under the National Aeronautics and Space Administration (NASA) Earth System Science Pathfinder Project (ESSP). To make use of the resulting data, a suite of algorithms[1] to infer a wide range of cirrus cloud properties has been developed to operate in concert with each of these satellites and, through major advancements in both instrumentation and remote sensing techniques, continuous progress has been made toward realizing the goal of globally mapping cirrus clouds. Both the NASA Cloud and Earth Radiant Energy (CERES) and the Moderate Resolution Imaging Spectrometer (MODIS) programs have developed and/or exploited these multi-spectral techniques to produce global distributions of cirrus properties and to investigate their effects on the Earth's climate (King et al. (1992); Wielicki et al. (1996)). In the spirit of these efforts, this paper presents an advanced version complete with error analysis of the algorithm commonly referred to as the split-window technique. It is not our intention to replace the work of these advanced programs but to demonstrate how the use of explicit cloud boundary information and the proper error characterization of retrieved cloud properties are important in determining uncertainties in related climate studies. Although we choose to focus on the split-window method, the physics underlying the other techniques could easily be incorporated into our algorithm and, in fact, we will show how this technique can be combined with ongoing research at Colorado State University to provide a retrieval of the vertical distribution of cirrus cloud properties with complete error diagnostics for the satellites of the NASA ESSP mission.

The split-window technique relies on differences in radiative properties for cloud particles at two wavelengths in the atmospheric window region of the infrared spectrum to estimate cloud optical depth and effective radius from satellite-observed brightness temperatures (Inoue (1985); Prabhakara et al. (1988)). An inherent short-coming of the original implementations of the approach is that the retrieved parameters are heavily dependent upon an assumed cloud thermodynamic temperature. Traditionally, a lack

[1]The interested reader is referred to Table 1 of Miller et al. (2000) which summarizes a broad cross-section of such algorithms.

of explicit cloud boundary information has resulted in significant biases in retrieved cloud properties (Miller et al. (2000)). Through the use of an optimal estimation based inversion (Rodgers (1976, 1990); Marks and Rodgers (1993)), the algorithm introduced in the present work is capable of incorporating explicit cloud boundary information from complementary sensors such as space-borne lidar or cloud radar providing to constrain cloud thermodynamic temperature in the algorithm.

The optimal estimation approach to inversion and its application to the split-window technique will be introduced in the next section. A new two-layer radiative transfer model for relating cirrus cloud optical depth and effective radius to infrared radiances in an efficient and accurate manner is developed and evaluated in Section 3.4. In Section 3.5.a, the algorithm is evaluated through a series of synthetic retrievals designed to demonstrate the salient features of the approach as well as to characterize uncertainties in retrieved optical depth and effective radius as a function of the accuracy of cloud boundary information employed. In Section 3.5.b the algorithm is applied to infrared radiances from the Visible and Infrared Scanner (VIRS) aboard the Tropical Rainfall Measurement Mission (TRMM) satellite in conjunction with cloud boundaries from the Atmospheric Radiation Measurement (ARM) program's Tropical Western Pacific (TWP) Nauru Island site to evaluate its performance with cloud boundary information of varying accuracy. The implications of these results for climate study are addressed in Section 3.5.c and relevant results and possible extensions of the technique are discussed in Section 3.6.

3. The Optimal Estimation Approach

Ultimately, estimates provided by cloud optical property retrievals are needed to improve our understanding of the mechanisms by which clouds interact with solar and terrestrial radiation to help shape the Earth's climate. Such applications require extensive spatial and temporal coverage, special care to remove any sources of systematic

errors in the retrieval method and rigorous estimates of the uncertainties in all products. Regrettably, this final requirement represents a significant shortcoming in many modern retrieval algorithms.

The approach adopted here is based on the physical principles that underlie the method introduced by (Prabhakara et al. (1988)). At the root of the method is the fact that ice particles on the order of 30 μm or smaller more efficiently absorb radiation at a wavelength of 12 μm than at 10.8 μm. As a result, cirrus clouds composed of small ice particles appear "colder" at 12 μm than at 10.8 μm. When examined at a variety of cirrus optical depths and effective radii, the relationship between $\Delta T_B = T_{B,10.8} - T_{B,12}$ and $T_{B,10.8}$ resembles an arch. The right foot of the arch corresponds to the clear-sky emitting temperature of the Earth while the left foot represents an optically thick cloud where $T_{B,10.8}$ and $T_{B,12}$ each approach the cloud thermodynamic temperature. Intermediate values provide information regarding the optical properties of the cloud. Theoretically derived relationships between ΔT_B and $T_{B,10.8}$ for a number of different cirrus clouds are illustrated in Figure 3.1[2].

Accurate specification of cloud temperature, as well as emitting temperature of the clear-sky, is clearly critical for a good retrieval. For a given ΔT_B and $T_{B,10.8}$ measurement, the split-window technique yields a different effective radius and optical depth for each cloud temperature. It should be noted from Figure 3.1 that the working range of the retrieval is limited to 10.8 μm optical depths up to about 2.0 and effective radii from about 5 to 25 μm, depending on the precise cloud thermodynamic temperature. Uncertainties in the clear-sky emitting temperature also make estimates of optical depths less than about 0.2 dubious.

The fact that the method is rooted in the interaction of cloud particles with infrared radiation, however, means that it can be applied without modification during the daytime and at night and is thus well suited for application to satellite platforms required for near-global observations. In the present study, as opposed to look-up tables that are

[2]These arches and all subsequent analyses are based on a TRMM satellite viewing angle of 45 degrees.

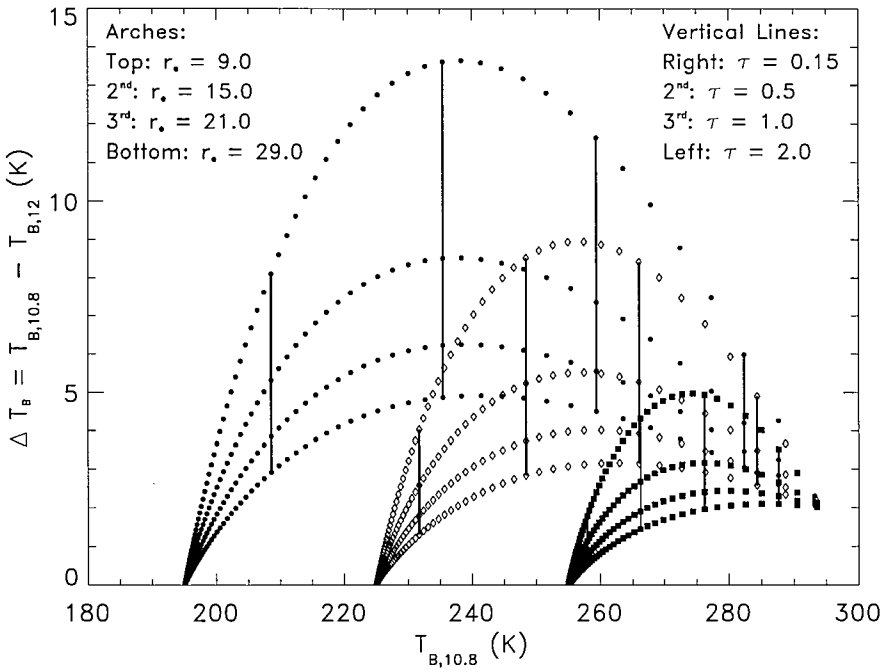

Figure 3.1: Relationship between ΔT_B and $T_{B,10.8}$ for a number of cirrus clouds with 10.8 μm optical depths ranging from 0 to 4 and effective radii ranging from 9 to 29 μm. Clouds with emitting temperatures of 195 K (filled circles), 225 K (open diamonds), and 255 K (filled squares) are modeled.

susceptible to biases introduced by the required assumption of cloud thermodynamic temperature and often lack rigorous uncertainty estimates, we adopt an optimal estimation implementation of the retrieval method (Rodgers (1976, 1990); Marks and Rodgers (1993)). The technique provides a framework for making use of the accuracy in the measurements and physical model to determine the strength of their influence on the retrieval and for propagating these errors through the estimation process to estimate uncertainties in all retrieved parameters. Furthermore, biases introduced by the assumption of a cloud thermodynamic temperature are mitigated by the introduction of cloud temperature as a variable parameter in the retrieval. While these benefits may not be exclusive to the optimal estimation approach, it provides the benefit of an elegant framework that is straightforward to implement and is well-suited to combining information from multiple

sensors provided the added computational cost is not prohibitive.

Recent studies by Engelen and Stephens (1997), Engelen and Stephens (1999), Miller et al. (2000), Austin and Stephens (2001), Stephens et al. (2001b), and L'Ecuyer and Stephens (2002) have applied the optimal estimation technique to retrievals of ozone, water vapor, cloud properties, rainfall, and aerosols from a combination of lidar, radar, and passive measurements at visible, infrared, and microwave wavelengths. Many of the mathematical details of the approach can be found in these references but a short summary is provided here for completeness. Letting $\hat{\mathbf{x}}$ denote the vector of cloud properties to be retrieved, the optimal estimation technique consists of minimizing a combination of the variance between the set of observations, $\mathbf{y}$, and a corresponding set of simulated measurements, $F(\hat{\mathbf{x}})$, and that between $\hat{\mathbf{x}}$ and a suitable *a priori* guess, $\mathbf{x}_a$. Assuming Gaussian statistics[3], this is accomplished by minimizing the scalar cost function,

$$\begin{aligned}\Phi(\hat{\mathbf{x}},\mathbf{y},\mathbf{x}_a) &= (\mathbf{y}-F(\hat{\mathbf{x}}))^T\,\mathbf{S}_y^{-1}\,(\mathbf{y}-F(\hat{\mathbf{x}})) \\ &+ (\hat{\mathbf{x}}-\mathbf{x}_a)^T\,\mathbf{S}_a^{-1}\,(\hat{\mathbf{x}}-\mathbf{x}_a) \qquad (3.1)\end{aligned}$$

with respect to $\mathbf{x}$. F denotes the physical model relating the cloud parameters to the observations called the "forward model", $\mathbf{S}_a$ is the *a priori* error covariance matrix, and $\mathbf{S}_y$ is the measurement error covariance matrix consisting of a combination of observation and the forward model uncertainties.

The values of $\hat{\mathbf{x}}$ for which Eqn. (3.1) is minimum can be found by Newtonian iteration via

$$\hat{\mathbf{x}}^{i+1}-\hat{\mathbf{x}}^{i}=\mathbf{S}_x\left[\mathbf{K}_i^T\mathbf{S}_y^{-1}\left(\mathbf{y}-\mathrm{F}(\hat{\mathbf{x}}^i)\right)+\mathbf{S}_a^{-1}\left(\mathbf{x}_a-\hat{\mathbf{x}}^i\right)\right] \qquad (3.2)$$

[3]In principle any non-Gaussian statistics could be invoked (this would change the details of the solution as described in the text). Rodgers (2000), however, notes that according to the Principle of Maximum Entropy, the Gaussian distribution is the most appropriate if only a mean and variance is known. Alternative distributions, unless known and rigorously justifiable, add spurious information to the retrieval and biases estimation of the most probable solution.

where

$$\mathbf{S}_x = \left(\mathbf{S}_a^{-1} + \mathbf{K}_i^T \mathbf{S}_y^{-1} \mathbf{K}_i\right)^{-1} \tag{3.3}$$

is the error covariance matrix of the estimated parameters accounting for uncertainties in the forward model, measurements, and *a priori* data. The Kernel or weighting function matrix, $\mathbf{K}$, is the Jacobian of the forward model with respect to the retrieval vector, with elements given by

$$K_{jk} = \frac{\partial F_j}{\partial x_k} \tag{3.4}$$

The iteration proceeds until such time as the covariance-weighted mean difference between successive estimates is much less than the number of independent variables in the retrieval vector, i.e.

$$\left(\hat{\mathbf{x}}^{i+1} - \hat{\mathbf{x}}^i\right) \mathbf{S}_y^{-1} \left(\hat{\mathbf{x}}^{i+1} - \hat{\mathbf{x}}^i\right) << N_x \tag{3.5}$$

Among the advantages of this approach is the fact that it allows the algorithm developer complete flexibility regarding the choice of retrieval parameters and observations. In principle any set of measurements can be used to retrieve any set of parameters provided one can define a forward model to suitably represent the relationship between them and assign uncertainties to this model and the observations themselves. Making use of this flexibility, we adopt a retrieval consisting of not only effective radius, r_e, and optical depth, τ, but which also includes cloud thermodynamic temperature, T_c, as an adjustable retrieval parameter. At the same time we add an estimate of cloud thermodynamic temperature to the measurement vector, in part to avoid defining a grossly under constrained problem but also to provide a framework for including direct estimates of T_c from complementary sensors. At first, it may seem strange to include T_c as both an observation and a retrieval parameter but it merely affords us the luxury of using T_c as a soft constraint on the retrieval. Ultimately the strength of this constraint is determined by the accuracy to which cloud temperature can be determined, σ_{T_c}. By including T_c in both the observation and retrieval vectors, its role smoothly varies from a purely retrieved result when σ_{T_c} is large to a pure observation that constrains the retrieval when

σ_{T_c} is small. At intermediate accuracies, T_c constrains the retrieval to search for solutions along arches corresponding to the observed cloud thermodynamic temperature but can be modified within its error bounds in cases where the combination of $T_{B,10.8}$, T_c, and ΔT_B are unphysical (eg. if ΔT_B is large but $T_{B,10.8} \sim T_c$, the T_c estimate must be too high). It will be shown that this approach leads to a significantly greater overall consistency between retrieval products and observations particularly in cases where at most a rough estimate of T_c is available.

4. The Forward Model

Application of Eqn. (3) requires a physical model for mapping $\mathbf{x} = (\tau, r_e, T_c)$ into the observation space defined by $\mathbf{y} = (T_{B,10.8}, \Delta T_B, T_c)$ and a rigorous assessment of its uncertainty.

a. Radiative Transfer Model

A two-layer radiative transfer model has been developed to simulate the 10.8 and 12.0 μm radiances as observed by a satellite as a function of cloud optical depth, effective radius, and cloud temperature. The model consists of an isothermal cirrus cloud overlying an emitting clear-sky layer and assumes that scattering is negligible at infrared wavelengths[4]. Under these assumptions, the observed radiance at the top of the atmosphere is the sum of clear-sky emission transmitted through the cirrus cloud plus emission by the cloud itself,

$$I_{obs} = I_{cs} e^{-\tau/\mu} + B(T_c)\left[1 - e^{-\tau/\mu}\right] \tag{3.6}$$

[4]This assumption requires some justification. Ice particles of radii 10-50 μm which may be found in cirrus clouds scatter approximately as much IR radiation as they absorb. When an ensemble of these particles are modeled in a typical cirrus cloud, however, Stephens (1980) showed that they lead to a total IR reflectance of only about 5 % or 10 Wm^{-1}. While this may be significant in some applications, errors introduced by the simple radiative transfer model will be far greater in the present study.

where τ is cloud optical depth, μ is the cosine of the solar zenith angle, and $B(T_c)$ is the Planck blackbody function for cloud temperature T_c.

The size and shape of the constituent cloud particles enters the model through their influence on optical depth. For a monodispersed distribution of spherical particles of radius r, the optical depth at a wavelength, λ, is

$$\tau_\lambda = \pi N_0 r^2 Q_{abs,\lambda} \Delta z \tag{3.7}$$

where N_0 is the number of particles per unit volume, $Q_{abs,\lambda}$ is the absorption efficiency, and Δz is the geometric thickness of the cloud. The ratio of the optical depths at 10.8 and 12.0 μm is simply the ratio of the absorption efficiencies at the two wavelengths, which are estimated using an anomalous diffraction theory approximation developed by Flatau (1992) for spherical particles,

$$Q_{abs} \approx 2\left[\frac{1}{2} + \frac{e^{-4\chi\kappa}}{4\chi\kappa} + \frac{e^{-4\chi\kappa}-1}{(4\chi\kappa)^2}\right] \tag{3.8}$$

κ is the imaginary part of the refractive index and $\chi = 2\pi r/\lambda$ is the size parameter. The accuracy of the ADT approximation relative to explicit Mie calculations for spherical particles is assessed in Flatau (1992) and leads to errors of less than 5

$$\frac{\tau_{12.0}}{\tau_{10.8}} = \frac{\int \pi Q_{abs,12.0}(r) r^2 n(r) dr}{\int \pi Q_{abs,10.8}(r) r^2 n(r) dr} \tag{3.9}$$

For the retrieval, a modified gamma distribution of spherical particles with variance equal to 2.0 is used (Dowling and Radke (1990)). Hereafter this distribution will be referred to as the model distribution for simplicity. The impact of these assumptions will be examined in detail in the following section to estimate an appropriate forward model error covariance matrix for use in the retrieval. It should be noted that, while Eqns. (3.8) and (3.9) hold only for spherical particles, the ratio of the optical depths for non-spherical particles can be estimated through more advanced methods, such as the finite-

difference time-domain method (FDTD) (Yang et al. (2001)) facilitating modifications to particle shape if necessary.

b. Model Calibration

Eqns. (3.6)-(3.9) constitute a simple, complete model governing the transmission of radiation through a cirrus cloud from which 10.8 and 12.0 μm brightness temperatures can be evaluated for any combination of cloud particle size distribution, optical depth, and cloud temperature. When compared to a more sophisticated radiative transfer model developed by Deeter and Evans (1998) (hereafter referred to as the DE model), differences emerge. Analysis of model differences for a variety of cases spanning the range of optical depths and effective radii over which the retrieval is to be applied suggest that they are functions of cloud temperature, optical depth, and effective radius. Since for certain cloud property combinations $T_{B,10.8}$ differences between models can be nearly 5 K, a correction was developed to improve agreement between the present and DE models to remove systematic biases from our results. Details regarding the correction can be found in Appendix A. With the correction, the simple two-layer model can be employed as opposed to the DE model with minimal loss of accuracy affording an increase in computation speed of approximately a factor of a hundred. This increase in speed is particularly important in the optimal estimation framework. Typically, five iterations are required to reach convergence at any pixel, with each iteration invoking seven executions of the forward model. Thus, the forward model is called an average of thirty-five times per pixel. The corrected model yields an accurate and computationally efficient solution that is, therefore, essential for processing the large amounts of satellite data required for global applications of the retrieval.

c. Error Covariance Matrices

Proper estimation of error covariance matrices is critical to the success of any optimal estimation retrieval. In the absence of additional information, the *a priori* guess is limited to a rough estimate of the climatological mean effective radius, optical depth, and emitting temperature of typical cirrus clouds. To account for the lack of quantitative information in the *a priori* guess, its covariance matrix is assigned to represent the full range of the cirrus properties for which the retrieval is applicable and is therefore reasonably well specified. Calibration errors in VIRS satellite measurements of brightness temperatures will be assumed to range from 1K for a cirrus cloud emitting at 220K to 1.5K for cloud emitting at 275K (Lyu et al. (2000)).

Determining forward model errors is the most challenging task and is the primary focus of this section. Since the cloud temperature error in the model is variable by design, we only need determine the error in I_{cs}, $T_{B,10.8}$ and ΔT_B associated with the forward model. The effects of I_{cs} on retrieved parameters are significantly smaller than those effects of cloud temperature, so I_{cs} is simply treated as a constant derived from the DE model employing a McClatchey Tropical Atmosphere (McClatchey et al. (1972). For an operational retrieval, however, a rigorous pixel by pixel estimation of clear-sky emitting temperature with error estimates should be made for accuracy.

Based on the discussion above, the forward model determines the theoretical $T_{B,10.8}$ and ΔT_B observed by a satellite for a given effective radius, optical depth, and cloud temperature. The model, however, is based on a set of assumptions that, if changed, can yield substantially different results. The most prominent of these assumptions is the choice of the 'model distribution'- a modified gamma cloud particle distribution of ice spheres with variance equal to two. If the cloud particle size distribution or particle habit are changed, then the absorption characteristics at both 10.8 and 12.0 μm change, leading to a new $T_{B,10.8}$ and ΔT_B. To estimate the expected error in model results associated with choice of distribution and habit, a variety of cloud particle size distributions each with the same effective radius for both ice spheres and hexagonal columns have

been substituted into the model and the resulting $T_{B,10.8}$ and ΔT_B compared over a wide range of optical depths and effective radii.

Five different modified gamma and four different lognormal cloud particle size distributions for both ice spheres and hexagonal columns were used. The modified gamma distribution is of the form

$$n(D) = N_t \frac{1}{\Gamma(\nu)} \left(\frac{D}{D_n}\right)^{\nu-1} \frac{1}{D_n} e^{-D/D_n} \tag{3.10}$$

where $n(D)$ is the number of ice crystals of size D, N_t is the number concentration, D_n is the characteristic diameter, and ν is the distribution variance (Stephens (1994)). The lognormal distribution is of the form

$$n(D) = \frac{1}{D \ln\sigma_g (2\pi)^{0.5}} \exp\left[\frac{(\ln D - \ln D_g)^2}{2(\ln\sigma_g)^2}\right] \tag{3.11}$$

where D_g is the geometric mean diameter and σ_g is the geometric standard deviation (Reist, 1993). Figure 3.2 shows each of the distributions generated using Eqns. (4.1) and (4.2) for an effective radius of 20 μm, where effective radius is defined as

$$r_e = \frac{\int_a^b n(r) r^3 dr}{\int_a^b n(r) r^2 dr} \tag{3.12}$$

where a and b are chosen such that the integrals converge.

For spherical particles, the ADT approximation in Eqn. (3.8) was used to determine the ratio of optical depths at 10.8 and 12.0 μm for the distribution. Differences in this ratio of optical depths between the test distributions and the model distribution determines the error in the ΔT_B value while the difference in the total optical depth between the two distributions determines the error in $T_{B,10.8}$. For hexagonal crystals, explicit calculations of the absorption efficiencies at 10.8 and 12.0 μm as a function of crystal size from (Yang et al. (2001)) are used. Due to current limitations in the understanding of absorption characteristics of other crystal habits at infrared wavelengths, estimation of

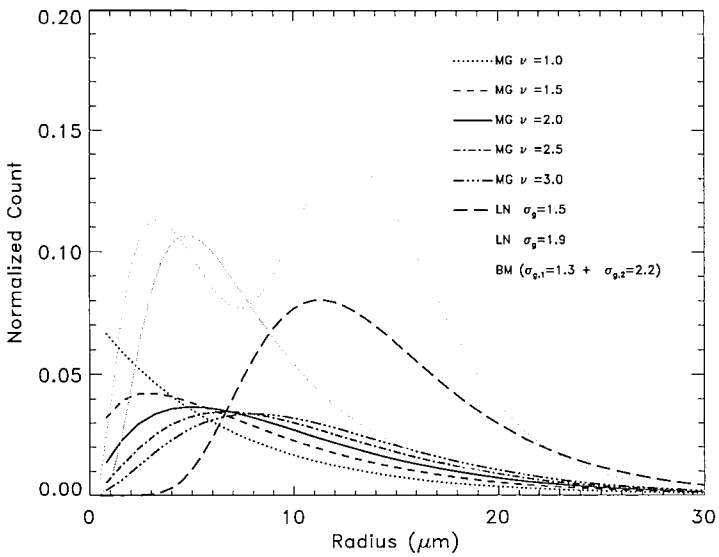

Figure 3.2: Size distributions used in estimating forward model error covariance matrices. Modified gamma distributions are designated MG, lognormal distributions LN, and the bi-modal distribution, which is simply the addition of 2 lognormal distributions, BM. The effective radius of each distribution is 20 μm.

model error incurred as a result of particle shape is limited to these hexagonal crystals. To facilitate comparisons between spherical and hexagonal crystals, all particles are represented as equivalent spherical distribution in which both the area and volume of the distribution is conserved (Francis et al. (1994); Mitchell and Arnott (1994); Grenfell and Warren (1999); Yang et al. (2001)).

Theoretical relationships between ΔT_B and $T_{B,10.8}$ (hereafter referred to as 'arch curves') generated for the cloud particle distributions of Figure 3.2 for both ice spheres and hexagonal crystals at a cloud temperature of 220 K are shown in Figure 3.3. The top set of curves show the variability associated with different spherical distributions while the bottom set corresponds to hexagon column distributions. Clearly, the variance between the two crystal habits exceeds the variance between size distributions with the same habit, consistent with the results of (Stephens et al. (1990)). Thus, we conclude that the variance between crystal habits dominates the measurement and forward model covariance matrix. Unfortunately, this variance is difficult to assess exactly given the

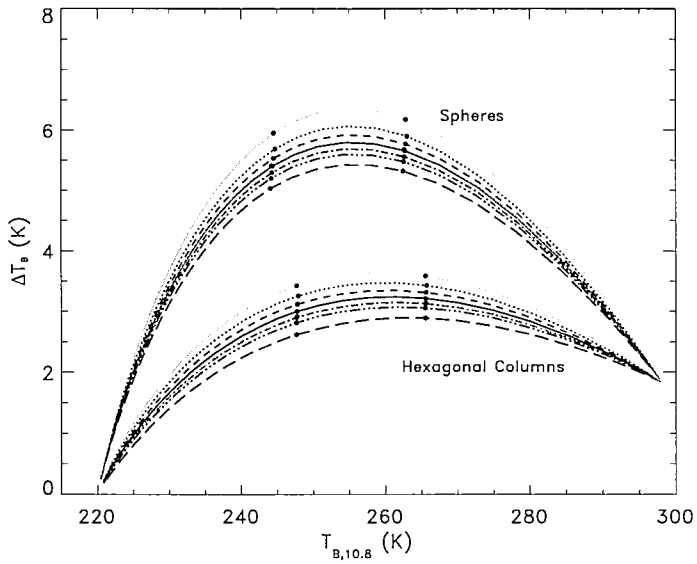

Figure 3.3: ΔT_B-$T_{B,10.8}$ relationships for a set of 220 K ice clouds. The upper set of curves correspond to each of the distributions in Figure 3.2 assuming spherical particles while the lower set corresponds to an equivalent set of distributions of hexagonal columns. The set of closed circles on the right correspond to a model distribution optical depth of 0.5 at 10.8 μm, while those on the left to an optical depth of 1.0 at 10.8 μm .

lack of absorption data for other crystal habits (eg. plates, rosettes, aggregates, etc.) and the generally complex mix of ice crystals observed in real clouds. Given that polycrystals scatter and absorb more like spheres, it is reasonable to assume that the difference between hexagonal columns and spherical crystals represents a pessimistic estimate of habit error. Thus, we might assume that an order of magnitude estimate of forward model uncertainties based on Figure 3.3 are representative of the maximum one would encounter using all possible habits. This assumption is supported by (Parol et al. (1991)) who calculated the ratio of optical depths at 10.8 and 12.0 μm for infinite cylinders and obtained similar results.

For the case illustrated in Figure 3.3, the difference in $T_{B,10.8}$ between the model distribution and hexagonal crystals is about 3 K when averaged over the working range of the optical depth retrieval at 10.8 μm. The average difference in ΔT_B between the model distribution and hexagonal crystals is about 2 K over the same range. The errors

depend weakly on both effective radius and cloud thermodynamic temperature since the magnitudes of both ΔT_B and $T_{B,10.8}$ depend on the choice of r_e and T_c. Smaller effective radii tend to yield a larger difference in ΔT_B but a smaller difference in $T_{B,10.8}$ between habits. Furthermore, the colder the cloud, the greater the absolute error in ΔT_B. As a result, the case shown, corresponding to a cold cloud at 220 K with an effective radius of 20 μm, is representative of conditions under which the errors are larger than average. Based on this argument and the estimates of VIRS calibration error, standard deviations of 1.5 and 2.5 K for ΔT_B and $T_{B,10.8}$, respectively, are used for the diagonal elements of the measurement covariance matrix in the retrieval. In an operational retrieval, these values should be determined as a function of cloud thermodynamic temperature and effective radius for a more rigorous result. For completeness,several different choices of ΔT_B and $T_{B,10.8}$ error are used in the synthetic retrievals that follow to illustrate how the retrieval is affected by the forward model accuracy.

As ΔT_B and $T_{B,10.8}$ are clearly correlated, it is also important to include some estimate of the off-diagonal elements of the measurement error covariance matrix. Taking the average difference between the model distribution and each of the test distributions described above for each of the variables, the covariance between ΔT_B and $T_{B,10.8}$ was found to be -3.5 when normalized by the appropriate standard deviations. Again, differences in habit dominate the magnitude and sign of the covariance. The correlation is negative since a decrease in ΔT_B relative to the model distribution is generally accompanied by a corresponding increase in $T_{B,10.8}$. Physically, this is a manifestation of the fact that hexagonal crystals have smaller absorption cross-sections at both 10.8 and 12 μm than equivalent volume to area spheres, reducing the ice cloud signal in both $T_{B,10.8}$ and ΔT_B. Thus more radiation from below the cloud emerges at TOA leading to an increase in $T_{B,10.8}$ and $T_{B,12}$ and a decrease in the difference between them.

It should be noted that there exist a number of additional sources of uncertainty that have not been addressed here, such as errors due to the cloud three-dimensional structure and sub-pixel variability. Evaluation of the impact of these error sources requires a more

rigorous treatment and are topics of ongoing research.

5. Algorithm Evaluation

The performance of the algorithm has been tested using a combination of synthetic retrievals and real-world retrievals making use of cloud boundary measurements from the Atmospheric Radiation Measurement (ARM) program's Tropical Western Pacific (TWP) site at Nauru Island. While synthetic retrievals may be somewhat biased by the fact that similar assumptions are often made in both forward and inverse calculations, they provide an invaluable tool for testing the behavior of the algorithm under controlled conditions. These studies must, however, be complemented with applications involving real observations. Selected results from both types of studies will be discussed below.

a. Synthetic Retrievals

A set of effective radii, optical depths, and cloud thermodynamic temperatures representative of typical cirrus clouds were applied in the two-layer model to produce synthetic 'observations' with which to test the algorithm. Random errors were simulated by adding Gaussian noise directly proportional to the standard deviation used in the measurement error covariance matrix to each of the synthesized $T_{B,10.8}$, ΔT_B, and cloud temperature measurements. This perturbed measurement vector was then run through the optimal estimation retrieval to assess the quality of the retrieved optical depth and effective radius. Each measurement vector was randomly perturbed five thousand times to produce a statistically significant distribution of errors about the measurements.

Figures 3.4 and 3.5 show the percentage error in retrieved optical depth and effective radius, respectively, for a cloud with a 10.8 μm optical depth of 0.8, an effective radius of 14 μm, and an emitting temperature of 225 K. Retrieval error is defined as the standard deviation of the retrievals divided by the expected mean expressed as a percent, $\sigma_i = \sqrt{(\mathbf{S_x})_{ii}} \,/\, x_{truth} * 100$, and is plotted as a function of error in the cloud

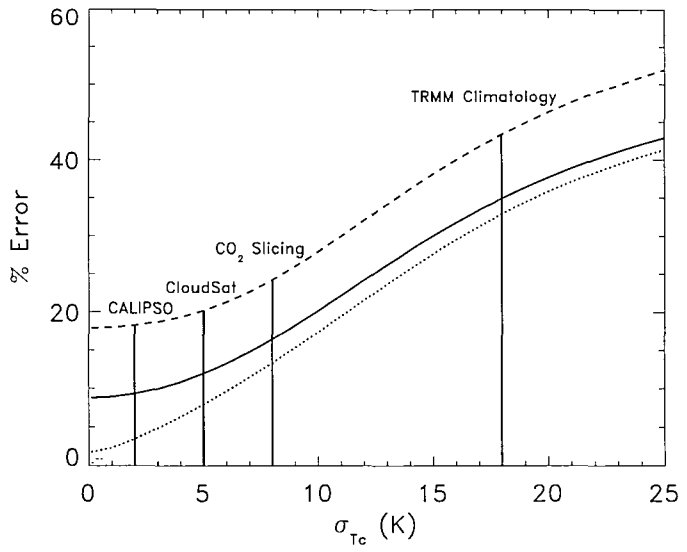

Figure 3.4: Error statistics for synthetic retrievals of 10.8 μm optical depth for different covariance matrix assumptions. The dotted line corresponds to a $\sigma_{\Delta T_B}$ of 0.5 K and a $\sigma_{T_{B,10.8}}$ of 0.5 K; the solid line to 1.5 K and 2.5K; and the dashed line to 3.0 K and 5.0 K. The vertical lines represent the estimated error in cloud thermodynamic temperature determined using a variety of techniques. Results are for an optical depth of 0.8, an effective radius of 14 μm, and cloud thermodynamic temperature of 225 K.

temperature measurement for three sets of $T_{B,10.8}$ and ΔT_B error assumptions. These figures illustrate retrieval performance for a given measurement with inherent random error. Gaussian statistics dictate that 68 percent of the randomly perturbed retrievals fall within one standard deviation from the retrieved mean. Clearly the lower the error in T_c estimate, the higher the probability of retrieving a value close to the truth. For fixed error in T_c, better estimates of $T_{B,10.8}$ and ΔT_B also yield better retrieval results. Note that the shapes of the curves, however, are different for the optical depth and effective radius cases. The optical depth retrievals show much greater sensitivity to T_c measurement error than effective radius. Furthermore, effective radii exhibit substantially larger relative errors than optical depths.

Also plotted on the figures are vertical lines corresponding to estimated accuracies in different techniques for determining T_c. Active systems such as, lidar and radar, for example, can be used to determine cloud boundaries that can, in turn, be related to cloud

temperature through the assumption of an atmospheric temperature profile. Uncertainties in these cases arise from a combination of the vertical resolution of the instrument and deviations from the vertical temperature profile. Uncertainties in lidar- and radar-based estimates of T_c are estimated to be 2 K and 5 K based on an expected accuracy of 2 K in atmospheric temperature profiles from numerical weather prediction models (Eyre et al. (1993)) and assuming vertical resolutions of 30 and 500 m characteristic of the CALIPSO lidar and the CloudSat cloud profiling radar (CPR)[5].

Passive techniques such as CO_2 slicing can also be used to estimate cloud-top pressure which can then be related to cloud temperature, again through assumption of a temperature profile. Based on the work of Menzel et al. (1992) and Baum and Wielicki (1994), a CO_2 slicing-derived cloud top pressure of 300 mb has a maximum random error of 50 mb. This translates to an error in cloud thermodynamic temperature of 8K.

One alternative to explicitly measuring cloud boundary information is to resort to a reasonable climatological mean value. In the present study a climatology of cloud thermodynamic temperature is made by matching infrared radiances and precipitation information from the TRMM satellite. As discussed in the next section, uncertainties in the resulting 'TRMM climatologies' are estimated to be about 18K.

Figures 3.4 and 3.5 show only statistics for those retrievals that converged to physically realistic values of effective radius, optical depth, and cloud thermodynamic temperature for all three pairs of $\sigma_{\Delta T_B}$ and $\sigma T_{B,10.8}$. Table 3.1 lists the number of convergent cases out of the 5000 perturbations for each combination of measurement error. Since cases with large error are more likely to be non-convergent, Figures 3.4 and 3.5 underestimate retrieval errors at high σ_{T_c} since the worst retrievals are all thrown out and not used in the statistics. To get a complete picture, the results from the number of non-convergent pixels must be considered together with the results in Figures 3.4 and 3.5 as it is just as undesirable to have a non-convergent retrieval as one with large uncertainty. It should also be noted that the standard deviations are not symmetric about truth, as the

[5]See CloudSat and CALIPSO web-pages for documentation of vertical resolutions, www.cloudsat.atmos.colostate.edu and www.-calipso.larc.nasa.gov/instrument.html

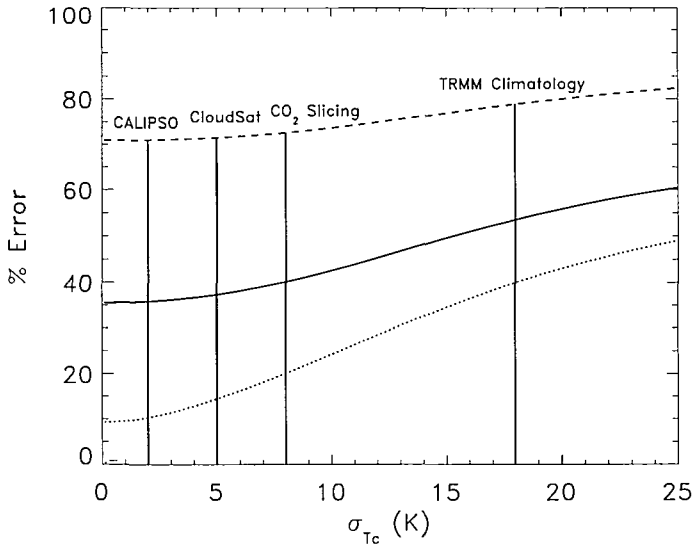

Figure 3.5: As in Figure 3.4 but for retrievals of effective radius.

retrieved mean does not always converge to the expected mean. Large error covariance matrices, for example, result in a bias in the retrieval since it becomes more influenced by the assumed *a priori* guess.

Table 3.1 also lists the mean effective radius, optical depth, and diagonal elements of the averaging kernel for all convergent retrievals. The averaging kernel can be loosely interpreted as the relative contribution of the measurements to the *a priori* guess in the retrieval (Rodgers (1990)). Values near unity are desirable as they indicate a heavy weighting of the measurements while values near zero characterize a retrieval which derives primarily from the *a priori* guess in which we have no confidence. Clearly, errors in retrieved optical depth and effective radius increase as σ_{T_c}, $\sigma_{T_{B,10.8}}$, and $\sigma_{\Delta T_B}$ increase. These qualitative trends are to be expected and reflect the mapping of measurement error into the cloud property parameter space. An advantage of the optimal estimation approach, however, is that retrieval error can be quantified. From Table 3.1, retrieved optical depth is more accurate than retrieved effective radius for a given measurement error covariance. For example, assuming errors of 1.5 K in $T_{B,10.8}$, 2.5 K in ΔT_B, and 2 K in T_c, retrieved optical depths are accurate to approximately 10 %, whereas uncertain-

$(\sigma_{\Delta T_B}, \sigma_{T_{B,10.8}})$	σ_{T_c}	Number	τ	r_e (μm)	A_τ	A_{r_e}
(0.5,0.5)	2.0	4944	0.80	14.24	1.00	0.99
	5.0	4953	0.81	14.16	1.00	0.99
	10.0	4931	0.83	13.91	1.00	0.94
	18.0	4877	0.85	13.50	0.99	0.92
	25.0	4833	0.87	13.25	0.99	0.88
(1.5,2.5)	2.0	4948	0.80	15.54	1.00	0.94
	5.0	4912	0.81	15.45	1.00	0.93
	10.0	4877	0.83	15.16	1.00	0.93
	18.0	4854	0.86	14.66	0.99	0.86
	25.0	4803	0.87	14.36	0.99	0.82
(3.0,5.0)	2.0	4875	0.81	16.51	1.00	0.75
	5.0	4867	0.82	16.42	1.00	0.75
	10.0	4860	0.84	16.10	0.99	0.73
	18.0	4788	0.87	15.56	0.99	0.70
	25.0	4731	0.92	15.24	0.98	0.67

Table 3.1: Optical depth and effective radius from selected synthetic retrievals. In all cases synthetic measurements assuming an optical depth of 0.8, an effective radius of 14 μm, and a cloud emitting temperature of 225 K were used. *A priori* initial guesses of $\tau = 1.5$, $r_e = 20\mu$m, and $T_c = 235K$ were used in all cases. All standard deviations, denoted σ, are in Kelvin. Number indicates the number of convergent retrievals out of the 5000 random perturbations of the measurement vector for the given error combinations.

	Case 1	Case 2	Case 3	Case 4	Case 5	Case 6	Case 7	Case 8
τ	0.8	1.8	0.8	1.8	0.8	1.8	0.8	1.8
r_e (μm)	14	14	14	14	22	22	22	22
T_c (K)	225	225	245	245	225	225	245	245

Table 3.2: Description of each of the eight synthetic retrieval cases.

ties in retrieved effective radius are, on average, 35 %. This result is explained by more careful examination of the physics underlying the retrieval. Optical depth is determined primarily by the $T_{B,10.8}$ measurement, whereas effective radius is heavily dependent on ΔT_B. An error of a few Kelvin in a $T_{B,10.8}$ measurement of 250 K amounts to an uncertainty of $\sim$1 % while a similar error in a ΔT_B measurement of 6 K corresponds to $\sim$50 % uncertainty. The result is substantially less inherent error in the optical depth estimate. These considerations also explain the fact that, while retrieved optical depths are very sensitive to the accuracy of the cloud thermodynamic temperature measurement regardless of the error in $T_{B,10.8}$ and ΔT_B, retrieved effective radii are not. Since uncertainties in optical depth due to errors in $T_{B,10.8}$ and ΔT_B are small, its accuracy is dictated by the error in T_c. As a result, optical depth estimates improve significantly for all curves as σ_{T_c} is reduced. Retrieved effective radii, however, are much more strongly dependent upon the error in $T_{B,10.8}$ and ΔT_B. If these errors are too large, the retrieval improves little regardless of the accuracy in cloud thermodynamic temperature.

It should be noted that, while the numerical values quoted in Table 3.1 apply only to the specific combination of optical depth, effective radius, and cloud temperature considered, results for other sets of cloud properties are qualitatively similar. To illustrate this, synthetic retrievals were also performed for the eight combinations of optical depth, effective radius, and cloud temperature summarized in Table 3.2.

In each case $\sigma_{\Delta T_B}$ and $\sigma_{T_{B,10.8}}$ were assumed to be 1.5 K and 2.5 K, respectively,

	σ_{T_c} (K)	Case 1	2	3	4	5	6	7	8	Avg.
	2.0	0.4	0.6	0.4	1.0	0.6	1.5	1.1	3.3	1.1
Bias	5.0	1.2	0.9	0.8	2.1	1.9	3.7	2.6	1.6	1.9
Error	10.0	3.7	1.7	1.4	6.6	6.0	6.1	6.0	1.2	4.1
	18.0	7.3	2.4	1.0	10.1	12.6	8.1	7.7	2.9	6.5
	2.0	9.3	14.2	13.3	25.1	9.3	15.1	13.5	27.0	15.8
Random	5.0	12.0	21.6	18.8	34.3	12.2	25.0	19.7	37.7	22.6
Error	10.0	20.4	29.7	32.5	40.6	21.9	35.5	36.9	45.1	32.8
	18.0	35.4	35.2	45.0	43.8	39.2	42.0	53.6	49.2	42.9

Table 3.3: Bias and random error in retrieved optical depth from each of the synthetic retrieval cases summarized in Table 3.2. Bias error indicates the percentage difference between the mean retrieved optical depth and the true optical depth. Random error is defined as the standard deviation divided by the mean of the retrieved optical depth for all convergent pixels, expressed as a percent.

consistent with the accuracy of the corrected two-layer model and under the assumption of spherical particles which obey a modified gamma distribution. Results for optical depth and effective radius are summarized in Tables 3.3 and 3.4, respectively.

General trends in each of these synthetic cases agree with those described above, but the precise magnitude of retrieval errors is case dependent. Again, a physical understanding of the retrieval suggests that some combinations of measurements will have larger errors than others. Consider again the theoretical arches presented in Figure 3.1. Errors are large in cases where small changes in ΔT_B or $T_{B,10.8}$ result in large changes in retrieved properties. For example, at a cloud thermodynamic temperature of 255 K, very small differences in ΔT_B separate effective radii of 15 μm and 25 μm. In that case, small errors in the measurement vector will lead to very large errors in the retrieved ef-

	σ_{T_c} (K)	Case 1	2	3	4	5	6	7	8	Avg.
	2.0	8.6	19.9	12.5	18.2	2.0	3.3	2.9	13.7	10.1
Bias	5.0	7.9	22.5	12.6	27.1	0.8	5.0	3.6	9.8	11.1
Error	10.0	5.6	26.5	13.4	38.8	2.5	7.0	4.8	4.7	12.9
	18.0	2.0	29.0	17.8	47.8	7.9	9.3	4.5	1.8	15.0
	2.0	34.9	72.1	52.6	95.1	40.6	56.8	48.6	66.3	58.4
Random	5.0	36.5	83.3	55.0	103	41.3	63.0	49.8	70.7	62.8
Error	10.0	41.8	99.0	62.6	112	43.9	71.5	53.9	75.7	70.0
	18.0	53.0	112	72.8	120	49.9	78.0	59.8	79.8	78.1

Table 3.4: As in Table 3.3 but for retrieved effective radius.

fective radius. Similarly, errors are small when the measurement vector is located such that random error in the measurements does not change the retrieved parameters. In other words, retrieval uncertainties reflect the sensitivity of the retrieved parameters to the observations being used to retrieve them. As with most retrievals, the best results are obtained when the forward model is very sensitive to the retrieval parameters.

b. Nauru Retrievals

Although synthetic retrievals provide useful information on algorithm performance, their validity rests entirely on the assumptions used in the numerical experiments. Physical measurements provide a much more rigorous and realistic means to examine algorithm performance. In this sub-section, infrared radiances from the VIRS instrument aboard TRMM are combined with cloud boundary information from the ARM Nauru field site to determine both advantages and disadvantages of the algorithm when applied in real-world situations.

The technique has been applied to all TRMM overpasses of Nauru Island (0.5 °S and 166.9 °E) from July through December, 1999 yielding 23 thin cirrus cases. Figure 3.6 shows the $T_{B,10.8}$, ΔT_B, and precipitation fields for one such case which took place on the morning of July 11, 1999. Nauru is located in the center of each field just north of the central cold $T_{B,10.8}$ band. The $T_{B,10.8}$ and ΔT_B values of 269 K and 5.5 K, respectively, suggest the presence of cirrus clouds likely forming from the detrainment of ice from the convective cells, visible in the corresponding precipitation field. Figure 3.7 shows the retrieved optical depth, effective radius, and cloud temperature for this case using a climatological estimate of cloud thermodynamic temperature determined by matching VIRS 10.8 μm brightness temperatures to the TRMM precipitation product 2A12 (Kummerow and Giglio (1994)). Assuming that cirrus clouds were formed from outflow near the top of tropical convective cells, a mean and standard deviation of T_c as a function of latitude are calculated by averaging $T_{B,10.8}$ values in regions where precipitation rate was greater than 5 mm h^{-1} and $T_{B,10.8}$ was sufficiently low to indicate

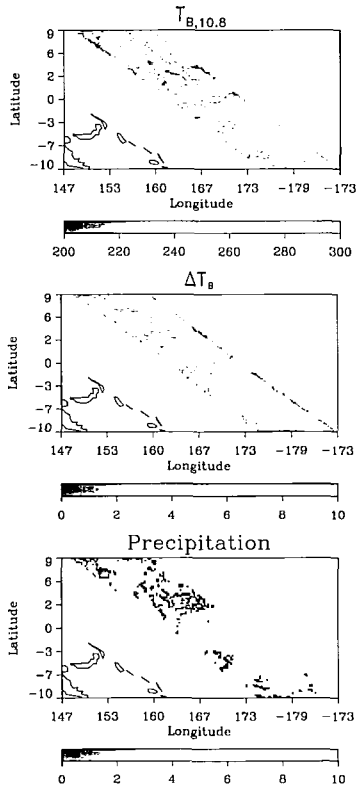

Figure 3.6: $T_{B,10.8}$ (in K), ΔT_B (in K), and precipitation fields (in mm h^{-1}) for a TRMM overpass of Nauru island on July 11, 1999. Nauru is located in the center of each field at 0.5 °S and 166.9 °E.

the presence of convection. The resulting cirrus cloud thermodynamic temperature for Nauru in the month of July is 218 $\pm$18 K. Figure 3.7 shows regions of thin cirrus clouds surround areas of convection, often exhibiting a smooth gradient with large values near convection tapering off to near zero further away. Retrieved effective radii are small, agreeing with the notion of large crystals settling out during detrainment (Prabhakara et al. (1988)). Another interesting feature in these results is the fact that although the error in the climatological estimate of T_c is quite large and despite the uniform initial guess employed over the entire orbit swath, the cloud temperature field exhibits fine-scale structure. This is due to the use of T_c as a dynamic variable in the algorithm which allows the cloud thermodynamic temperature estimate to adjust through the heavy influence of the $T_{B,10.8}$ measurements in the Kernel matrix, $\mathbf{K}$.

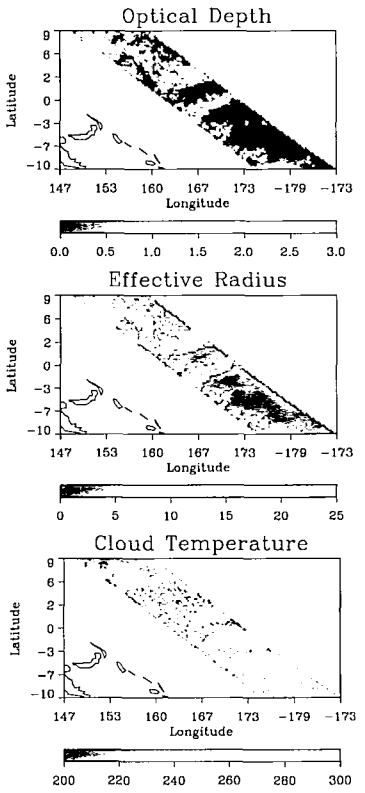

Figure 3.7: Retrieved optical depth, effective radius (in μm), and cloud thermodynamic temperature (in K) using TRMM climatology estimate of cloud temperature for the TRMM orbit in Figure 3.6. Gray pixels represent areas of optically thick, precipitating cloud.

While the potential for global observations afforded by satellites is clear, the lack of explicit cloud boundary information in the TRMM observations alone restricts the remainder of this study to the 23 cirrus clouds found directly over Nauru Island while we await the launch of future satellite missions. For each case cloud boundary information was determined by use of the ARM derived cloud-boundary product based on a combination of millimeter wavelength cloud radar, ceilometer, and lidar data [6]. Figure 3.8 shows the vertical distribution of thin cirrus clouds over Nauru for the day of the TRMM orbit case shown in Figures 3.6 and 3.7. Cloud temperature was determined by relating these cloud boundaries to temperature profiles determined from ARM sonde data. Microphysical parameters over Nauru using explicit cloud boundary information

[6]Nauru data is obtained from the ARM program website, www.arm.gov

are compared to a retrieval using the less accurate climatological estimate of T_c in Figure 3.9.

The most obvious feature in the results is the presence of two distinct clusters of points. While application of the split-window approach in the absence of explicit cloud boundary information indicates the presences of cirrus clouds in all cases, more careful examination of the ARM data suggests that the satellite actually observed a combination of cirrus and low-level water clouds in a number of scenes (denoted by diamonds) and pure liquid clouds (open boxes). The presence of the low level clouds effectively changes the right foot of the arch to $T_{B,10.8}$ and ΔT_B values characteristic of the underlying clouds rather than the clear-sky atmosphere causing spurious results. In an operational retrieval, use of lidar to define cloud boundaries would provide a means to immediately discard such ambiguous cases.

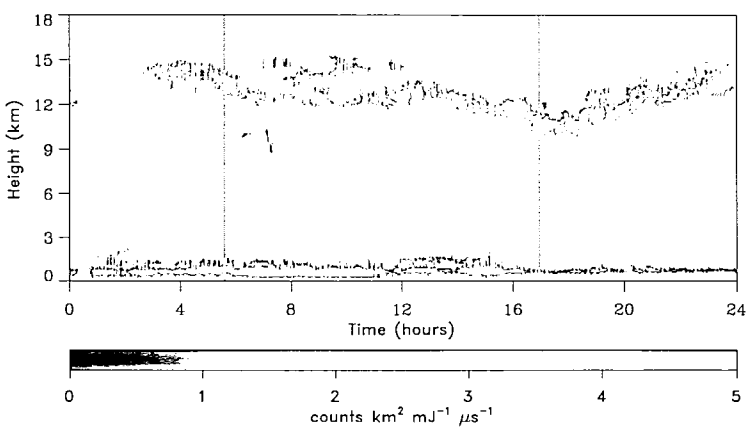

Figure 3.8: The normalized corrected relative backscatter from micropulse lidar located at the ARM site on Nauru. The two gray lines indicate the times of TRMM overpasses, the morning overpass corresponds to the observations and retrieval results shown in Figures 3.6 and 3.7.

Retrieved optical depth and effective radius from the two retrievals exhibit reasonable agreement for the thin cirrus cases (open circles). Relative differences are larger for effective radius ($\sim$ 30 %) than for optical depth ($\sim$ 10 %), in agreement with dif-

ferences in the sensitivity of the measurements to each. For the pure water cloud cases (open boxes), differences in retrieved properties are large because the estimates of T_c are significantly different. In one case, effective radius changes from 22 to 11 μm and the optical depth from 0.35 to 0.83 in the presence of explicit T_c information. So, even if the algorithm were applicable in the case of a thin, low level cloud, uncertainties in T_c will result in significant retrieval biases in the absence of cloud boundary information.

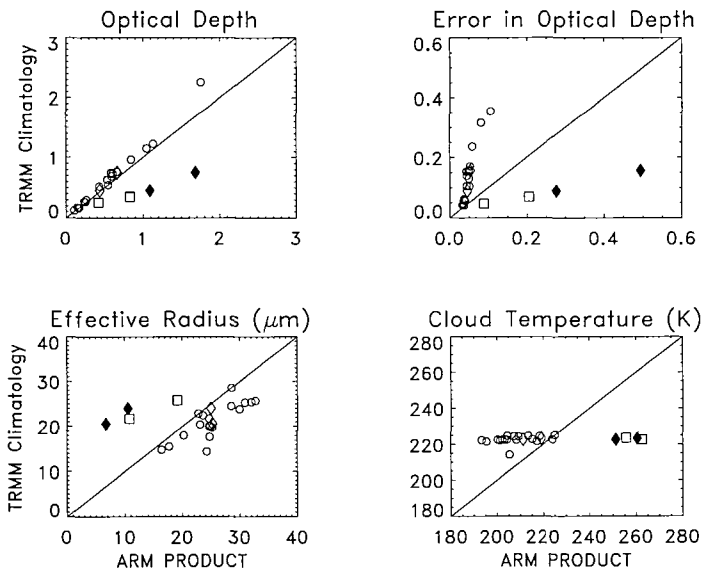

Figure 3.9: Scatter plots of retrieved optical depth, effective radius (in μm), cloud temperature (in K), and error in optical depth using estimates of cloud temperature from TRMM climatology vs. that from the ARM cloud boundary product. Open circles represent thin cirrus clouds. Open boxes represent water clouds. Open diamonds and filled diamonds represent cirrus clouds and water clouds, respectively, for cases where the satellite field of view was filled by both types of cloud at the same time. A one-to-one line has been plotted on each graph for reference.

The plot in the upper right of Figure 3.9 compares optical depth retrieval error from both retrievals. Retrieval error as defined in Eqn. (3) is a function of both measurement error and the sensitivity of the model to retrieved parameters. For the ice cloud cases, error in retrieved optical depth is significantly smaller when explicit cloud boundary information is used relative to the TRMM climatology case. In the cases with water cloud contamination, however, error appears larger in the presence of explicit cloud boundary

information. This is an artifact of the increased model sensitivity in the presence of large optical depth and small effective radii. As seen from Figure 3.1, small changes in effective radius and optical depth have little effect on $T_{B,10.8}$ and ΔT_B near the bottom of the arches but have a large effect near the top. Thus the apparent increase in error when ARM cloud boundary product is used result from the fact that optical depths are larger and effective radii smaller than in the TRMM climatology case.

Finally, agreement between the retrieved cloud temperatures is poor in general. With the exception of the single optically thick cirrus cloud, T_c's are limited to near the climatological mean of 218K in the TRMM climatology retrievals, whereas the ARM cloud boundary cases remain close to the measured T_c. Again, it is the striking difference between the two initial estimates of T_c that cause the differences in the other plots.

c. *Implications for Studying Cloud-Radiation-Climate Interactions*

Estimates of the microphysical and optical properties of cirrus clouds, make it possible to study their impact on climate through their interactions with solar and terrestrial radiation. Cirrus clouds both warm the atmosphere by trapping longwave radiation emitted by the Earth's surface and cool it by reflecting incoming solar radiation. Their net effect on the environment is determined by the relative magnitudes of these two processes which depend, in turn, on the absorption and emission properties of the constituent cloud particles. The goal of all space-based cirrus cloud microphysical retrievals is to constrain these quantities through direct estimation of the size and concentration of these particles.

To estimate the impact of explicit cloud boundary information in studying the role of cirrus in the radiation budget, a number of the Nauru retrievals have been used in broadband radiative transfer calculations. Ice water path (IWP) derived from retrieved 10.8 μm optical depths, retrieved effective radii, and cloud height estimated from retrieved cloud thermodynamic temperature were used as input to the BUGSrad broadband radiative transfer model to calculate upwelling and downwelling longwave and shortwave

fluxes at the top of the atmosphere (TOA) and surface (SFC). The BUGSrad model, which is currently implemented in the Colorado State University (CSU) general circulation model (GCM), employs the δ-two-stream approximation to the radiative transfer Eqn. (Stephens and Webster (1979); Ritter and Geleyn (1992); Stephens et al. (2001a)) over six shortwave and twelve longwave spectral bands. The model, explicitly accounts for the effects of scattering, absorption and emission from liquid and ice clouds using the parameterization of cloud optical properties introduced in Stephens et al. (1990), and includes gaseous absorption through the correlated k-distribution method of Fu and Liou (1992). In the present application, atmospheric temperature and humidity profiles are assumed to follow the McClatchey tropical atmosphere and the all calculations are made at local noon for simplicity.

Results are summarized for three cases in Table 3.5 chosen to be representative of a number of different scenes to which space-based measurements are likely to be applied.

The first case, observed on July 11, 1999, corresponds to a high, thin cirrus cloud, ideally suited for retrievals making use of split-window radiances. The second case, occurring later that day, consists of another high cirrus cloud but one that is approximately four times thicker than the first near the upper limit of optical thickness for which meaningful results can be obtained using this technique. The final case is a much lower cloud with an emitting temperature near 260 K. By virtue of its altitude, this cloud is likely composed of liquid droplets but this information is difficult to determine using window radiances alone increasing the probability of misinterpreting it as a thin cloud in the absence of explicit cloud boundary information.

In each of the first two cases cloud thermodynamic temperatures derived from the ARM cloud boundary product both modify the magnitude and increase the accuracy of all fluxes. Uncertainties are decreased by a factor of two in the thin cirrus case and three to four in the presence of the thicker cloud. Furthermore, in the absence of cloud boundary information, retrieved T_c's are generally close to the initial guess of 218 K failing to reflect large differences in vertical boundaries of the three cases. As a result,

Date	Lidar	$\tau_{10.8}$	r_e (μm)	T_c (K)	$F^{\uparrow}_{LW,TOA}$	$F^{\uparrow}_{SW,TOA}$	$F^{\downarrow}_{LW,SFC}$
July 11, 1999	No	0.52	20.0	223	186 ± 20	262 ± 6	418.7 ± 0.2
July 11, 1999	Yes	0.45	23.4	207	185 ± 8	259 ± 3	418.1 ± 0.1
July 11, 1999	No	2.3	14.1	214	112 ± 34	347 ± 99	420.5 ± 0.5
July 11, 1999	Yes	2.0	19.1	210	119 ± 11	320 ± 20	418.7 ± 0.2
Oct. 16, 1999	No	0.35	21.8	223	200 ± 16	255 ± 5	418.2 ± 0.1
Oct. 16, 1999	Yes	0.74	12.1	260	207 ± 10	277 ± 13	422.6 ± 0.7

Table 3.5: Broadband radiative fluxes (in Wm^{-2}) from BUGSrad for selected Nauru ice cloud retrievals. Horizontal lines delineate the three cases investigated. Two sets of fluxes are computed for each case, corresponding to retrievals without (upper set) and with (lower set) explicit cloud boundary information, respectively. Uncertainties, denoted by $\pm$ X, are estimated by perturbing retrieved cloud properties by their errors as established in the estimation process.

the vertical placement of the cloud heating in the atmosphere is poorly constrained in these retrievals which can have serious consequences in modeling global circulations (eg. Hartmann et al. (1984) and Lau and Peng (1987)).

In the third case, fluxes appear to be better constrained in the absence of cloud boundary information. This is deceiving since the cloud is likely actually a liquid cloud scene to which the retrieval shouldn't be applied. In this case, to match the 10.8 and 12 μm radiances observed by TRMM the algorithm creates an equivalent thin ice cloud consisting of 22 μm particles and emitting at 223 K. Explicit cloud boundary information results in a much thicker cloud consisting of 11 μm particles but emitting at a more appropriate 263 K. Since the radiative fluxes are most sensitive to small changes in effective radius when particles are small to begin with, their uncertainties are largest when cloud boundaries are constrained. Operationally, however, the presence of cloud boundary information allows the algorithm to flag this scene as a possible liquid cloud while its absence could lead to the very serious error of a complete misclassification.

It is important to note that, in all three cases, cloud boundary information has little influence on downwelling longwave radiation at the Earth's surface. This reflects the fact that downwelling radiation at the surface is due to emission from water vapor in the moist tropical atmosphere. Conversely, increased reflection of incoming solar radiation to space directly reduces downwelling shortwave radiation incident at the surface thus the errors in the two shortwave fluxes are strongly correlated.

Considering the fact that approximately a third of the planet is covered by cirrus at any given time (Liou (1986)), one can imagine the impact of such errors when integrated on large scales. The potential increase in accuracy afforded by the combination of explicit cloud boundary information and infrared observations is very promising in light of these considerations. For example, assuming cirrus cloud retrieval errors lead to average uncertainties in longwave fluxes at TOA of $\sim$30 Wm^{-2}, the absence of cloud boundaries leads to errors in global estimates of outgoing longwave radiation (OLR) as large as 10 Wm^{-2}. In practice the random component of this uncertainty will be substan-

tially reduced in the averaging process but we have no way of separating systematic and random errors at this time. Explicit estimates of cloud boundaries reduce average TOA longwave flux uncertainties to $\sim$10 Wm^{-2} and corresponding global OLR errors to $\sim$3 Wm^{-2}. For comparison purposes, the magnitude of the global-mean radiative effects of aerosols (both direct and indirect) are expected to be on the order of 1-2 Wm^{-2} while the longwave radiative signature of atmospheric CO_2 is $\sim$1.5 Wm^{-2} (IPCC (1995)). Clearly, improved estimates of ice cloud microphysical and optical properties afforded by including explicit cloud boundary information are critical to the problem of establishing observational evidence for climate variability resulting from anthropogenically induced changes in either of these two important atmospheric constituents.

6. Conclusions

An optimal estimation algorithm that combines explicit cloud boundary information with the split-window approach to estimate the microphysical properties of thin cirrus clouds has been introduced. The inclusion of explicit cloud boundary information is found to significantly reduce the biases inherent in traditional implementations of the of the approach. Furthermore, the optimal estimation framework provides error diagnostics for all retrieved parameters often lacking in other retrievals and facilitates addition of information from complementary sensors into the retrieval. Ackerman et al. (1990) for example, show that 8.5 μm radiances can be used in conjunction with those at window wavelengths to distinguish between water and ice clouds. Such information can easily be added to the algorithm providing a thermodynamic phase cloud mask, increasing its speed and accuracy when applied on global scales. In principle, a retrieval of cirrus properties could be performed from any data set that includes a direct estimate of cloud thermodynamic temperature, T_c, using the forward model developed here.

Synthetic retrievals indicate that the more accurate the estimate of T_c, the higher the probability of obtaining an accurate retrieval given a measurement with random er-

ror. Retrieval errors provided by the optimal estimation approach suggest that optical depth is determined significantly more accurately than effective radius, an artifact of the sensitivity of the forward model physics to each of these parameters. For an error in cloud temperature of 2 K, characteristic of lidar-based estimates of cloud thermodynamic temperature, the average error in retrieved optical depth and effective radius are $\sim$15 and $\sim$60 percent, respectively, significantly better than retrievals performed with less accurate cloud temperature information. Application of the algorithm to coincident measurements of infrared radiances from TRMM and cloud boundary measurements from the ARM Nauru site confirms these results. Differences between retrievals using accurate cloud boundary information and those performed with a less accurate climatological estimate of T_c were on the order of 10 and 30 percent for optical depth and effective radius, respectively, while retrieval uncertainties were generally much larger in the absence of cloud boundary information. Furthermore, cloud boundary information proves invaluable in eliminating the potential for ambiguities in cases where the satellite field of view observed either multiple cloud layers or water clouds.

If one third of the planet is assumed to be covered by cirrus clouds at any given time, the absence of cloud boundaries in the present work leads to errors in global estimates of outgoing longwave radiation (OLR) as large as 10 Wm^{-2}. Accurate estimates of cloud boundaries are found to reduce global OLR errors to $\sim$3 Wm^{-2}. When compared to IPCC estimates of the global-mean radiative effects of aerosols (1-2 Wm^{-2}) and CO_2 ($\sim$1.5 Wm^{-2}) it is clear that improved estimates of ice cloud microphysical and optical properties afforded by including explicit cloud boundary information are critical to the problem of establishing observational evidence to constrain the climatic impact of either of these highly variable atmospheric constituents.

Co-located active and passive measurements will soon be available on a global scale with coincident measurements from the Earth Observing System (EOS) Aqua, CALIPSO, and CloudSat satellites which are scheduled to fly in formation in early 2004. Infrared radiances from the MODIS instrument aboard Aqua can be combined with li-

dar data from CALIPSO, or, equivalently, cloud radar data from the 94 GHz CPR, to retrieve thin cirrus clouds globally. The work presented here, for example, could be used in conjunction with a retrieval scheme developed by Stephens et al. [2002] for an estimate of the vertical distribution of cloud microphysical properties, as depicted in Figure 3.10. An optical depth generated by the combination of active and passive measurements as described in this paper provides a constraint in the Stephens et al. [2002] algorithm. The vertical distribution of both particle size and ice water content is then generated from the vertical profile of radar reflectivities observed by CloudSat initially used to supply cloud boundary information in the optical depth retrieval. Furthermore, provided suitable forward models are developed, information from the visible or near-infrared channels on MODIS can be incorporated to further augment the flexibility of the retrieval and increase its accuracy. The resulting climatology fits well within the objectives of all three missions offering the potential to significantly improve characterization of cirrus cloud extent and microphysical properties necessary to understand the physical processes underlying climate variability and change.

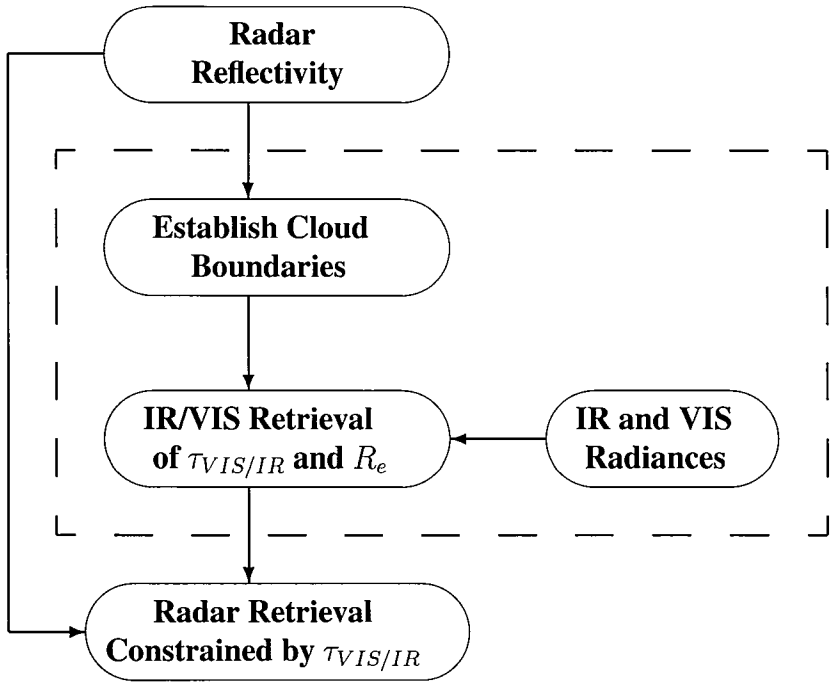

Figure 3.10: Schematic representation of a methodology for retrieving vertical distributions of cirrus cloud microphysical properties from a combination of active and passive observations. The elements of the approach that are explicitly addressed in this paper are highlighted with the dashed box.

Acknowledgments

We thank Dr. Ping Yang for his assistance in determining cloud particle absorption properties and Drs Merritt Deeter and Frank Evans for allowing us to use their forward model for calibrating our own model. Dr. Angela Bendetti provided many useful insights into our problem. Finally, we thank each of the three anonymous reviewers for their thorough reviews and their helpful comments. Nauru data were obtained from the Atmospheric Radiation Measurement (ARM) Program sponsored by the U.S. Department of Energy, Office of Science, Office of Biological and Environmental Research, Environmental Sciences Division. Funding for this work was provided by NASA research grants NAS5-99237 (TRMM), NAS1-99103 (CALIPSO), and NAG5-7719 (CloudSat).

Chapter 4

Channel Selection for Ice Cloud Microphysical Property Retrievals over the Global Oceans

1. Introduction

In the previous chapter, an advanced version of the split- window technique was used as an illustrative example to quantify the relative importance of uncertainties in cloud and atmospheric state variables on the retrieval of ice cloud microphysical properties. Chapter 4 exploits the optimal- estimation retrieval framework and the forward model error covariance methodologies developed in the split- window paper but applies them at a much more general level. Instead of examining retrieval performance for a variety of pre- conceived retrieval techniques, such as the split- window approach, a formal information content analysis is used to select objectively the ideal combination of measurements for an ice cloud property retrieval scheme given information from each the visible, near- infrared, and infrared spectral regions.

The information content methodology as implemented by L'Ecuyer et al. (2004) is used to objectively select the optimal combination of measurements for an estimation-

based ice cloud retrieval scheme given a realistic assessment of the current knowledge of the ice cloud problem. The method developed uses information theoretical concepts elucidated by Shannon and Weaver (1949) and on the application of their technique to atmospheric science by Rodgers (2000). Channel selection is made objective by quantifying the amount of information contained in the spectral measurements and calculating their effective signal to noise ratio in relation the desired set of retrieval parameters. This is accomplished practically through analysis of the retrieval covariance matrix, which holds the key for understanding and quantifying differences between a different retrieval procedures and observational data. Although this analysis is for a theoretical retrieval combining simulated measurements from the Moderate Resolution Imaging Spectroradiometer (MODIS) with the CloudSat Cloud Profiling Radar (CPR) above an ocean surface, the general methodology could be applied to any available instrument package. The sensitivities and uncertainties used in determination of this effective signal to noise ratio for the MODIS channels listed in Table 4.1 will be examined across the climatological range of ice cloud properties to determine which channels are most useful dependent upon the state of the atmosphere.

The calculations are made possible only by the recent development of optical properties for a variety of non- spherical ice crystals at the MODIS wavelengths (Baran et al. (2001); Yang et al. (2000, 2003)), allowing a reasonable estimate of the uncertainties in satellite- viewed radiances resulting from our assumptions of cloud microphysical properties. The results will show that the optimal combination of channels for an ice cloud retrieval is highly case dependent, meaning that there is no ideal combination of two or three channels that will always ensure an accurate retrieval. We therefore propose a five-channel, estimation- based retrieval scheme that uses a combination of visible, near- infrared, and infrared channels weighted by appropriate estimates of their errors to place emphasis on those channels which contain the most information given our best estimate of the state of the atmosphere. Algorithmic details and validation will be the subject of a future paper. It is hoped an estimate of cloud properties with associated uncertain-

ties based on an honest assessment of ice cloud physics from this retrieval scheme will be useful both in determining the extent to which these clouds can be measured and in assessing their role in climate variability.

Section 4.2 describes the forward model used to estimate satellite-observed radiances for given cloud and atmospheric properties. Section 4.3 discusses the sensitivity of these top of the atmospheric (TOA) radiances to small perturbations in cloud and atmospheric properties to determine which wavelengths potentially contain the most information given the atmospheric state. Since an estimate of both sensitivity and uncertainty is required to compute an effective signal to noise ratio as defined in Part I, Section 4.4 focuses on an estimate of forward model error due to uncertainties in ice crystal shape, drop size distribution,and atmospheric profile. Section 4.5 presents a formal information content analysis used to select those channels which contain the most information given a variety of expected climatological conditions while Section 4.6 explores the practical implications of these results for an operational retrieval.

2. The Forward Model

A 48-stream adding and doubling radiative transfer model was used to calculate top of the atmosphere radiances assuming a plane parallel atmosphere. The solution of the radiative transfer equation for this technique is well-documented in the literature and will be omitted here for brevity. Application of this numerical model to the real- world cirrus cloud problem is only insightful when rigorous, realistic physical assumptions are used as input for the model. An accurate representation of atmospheric profile, surface reflection, and cloud microphysical properties is crucial to understanding what information actually can be retrieved for a given instrument package. The base physical assumptions used in the forward model for the sensitivity studies of Section 4.3 will be described briefly. Atmospheric absorption in our model was approximated by correlated- k distributions specifically developed for the MODIS wave bands by Kratz

MODIS channel	wavelength	MODIS channel	wavelength
1	0.62-0.67	27	6.53-6.90
2	0.84-0.88	29	8.40-8.70
5	1.23-1.35	31	10.78-11.28
6	1.63-1.64	32	11.77-12.27
7	2.10-2.15	33	13.18-13.49
19	0.91-0.96	34	13.48-13.78
20	3.66-3.84	35	13.78-14.08
23	4.02-4.08	36	14.08-14.38
26	1.36-1.39		

Table 4.1: MODIS channels evaluated for information content analysis.

(1995), where the vertical distribution of gases and temperature were defined by the McClatchey Tropical Atmosphere (McClatchey et al. (1972)). The surface was assumed to be an isotropically reflecting ocean surface with visible albedo of 0.1 and infrared albedo of 0.01. Cirrus clouds were assumed to be 1 km thick and at the same temperature as the layer of the atmosphere in which they were embedded. The clouds were composed of randomly oriented randomized hexagonal ice aggregates developed by Baran et al. (2001), arranged in a modified gamma size distribution of the form,

$$n(D) = N_t \frac{1}{\Gamma(\nu)} \left(\frac{D}{D_n}\right)^{\nu-1} \frac{1}{D_n} e^{-D/D_n} \tag{4.1}$$

with variance parameter, ν, equal to 2, $n(D)$ is the number of ice crystals of size D, N_t is the number concentration, and D_n is the characteristic diameter (Stephens (1994)). The basis for choosing these crystals is that Baran et al. (2003) showed that the single scatter properties for these polycrystals combined with a modified Henyey- Greenstein phase function better explained observed radiances than the optical properties for more pristine crystal habits. Since these aggregates had strongly forward-peaked phase functions, a modified form of the Delta- M scaling technique (Wiscombe (1977)) recently developed by Mitrescu and Stephens (2004) was used to accurately calculate radiance while maintaining computational efficiency. Both the observation angle and the solar zenith angle were at nadir.

3. Sensitivity Studies

The retrieval of cloud properties from satellite- based measurements depends on the ability to relate observed radiances back to a unique set of desired cloud properties. Those measurements that show the greatest change or sensitivity to small changes in cloud microphysical properties are potentially the most useful for a cloud retrieval. Traditional retrieval schemes are based on *a priori* knowledge of these sensitivities, e.g. the split-window technique ultimately depends upon the sensitivity of radiance measurements re-

sulting from a difference in the refractive index for ice cloud particles at wavelengths in the window region. The magnitude of these sensitivities, however, is heavily dependent upon both wavelength and the state of the atmosphere. The split- window technique, see Figure 3.1, only has sensitivity for optically thin clouds with relatively small effective radius. An ideal retrieval scheme should be based on the proper selection of those channels with the greatest sensitivity for the current state of the atmosphere. Thus, a series of sensitivity studies were run for each of the MODIS wavelengths listed in Table 4.1 to determine how satellite observed radiances change for small perturbations of the desired retrieval parameters. Although these results will be specifically for the use of the Baran ice aggregate, it should be noted that other crystal habits exhibited very similar sensitivities or trends in radiance albeit different magnitudes, e.g. see Figure 2.7.

Sensitivity studies were run for cloud particle effective radius, ice water path, cloud temperature, and surface albedo. Each of these parameters were perturbed while holding the other parameters fixed to determine the magnitude of the radiance change at the top of the atmosphere for a given change in the varied parameter. It should be noted that for the perturbations of effective radius, the ice crystal size distribution number concentration was necessarily varied to fix ice water path (IWP), meaning that cloud optical depth increases with both decreasing effective radius and increasing IWP for these studies. Synthetic radiances were calculated for small perturbations about cloud effective radii between 6 μm to 50 μm, IWP between 1 g/m^2 and 250 g/m^2, cloud heights between 8 and 15 km, and the base surface albedos of 0.1 for the visible and near-infrared and 0.01 for the infrared channels. IWP and effective radius combinations were chosen to ensure that cloud optical depths, Figure 4.1, varied across the expected range for cirrus clouds at each MODIS wavelength. Since it is impractical to present results from all of these sensitivity studies, a few sample cases will be examined to demonstrate that our forward model and its assumptions are capturing the basic physics of the ice cloud problem. Although the sample cases are chosen for their well- known physical properties, as visualized in Figures 3.1 and 2.7, it is important to remember

that all channels in Table 4.1 will be evaluated in an un-biased manner in the information content analysis of Section 4.5 to objectively select the most useful channel for the given state of the atmosphere.

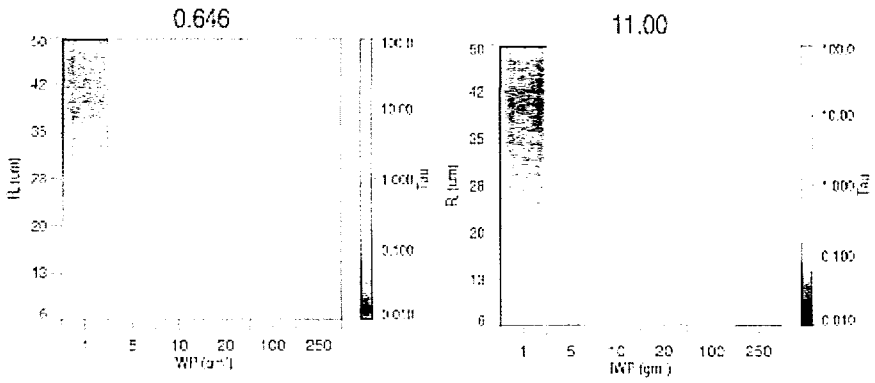

Figure 4.1: 0.64 μm and 11.0 μm optical depths for given effective radius- IWP ice clouds evaluated in sensitivity studies.

Figures 4.2a, 4.2b, and 4.2c show example results from the sensitivity studies for the 0.65 μm, 2.13 μm, and 11.0 μm channels, respectively, as a function of effective radius and ice water path for a cloud at 9 km. The values in the three panels represent from left to right the normalized change in radiance, $\frac{x}{I}\frac{dI}{dx}$, given a change in effective radius, ice water path, and cloud temperature, respectively, holding the other retrievable parameters fixed. Surface albedo effects are generally small and unimportant for the

highly absorbing ocean background and will be neglected for the remainder of the paper. For an operational retrieval over land, of course, albedo will become very important and need consideration. Figure 4.2a suggests that the 0.66 μm channel is sensitive to both effective radius and IWP but not to cloud temperature. These results agree with our physical intuition into the problem. The conservative scattering 0.66 μm channel is useful in retrieving cloud optical depth, as satellite- observed radiances at this wavelength are primarily a function of cloud optical depth. For our sensitivity studies, this property leads to the observed sensitivity for perturbations of both IWP and effective radius as both act to determine optical depth. Sensitivities to IWP and effective radius are similar but opposite is sign as decreasing effective radius increases optical depth, with generally good sensitivity except for the optically thick and thin clouds. The thickest clouds have low sensitivity as the reflectance function slowly converges as optical depth becomes large, see Figure 2.7. The thin clouds have poor sensitivity due to a complex interaction of the directly backscattered radiation and the forward scattered radiation reflected off the ocean. As expected, the 0.65 μm channel shows little sensitivity to cloud height perturbations as gaseous absorption is negligible small in this channel.

The sensitivity studies for the 2.13 μm channel in Figure 4.2b are very similar to those of the 0.66 μm channel in that they exhibit sensitivity to both IWP and effective radius but not cloud temperature. The non- conservative scattering 2.13 μm channel is useful in retrieving cloud particle effective radius, as backscattered radiation now becomes dependent upon particle size. Sensitivity to perturbed effective radius is again generally good, except for the low IWP cases where Figure 2.7 suggests we would expect the smallest sensitivity. Sensitivity to both IWP and cloud temperature is similar in trend to that of the 0.65 μm channel for similar reasons.

Figure 4.2c suggests that the infrared 11.0 μm channel displays sensitivity to effective radius, IWP, and cloud temperature. This sensitivity, however, is limited to IWP-effective radius combinations that result in intermediate optical depths from one to about five, agreeing very well with the working range of the split- window retrieval technique

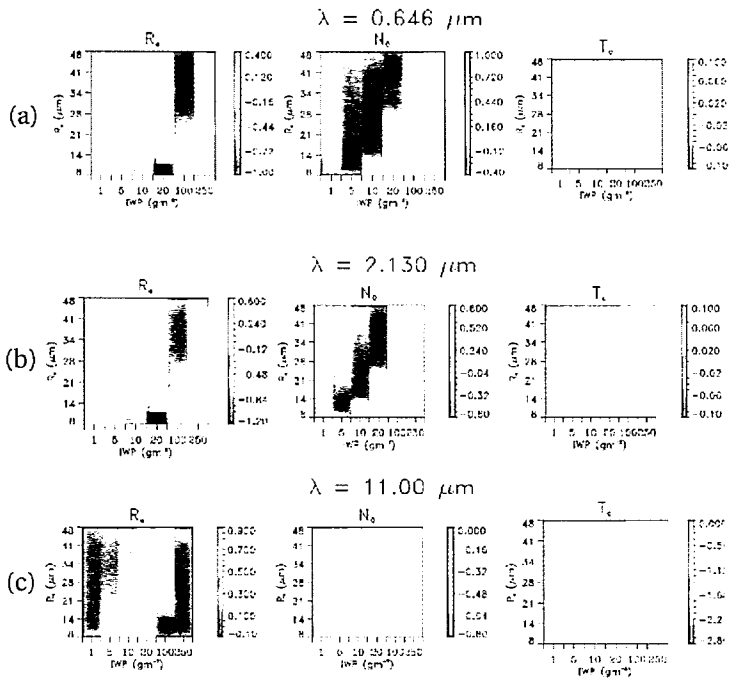

Figure 4.2: Sensitivities to effective radius, IWP (No), and cloud temperature for the 0.65, 2.13, and 11.00 μm MODIS channels are shown in Figures a, b, and c, respectively, for the given effective radius- IWP combinations for a cloud height of 9 km. Sensitivities indicate normalized change in top of the atmosphere radiance given a change in the specified variable while holding the other two fixed.

as seen in Figure 3.1. If the cloud becomes too thick, emission is that of a Planck blackbody emitting at cloud temperature so that further perturbations cannot change the radiance. If the cloud is too thin, surface emission dominates and the contribution from the cloud is negligible. Sensitivity to cloud height increases with increasing optical depth, becoming important for thick clouds when the emission from the cloud and not the surface begins to dominate the radiance measurement.

4. Uncertainty Analysis

Information content of a set of measurements depends not only on the sensitivity of measurements to retrieved cloud parameters, but also on the error associated with each

of these measurements both from the instrument itself and from the *a priori* assumptions as discussed in the introduction. Instrument error primarily results from calibration issues and is on the order of a few percent (Guenther et al. (1996)). Error from forward model assumptions required to simulate radiances, however, is generally much larger. The remainder of this section will focus on the quantification of these errors for the MODIS channels listed in Table 4.1. Uncertainties in radiances associated with our choices of ice crystal habit, cloud particle size distribution, and atmospheric temperature and relative humidity profiles were determined by calculating TOA radiances for the base case assumptions described in Section 4.3 and then comparing these results with radiances found using alternate assumptions. Further uncertainties associated with 3-D radiative transfer effects and multi- layer clouds, although certainly important, are beyond the scope of this paper and will be neglected.

The assumption of crystal habit and associated optical properties will heavily influence cirrus cloud retrieval results. Cooper et al. (2003) showed that uncertainties in ice crystal habit were important in determining overall retrieval accuracy for a modified version of the infrared split- window technique. Errors from habit assumptions should be expected to be even greater for the visible and near- infrared channels where large single-scatter albedos could result in significant multiple- scattering. Radiative transfer calculations were run for a variety of crystal habits developed by Yang et al. (2000, 2003) and compared to those using the Baran et al. (2001) randomly oriented randomized hexagonal ice aggregates. Calculations were made at the visible and near- infrared wavelengths for columns, plates, bullets, rough aggregates, and smooth aggregates and at the infrared wavelengths for droxtels and aggregates. To facilitate comparisons between the different types of ice habits, the Baran aggregates were converted to an equivalent set of Yang crystals by conserving both IWP and volume to area ratio for the crystal types (Francis et al. (1994); Mitchell and Arnott (1994); Grenfell and Warren (1999); Yang et al. (2001)). A ball-park estimate of the error in radiance associated with habit choice is then obtained from the normalized average absolute difference between the Baran aggregates

and all Yang crystals. Error estimates were run at each of the effective radius, ice water path, and cloud temperature combinations run in the sensitivity studies. Errors in the visible channels can be as large as a factor of 2 as but are more typically around 20 to 30 percent, errors for the infrared channels are generally less than about 5 percent. One interesting finding from this error analysis is that the fractional errors in the 3.78 and 4.05 μm radiances are significantly greater during the day than the night due to the large uncertainties associated with the scattering of the direct solar beam.

Model errors associated with particle size distribution were assessed by substituting the modified gamma distribution with variance parameter equal to two used in sensitivity studies with both a different modified gamma distribution with variance parameter equal to 3 and a lognormal distribution. The lognormal distribution is of the form

$$n(D) = \frac{1}{D\ln\sigma_g(2\pi)^{0.5}}\exp\left[\frac{(\ln D - \ln D_g)^2}{2(\ln\sigma_g)^2}\right] \tag{4.2}$$

where D_g is the geometric mean diameter and σ_g is the geometric standard deviation (Reist (1994)). Unlike those associated with crystal habit, uncertainties in radiance due to particle size distribution assumptions were generally under a few percent for all wavelengths, agreeing well with previous work (Stephens et al. (1990); Cooper et al. (2003)).

Uncertainties in determination of atmospheric temperature and moisture profiles were found to be important for the infrared channels but not for the visible and near-infrared channels. Temperature error was assumed to be 2 K based on expected uncertainties in temperature profiles derived from numerical weather predation models (Eyre et al. (1993)) which would be used to constrain an operational retrieval. Resulting errors in infrared radiance measurements varied from about 3 to 8 percent due to the non- linear nature of the Planck function. Relative humidity was perturbed 30 percent for atmospheric levels above 500 mb and 15 percent for those levels at or below 500 mb. These assumptions resulted in errors less than 3 percent for all channels. Visible

channels are not affected by temperature errors as atmospheric absorption only weakly depends on temperature. Similarly, sensitivity to moisture assumptions was small for the visible channels as the high cirrus clouds were generally above the peak of the weighting functions for these channels.

Figure 4.3 illustrates the total error due to a combination of all of these uncertainties listed above for the 0.66, 2.13, and 11.0 μm channels for a cloud at 9 km and for the IWP- effective radius combinations used in the sensitivity studies. Each of the above sources are considered un- correlated, so total error is simply the sum of the squares of the individual sources. Figure 4.3 shows that error is clearly dependent upon the state of the atmosphere, with generally large errors in the visible channel dominated by habit effects and comparatively small errors in the infrared resulting from a mixture of uncertainties in habit, temperature, and moisture assumptions.

5. Information Content Analysis

An information content analysis based on the techniques of Shannon and Weaver (1949) and Rodgers (2000) as described in Part I of this paper was performed using the results of the sensitivity and uncertainty studies to determine the optimal channels for a theoretical cirrus cloud retrieval using the MODIS instrument. A brief summary of salient features of the information content methodology is included here for completeness. In these analyses, information, H, is considered the difference in entropy, S, between two states, P_1 and P_2,

$$H = S(P_1) - S(P_2) \tag{4.3}$$

If a Gaussian distribution is assumed for both states, Rodgers shows that information can be re- written in terms of the distribution covariances, $\mathbf{S_1}$ and $\mathbf{S_2}$,

$$H = \frac{1}{2} log_2 \left| \mathbf{S_1 S_2}^{-1} \right| \tag{4.4}$$

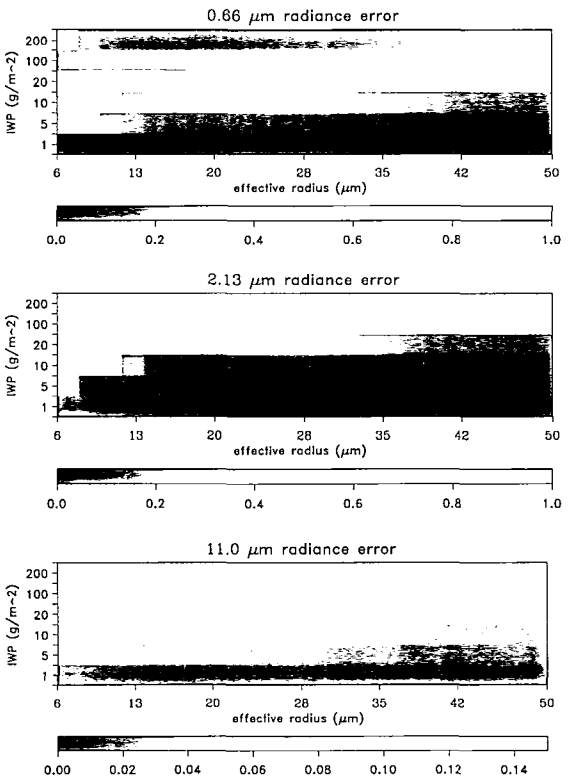

Figure 4.3: Combined fractional uncertainties in MODIS radiances due to assumptions of ice crystal habit, crystal size distribution, atmosphere profile, and instrument noise as a function of IWP and effective radius for an ice cloud at 9km.

The initial state covariance is simply the *a priori* error covariance matrix, $\mathbf{S_a}$, and is estimated from the expected climatological range of ice cloud properties. The final state covariance may be considered the error covariance matrix for retrieved cloud properties, $\mathbf{S_x}$, defined mathematically as,

$$\mathbf{S}_x = \left(\mathbf{S}_a^{-1} + \mathbf{K}^T\mathbf{S}_y^{-1}\mathbf{K}\right)^{-1} \tag{4.5}$$

where $\mathbf{K}$ is the Jacobian determined from the sensitivity studies of Section 4.3 and $\mathbf{S_y}$ is the forward model and measurement covariance matrix determined from the uncertainty analyses of Section 4.4. Use of these assumptions in Equation 4.4 yields a form for H which is defined entirely in terms of the work described in the proceeding sections,

$$H = \frac{1}{2} log_2 \left| \mathbf{S_a} \left(\mathbf{K^T S_y^{-1} K} + \mathbf{S_a^{-1}} \right)^{-1} \right| \tag{4.6}$$

Separate analyses were run for each of the IWP, effective radius, and cloud height combinations described in the sensitivity studies for both daytime and nighttime retrievals and for retrievals with and without complementary information from the CloudSat CPR. In addition, an information content analysis was performed assuming equal error at all channels and atmospheric states to determine the influence of our heavily-case dependent error characterization upon final channel selection. We do not have adequate space to discuss the results from all these runs, so instead we will first focus on specific examples to show that the mathematical results agree with our physical intuition of the problem. To prevent an over simplification of the ice cloud retrieval problem, however, we must then turn to a graphic representation of the multitude of cases to properly convey the complexity of the problem and its practical implications for an operational retrieval.

Figure 4.4 shows a sample information spectrum for an optically thick cirrus cloud at 9km with effective radius of 16 μm and IWP of 100 g/m^2, a combination producing a 0.64 μm optical depth near 11.0. The initial entropy is defined by the total number of possible states associated with our *a priori* characterization of the atmosphere, $\mathbf{S_a}$. For our cases constrained by CloudSat and MODIS information, initial entropy would result from all possible states assuming standard deviations for *a priori* assumptions of 25.0 μm for effective radius, 200 g/m^2 for IWP, and 1.5 K for cloud temperature and a uncertainty in surface albedo of 10 %. Once a measurement is added, however, the entropy or, alternately, the number of possible atmospheric states is reduced to only those consistent with that measurement. The basic idea of these figures is to identify the channel with the most independent information relative to the *a priori* state, remove that channel, and then re- run the analysis to find the channel with the most independent information for the new state constrained with the first measurement, and so on. In Figure 4.4, the top solid curve shows that the 0.64 μm channel contained the most information relative to

the *a priori*. Since the MODIS measurements may be strongly correlated, the selection of one channel will limit the independent information in a similar channel, e.g. in this case the selection of the 0.64 μm channel results in a significant decrease in potential information in the 0.86 μm channel. The middle, dotted curve suggests that the 2.13 μm channel contained the most information for the remaining channels for the *a priori* state constrained by the 0.64 μm channel. No additional channels were considered useful as their addition did not reduce the entropy given inherent noise in the system. As expected, this information content analysis suggests that a retrieval scheme based on the NK approach would be highly effective for this thick cloud case.

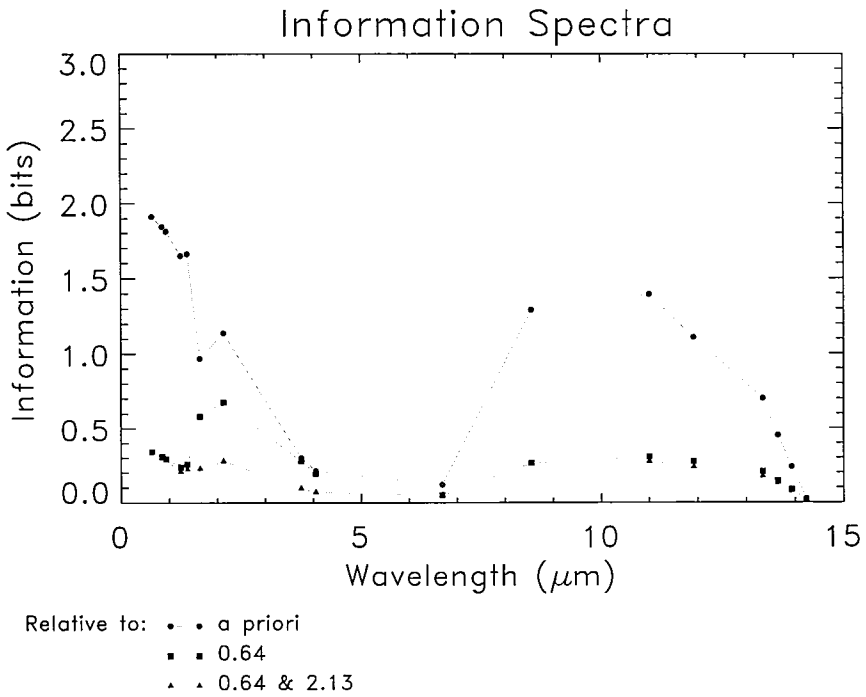

Figure 4.4: Information spectrum analysis for an ice cloud with effective radius of 16 μm, IWP of 100 g/m^2, and cloud height at 9 km.

The selection of channels for this optically thick cloud case agrees well with expectations based on our physical understanding of the problem. The 0.64 μm and 2.13 μm channels have sensitivity to IWP and effective radius, respectively, as seen in Figure 2.7. In turn, this expectation can be verified using the mathematical framework of the infor-

mation content analysis. Figure 4.5 presents the singular value analysis for this base case of Figure 4.4. The number of singular values that exceed the noise level of 1.0 indicate the number of retrievable parameters that can be inferred from the entire seventeen channel data set, in this case it is three. The singular vectors indicate the linear combination of retrievable parameters for each singular value, so for the top left panel IWP (number concentration, N_0) has the largest absolute value and therefore corresponds to the primary information in the system. Effective radius and cloud temperature information correspond to the second and third singular values, respectively. Of course, if we only used the 0.64 μm and 2.13 μm channels that were selected for this case, we could only retrieve IWP and effective radius. The use of some combination of the remaining channels would improve our cloud temperature retrieval, but since the singular value is small the increase in retrieval accuracy may not justify the necessary increase in computational effort.

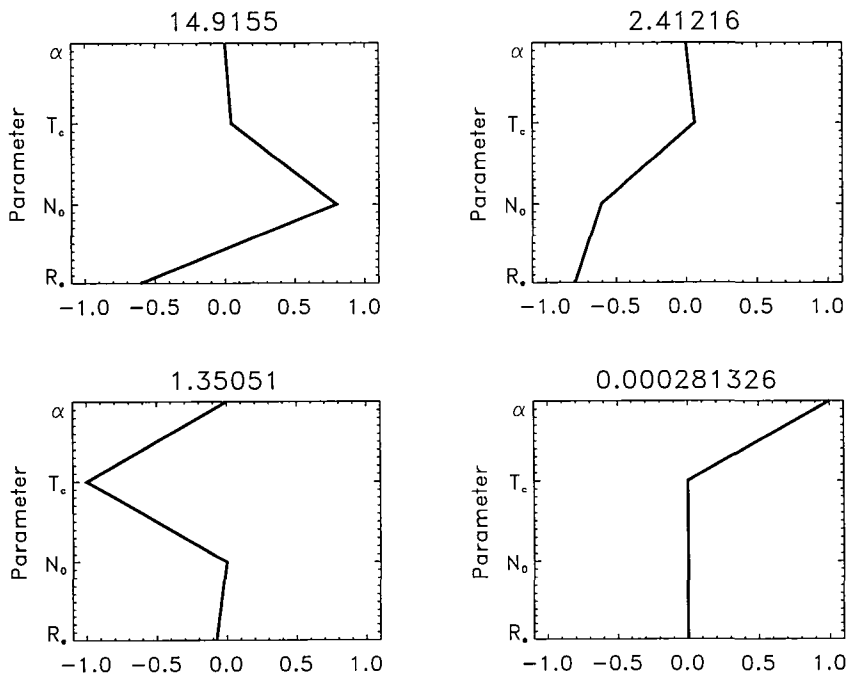

Figure 4.5: Singular value analysis for the ice cloud of Figure 4.4.

We then changed each of the parameters individually in the base cirrus cloud case to show that different cloud states require different combinations of channels to maximize information content. Figure 4.6 shows the information spectra for a thin cirrus cloud with the same effective radius and cloud height as in Figure 4.4 but now with an IWP of 10 g/m^2, producing a 0.64 μm optical depth of 1.1. The optimal combination of channels for this thin cirrus case are the 4.05 and 11.9 μm measurements in that order, suggesting that two emission based channels in a split- window type approach provide the most information for this thin cloud case. These selected channels are not un-expected, as the split- window technique has sensitivity for optically thin clouds but not for the thick cloud of the base case, see Figure 3.1. Although the visible channels chosen for the base case also have sensitivity to thin cirrus, the relatively large errors for these channels due to *a priori* assumptions of crystal habit ultimately limit their utility.

Figure 4.7 shows the information spectrum for a cirrus cloud with the same effective radius and IWP as in Figure 4.4 but now for a cirrus cloud at a height of 14 km. In this case, the 8.55, 11.0, and 2.13 μm channels are sequentially selected. The increased thermal contrast between the surface and the high cloud results in more information for the MODIS measurements, allowing the two infrared and one near- infrared channel to be selected. Although not entirely accurate quantitatively since we are using different channels, the easiest way to qualitatively understand why the high cloud case should have more information than the low cloud case is to examine the split- window arches of Figure 3.1. Although the arches for the cold cloud are much larger than those for the warm cloud, they both represent the same number of possible cloud states. A set of measurements with a well- defined uncertainty range define a set of possible optical depth and effective radius combinations in brightness temperature space. Since these solutions are more spread out for a colder cloud, the same set of measurements necessarily result in fewer possible solutions for the cold cloud case than the warm cloud case. Since the *a priori* space is the same for both clouds, the measurements should contain more information for the cold cloud case by definition, as suggested by the increased

number of useful measurements in Figure 4.7.

Figure 4.8 shows the information spectrum for the optically thick cirrus at a cloud height of 9 km but now with an effective radius of 40 μm, resulting in a 0.64 μm optical depth of 4.7. In this case, only the 11.9 μm channel was considered useful which the singular value analysis directly relates to IWP. This result is a direct consequence of the fact that neither visible nor infrared approaches have sensitivity at large effective radius.

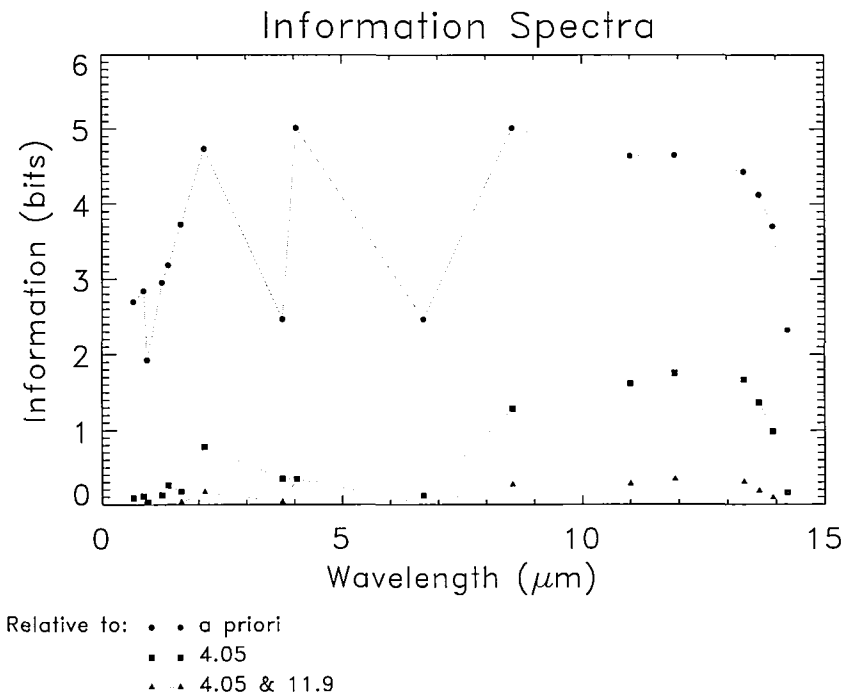

Figure 4.6: Information spectrum analysis for an ice cloud with effective radius of 16 μm, IWP of 10 g/m^2, and cloud height at 9 km.

Each of the four cases described above require a different combination of channels to maximize information content. Although each of these combinations could generally be explained in terms of our understanding of the underlying physics of the problem, it should be noted that these cases were selected for their relative ease in interpretation. Many other cases representing intermediate conditions for which the physical relationships between radiances and retrieval parameters are transitioning between regimes are more ambiguous, making it difficult to infer the optimal combination of channels before

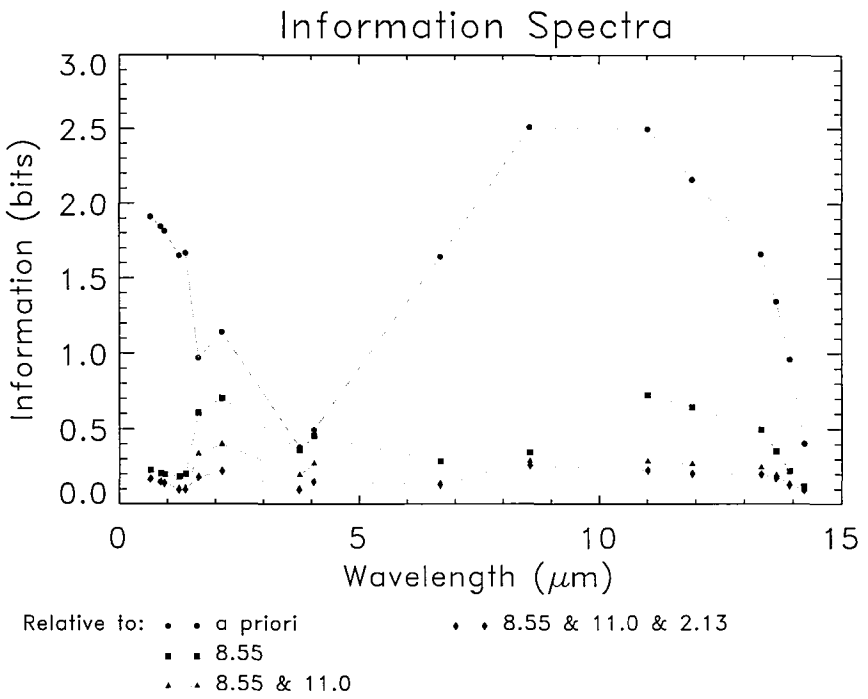

Figure 4.7: Information spectrum analysis for an ice cloud with effective radius of 16 μm, IWP of 100 g/m^2, and cloud height of 14 km.

performing the information content analysis. Figure 4.9 shows the first, second, third, and fourth channel selected for each of the IWP- effective radius combinations for the 9 km cirrus cloud case constrained with CloudSat cloud boundary information. Individual channels have been grouped according to their sensitivity characteristics for clarity of presentation. Dark blue represents the conservative scattering channels; light blue the non- conservative scattering channels; green the water vapor channels; yellow the SWIR (solar and emitting 3.78 and 4.05 μm) channels; orange the infrared channels; and red the CO_2 slicing channels. For some cases, such as most large IWP clouds, the optimal channels are simply a combination of scattering and non- conservative shortwave scattering as discussed above. Similarly, moderately thin clouds with small effective radius require the expected combination of an infrared channel with another infrared, SWIR, or CO_2 slicing channel to maximize information content. The exact transition between these regimes, however, is not intuitively obvious nor is it independent of other variable

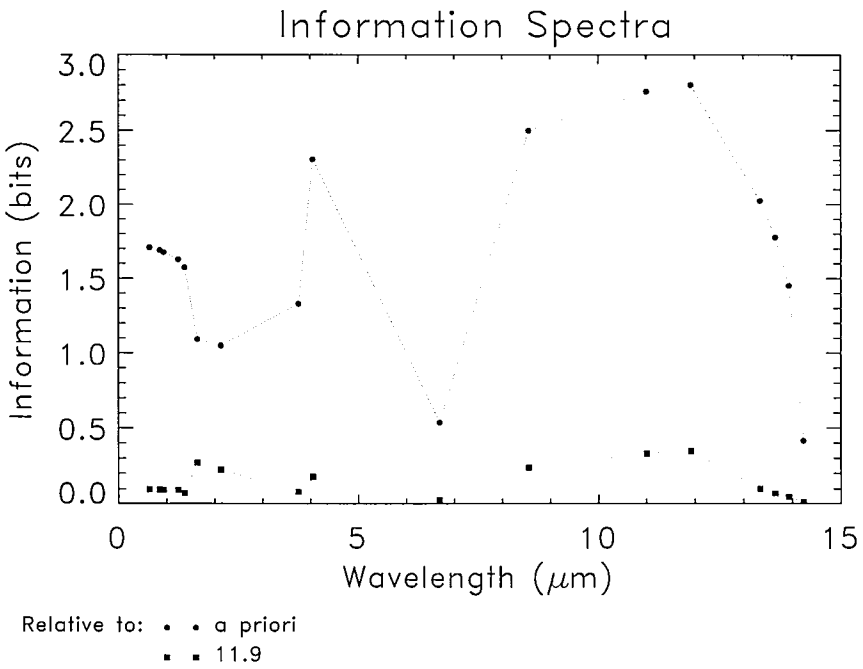

Figure 4.8: Information spectrum analysis for an ice cloud with effective radius of 40 μm, IWP of 100 g/m^2, and cloud height at 9 km.

such as cloud height or surface type. Often in other cases, such as large effective radius, only one conservative scattering, SWIR, or infrared channel provides independent information for the retrieval, and while the mathematical explanation for the specific wavelength chosen can always be traced backed through the methodology, it is not always intuitively obvious from a physical perspective why one type of channel is more useful than the others. This idea that the ideal combination of channels needed to maximize information content changes as a function of state of the atmosphere in a complex manner has important implications for the development of a ice cloud retrieval scheme and will be discussed in Section 4.6.

The analyses of Figures 4.4 to 4.8 were based both on our best estimate of measurement and forward model uncertainty as outlined in Section 4.4 and on a retrieval scheme constrained with both CloudSat cloud boundary and MODIS albedo information. Information content under less ideal retrieval conditions, namely retrievals without

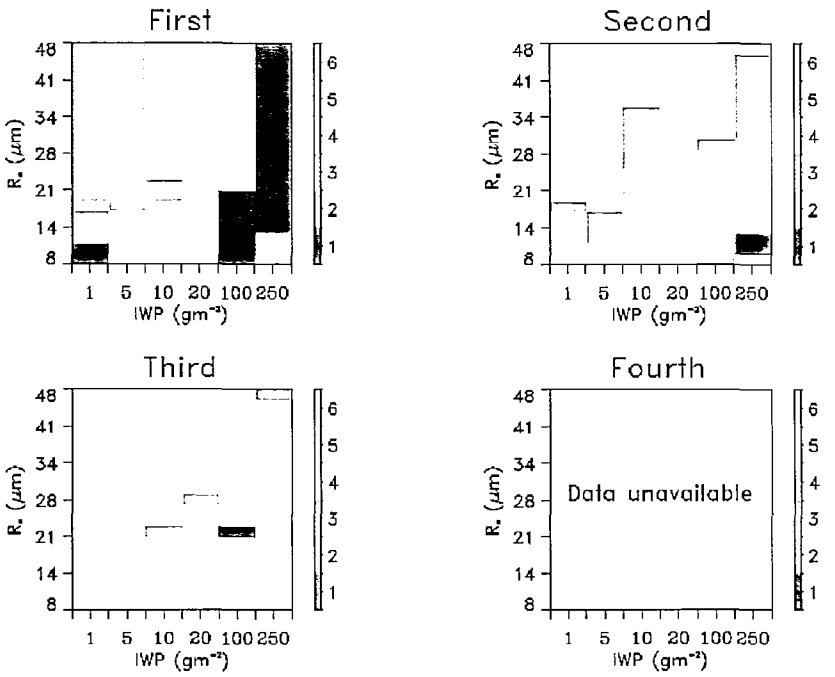

Figure 4.9: The selection of the first, second, third, and fourth channel for each of the IWP- effective radius combinations for the 9 km cirrus cloud case constrained with CloudSat cloud boundary information. The channels are not shown as individual channels but reported in groups with similar characteristics for clarity of presentation. Dark blue represents the conservative scattering channels; light blue the non- conservative scattering channels; green the water vapor channels; yellow the SWIR (solar and emitting 3.78 and 4.05 μm) channels; orange the infrared channels; and red the CO_2 slicing channels.The absence of color indicates the addition of measurements did not add any information relative to the noise of the analysis.

co-incident CloudSat radar profiles and at nighttime, is now examined. As Cooper et al. (2003) showed that retrieval results were heavily dependent upon proper error characterization, we also consider the impact of improper representation of forward model errors on optimal channel selection.

We first relaxed the standard deviation of our cloud temperature uncertainties from 1.5 K to 15 K and the albedo uncertainty from 10 percent to 30 percent, essentially mimicking an observational system dependent upon climatology as a constraint. Figure 4.10 shows that the ideal combination of measurements necessary to maximize information content for these assumptions are the 11.0 and 11.9 μm infrared channels in addition to

the 0.66 and 2.13 μm channels chosen for the CloudSat base case of Figure 4.4. These additional channels are now needed to supply cloud temperature information that was previously constrained by CloudSat cloud boundary information. This example also brings up the fact that the MODIS measurements contain more information when used without CloudSat than when used with it. Figure 4.11 shows that for many IWP and effective radius combinations, often three or even four channels are needed to optimize information content without CloudSat as compared to the usual two or maybe three measurements needed for the with CloudSat case. While this result may be counter-intuitive, it is important to remember that the case with CloudSat has smaller retrieval error as it effectively constrains the final solution to a smaller set of possible states than case the without CloudSat, as seen in Figures 4.12b and 4.12c. The increased information as displayed in Figure 4.12a simply results from the fact that the *a priori* state is much smaller for the case with CloudSat radar profiles and therefore results in less possible information for the MODIS measurements by definition.

Figure 4.13 explores the information content for a night-time retrieval for the base cloud case of Figure 4.4. Since we have no visible information, the 4.05 and 11.0 μm channels are selected yielding a split- window type approach. The 4.05 μm SWIR channel becomes much more useful during the nighttime, simply because of the loss of the large uncertainties associated with the scattering of the direct solar beam in daytime. Both the nighttime and without CloudSat cases emphasize the notion that the optimal channels needed to maximize information content not only dependent on the state of the atmosphere but also the uncertainties characteristic of the observing system.

This last point is further emphasized by performing an information content analysis assuming that errors in radiance from assumptions of cloud microphysics and atmospheric profile were a constant 10 percent for all channels and all atmospheric states. This assumption essentially mimics the approaches taken by those cloud retrieval schemes that do not explicitly account for radiance error. As Figure 4.3 shows, a flat error of 10 percent essentially reduces the error in most shortwave channels and increases the error

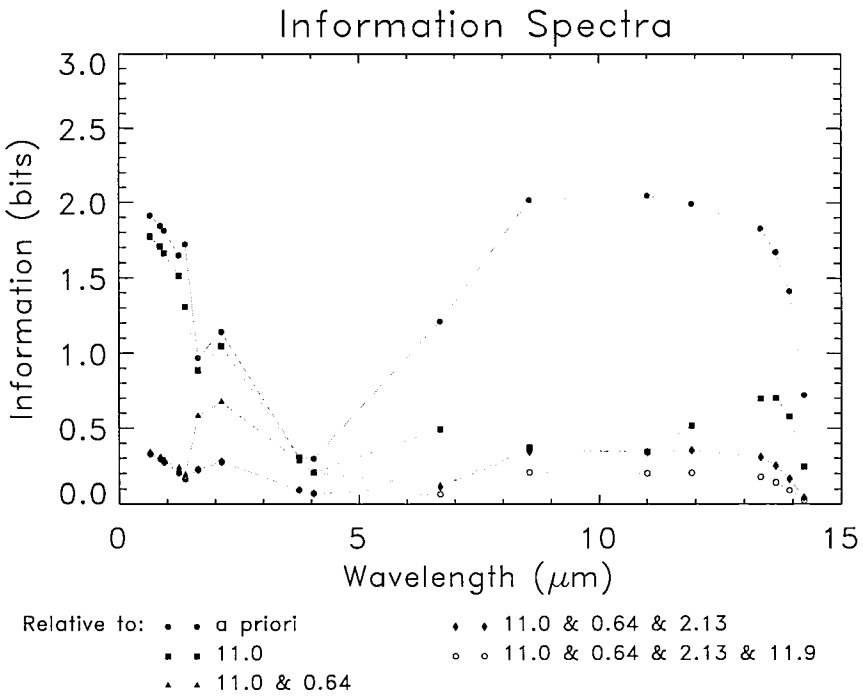

Figure 4.10: Information spectrum analysis for the ice cloud of Figure 4.4 but now for the scenario in which complementary CloudSat radar profiles are not available.

in the longwave channels. Figure 4.14 shows that for the thin cloud case of Figure 4.6, the optimal combination of measurements change from the 4.05 and 11.9 μm channels found with realistic errors to the 1.37 and 3.74 μm with flat errors. The retrieval approach essentially shifts from a split- window to a NK type approach, highlighting the need for realistic treatment of errors to maximize retrieval information as a function of state of the atmosphere. This flat error case also stresses the importance of the objective approach for channel selection. Our general physical understanding as supported by the singular vector analysis of Figure 4.15 suggests that the selected channels provide IWP and effective radius information. Indeed, the 3.74 μm should have sensitivity to effective radius (Stone et al. (1990)) and the 1.37 μm to IWP (Gao and Kaufman (1995)), but it is not clear why these channels are more useful than similar behaved channels. It is only the formal information content approach that allows the un- biased selection of the ideal channels.

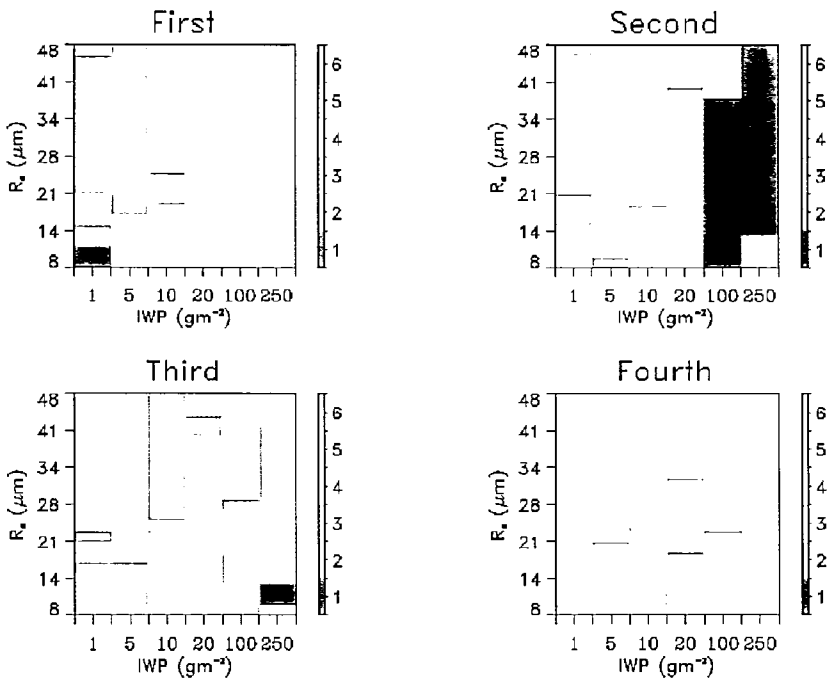

Figure 4.11: The selection of the first, second, third, and fourth channel for each of the IWP- effective radius combinations for the 9 km cirrus cloud case that is dependent upon a climatological constraint for cloud boundary information. The channels are not shown as individual channels but reported in groups with similar characteristics for clarity of presentation. The absence of color indicates the addition of measurements did not add any information relative to the noise of the analysis.

6. Implications for Global Retrieval Approach

Different combinations of channels were selected for each of the different cloud cases examined above, meaning no combination of two or three channels can ensure an accurate retrieval under all conditions given uncertainties in cloud microphysical properties. Since using different channels for an operational retrieval for each pixel is impractical and can lead to discontinuities in global products at the interfaces between different techniques, we instead suggest a retrieval scheme composed of the same five channels regardless of scene. Based upon the nearly 800 cloud cases in this analysis, the retrieval scheme should consist of a combination of error- weighted visible, near- infrared, and infrared channels chosen to use the inherent sensitivities in each of these regions to

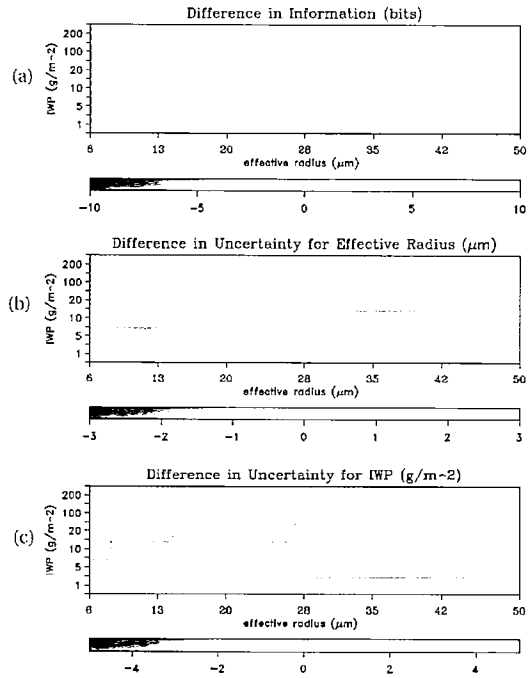

Figure 4.12: Figure a shows the difference in information from all MODIS channels used without and with complementary CloudSat cloud boundary information. Figures b and c show the difference in retrieval uncertainty for effective radius and IWP, respectively, again for without and with CloudSat information.

ensure high information content across expected cloud and atmospheric conditions.

To facilitate an understanding of the potential for this error- weighted, multiple-channel retrieval approach, the information content analysis is applied to a theoretical five- channel retrieval scheme, consisting of the 0.66, 2.13, 4.05, 11.0, and 13.3 μm channels as seen in Figure 4.16. The bottom right plot of Figure 4.16 shows the total information from all MODIS channels as a function of effective radius and IWP for a cirrus cloud at 9 km with the *a priori* assumptions described above for our base case. The other panels of Figure 4.16 represent the fractional information resulting from the addition of each channel into a theoretical retrieval. The upper left plot for 11.0 μm represents the fractional information contained in that channel alone, the 0.646 μm plot represents the fractional information by using that channel with the 11.0 μm channel,

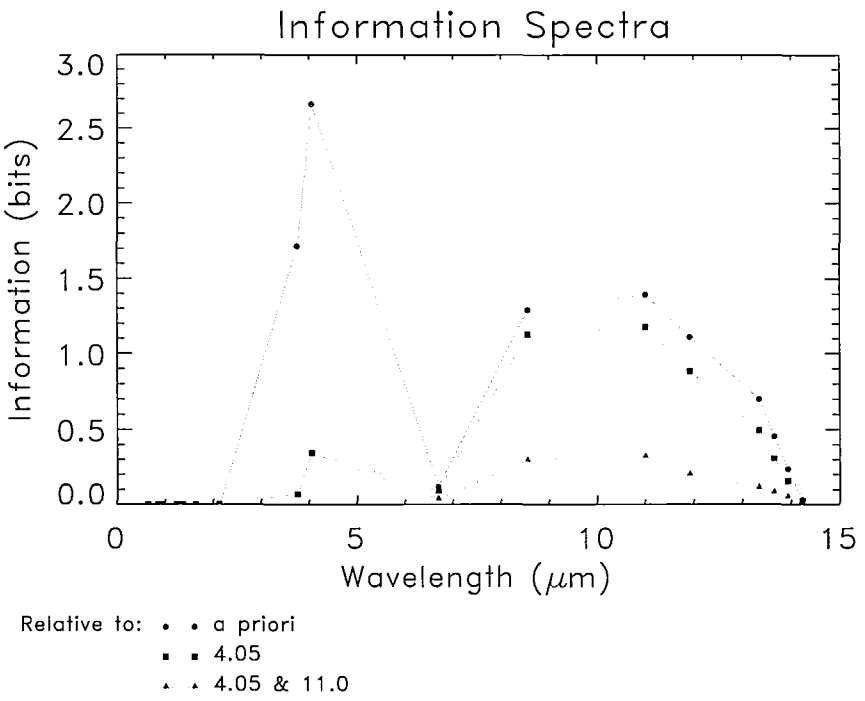

Figure 4.13: Information spectrum analysis for the ice cloud case of Figure 4.4 but now for a night-time retrieval.

and so on until we have the fractional information for the five channels as designated by the 13.34 μm plot. Figure 4.16 shows that the theoretical five- channel retrieval scheme captures a significant fraction of total information for most IWP- effective radius combinations for a cirrus cloud at 9km. Although the scheme is least effective for the large IWP cases, it still captures nearly 80 % of the total information. The addition of more channels to the retrieval scheme would be superfluous as the little remaining information is spread out more or less equally among the remaining MODIS channels.

The advantages of a unified five- channel approach best can be appreciated by comparing information content analysis from this approach with traditional multi- spectral retrieval schemes such as the split- window and NK methods. Panel 2 of Figure 4.17 shows the information content analysis for the traditional split- window approach, using just the 11.0 and 12.0 μm channels. As expected, the use of these two channels provides a significant amount of information for optically thin clouds, as designated by the sig-

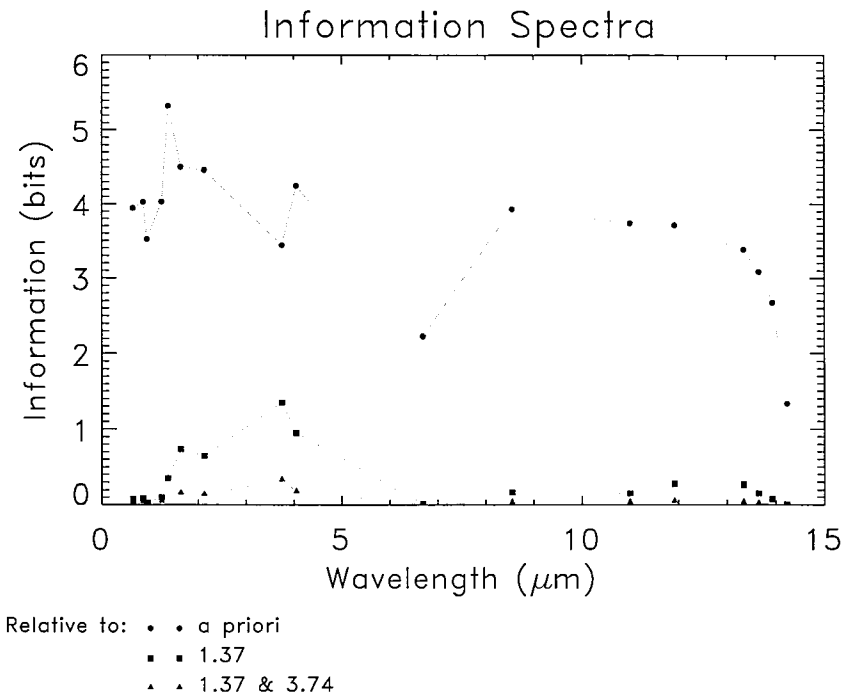

Figure 4.14: Information spectrum analysis for an ice cloud with effective radius of 16 μm, IWP of 10 g/m^2, and cloud height at 9 km as in Figure 4.6 but now assuming constant error of 10 percent for all channels and states of the atmosphere.

nificant amount of oranges and reds on the second panel. The information content for very thin and for thick clouds, however, is poor. It is only the addition of the visible and near- infrared channels to this retrieval scheme, e.g. the third and fourth panels of Figure 4.17, that allow us to optimize retrieval information content for most combinations of effective radius and IWP. Similarly, Panel 2 of Figure 4.18 shows the information content analysis for a NK type approach using the 2.13 and 0.646 μm channels. Although these two channels capture significant amounts of information for some combinations of effective radius and IWP, they perform poorly for others. It is only the addition of the infrared and SWIR channels, e.g. the third and fourth panels of Figure 4.18, that allow for a retrieval with high information content for all expected states of the atmosphere. The practical implications of these differences in information for operational retrieval schemes in terms of both retrieval bias and random error will be the focus of a future

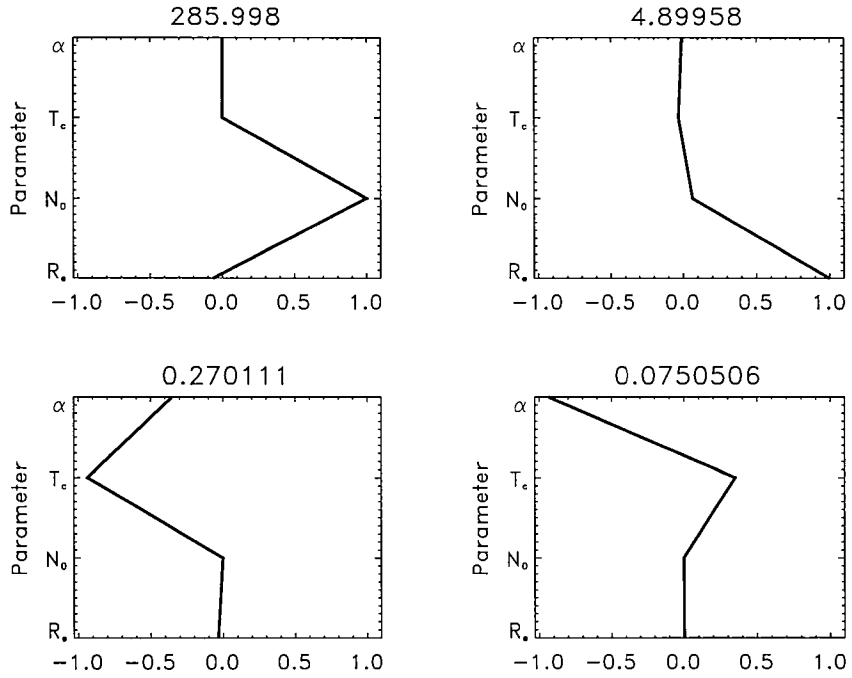

Figure 4.15: Singular value analysis for the ice cloud of Figure 4.14.

work.

7. Conclusions

In this work, a formal information content analysis presented in Part I has been used to objectively select the optimal combination of MODIS measurements for an ice cloud microphysical property retrieval scheme when constrained by CloudSat CPR cloud boundary information. Channel selection is determined through a realistic characterization of not only the sensitivity of TOA radiances to desired retrieval parameters but also to the uncertainties resulting from both the measurements themselves and from the forward model assumptions used in translating between observation and retrieval space. The channels selected for the retrieval are strongly dependent upon both cloud and atmospheric properties and the uncertainties characteristic to the observation system. Due to

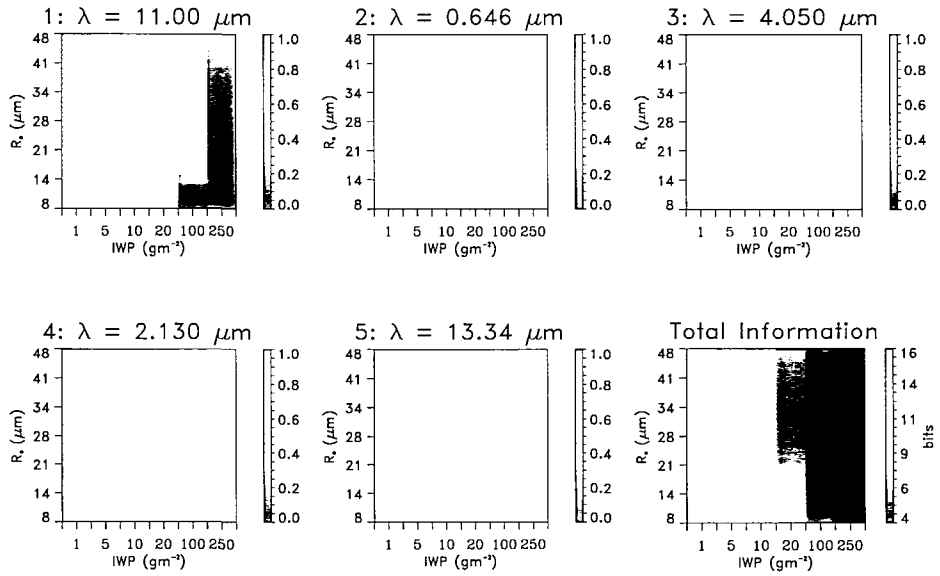

Figure 4.16: Fractional information content analysis for our proposed five channel retrieval scheme as a function of IWP and effective radius for an ice cloud at 9 km. The bottom right panel shows total information for all 17 MODIS channels. Each of panels labeled 1 to 5 indicate the fractional information from each channel added sequentially.

the complexities of these sensitivities to atmospheric state and the need for a consistent retrieval scheme for an operational retrieval, we suggest a five channel retrieval approach consisting of a combination of error- weighted visible, near- infrared, and infrared channels. Such an approach can be adopted independent of scene since it makes use of the inherent sensitivities in each of these spectral regions to ensure high information content regardless of cloud and atmospheric properties. Tentatively, the 0.64, 2.11, 4.05, 11.0, and 13.3 μm channels are suggested, but it should be noted that any of these channels could be replaced by another channel with similar characteristics with little loss in retrieval information. The optimal- estimation based retrieval framework (Rodgers (1976); Marks and Rodgers (1993)), which can incorporate information from multiple sensors and provide a built in set of diagnostics to quantify retrieval and measurement uncertainties, will provide the ideal means to implement this flexible, error-weighted

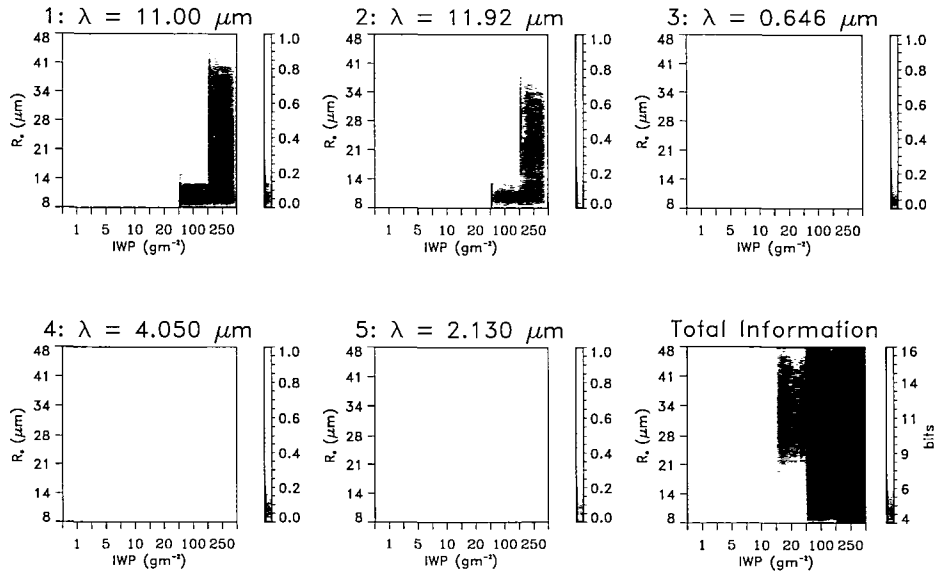

Figure 4.17: Fractional information content analysis for the spit- window retrieval scheme as a function of IWP and effective radius for an ice cloud at 9 km. The number 2 panel shows the fractional information from the split- window approach, the number 5 panel the fractional information from our proposed five- channel retrieval scheme.

retrieval approach. Application of such a unified retrieval approach would have the additional benefit of providing consistency in retrieved cloud products across different satellite and field measurement campaigns.

The analyses presented here apply only to single- layer clouds overlying an isotropically, reflecting ocean surface with a simple observation geometry of an overhead sun with nadir observation angle. Although much additional work in quantifying measurement and forward model error covariances for a variety of different land surfaces and retrieval geometries is needed for the development of an operational retrieval, the complete methodology for this work as outlined here and in Part I is already in place. In fact, the formal information content methodology presented in both part I and this paper should be considered at a more general level than just the retrieval of cloud microphysical properties. To realize the full potential of the rigorous information content analyses

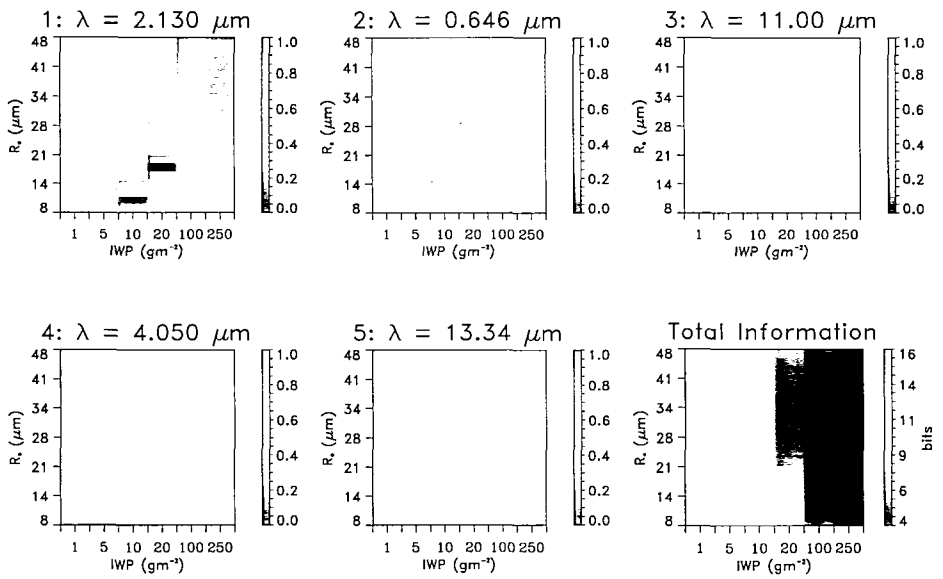

Figure 4.18: Fractional information content analysis for the NK retrieval scheme as a function of IWP and effective radius for an ice cloud at 9 km. The number 2 panel shows the fractional information from the NK approach, the number 5 panel the fractional information from our proposed five- channel retrieval scheme.

outlined here, they should be applied in the developmental stages of future satellite missions to systematically develop instruments from the ground up. In principle a detailed analysis of a wide variety of potential wavelengths could be performed to determine the subset that provide the most information for the desired application based on the accuracies to which they can be modeled and their sensitivities to the retrieval parameters. Then this information could be used to design an optimal channel configuration upon which an instrument could be constructed.

Although examining the reduction of entropy for various retrieval schemes and uncertainty estimates has proved illuminating, the validation of these results is necessary and will be the subject of the next chapter. The implications of the relative differences in total information for various retrieval schemes will be quantified in terms of retrieval bias and random error. Furthermore, the use of real- world data will investigate the

practical utility of our proposed five- channel retrieval scheme and help determine the validity of many of our assumptions. It is hoped this estimate of cloud properties with associated uncertainties based on a realistic assessment of ice cloud physics from this retrieval scheme will be useful in determining what we are capable of knowing about ice clouds and their role in climate processes.

Chapter 5

Assessment of a Five- Channel Estimation- Based Ice Cloud Property Retrieval Scheme over the Global Ocean

1. Introduction

In the previous chapter, a rigorous information content analysis (Shannon and Weaver (1949); Rodgers (2000); L'Ecuyer et al. (2004)) was performed to determine the ideal combination of MODIS channels for an ice cloud microphysical property retrieval scheme constrained with CloudSat cloud boundary information. The channels selected were those that reduced the entropy of the solution space the most, or in terms of the optimal estimation- based retrieval scheme, were those that had the highest ratio between the *a priori* error covariance matrix, S_a, and the retrieval error covariance matrix, S_x. The optimal combination of MODIS channels was found to be heavily dependent upon the state of the atmosphere. As such, a five- channel retrieval scheme consisting of a combination of error- weighted visible, near- infrared, and infrared channels was suggested

to take advantage of the inherent sensitivities found in each of these spectral regions to ensure high information content regardless of the state of the atmosphere. The 0.64 μm, 2.1 μm, 4.05 μm, 11.0 μm, and 13.3 μm channels were tentatively selected for the retrieval scheme, but it should be noted that each of these channels could be replaced by a channel with similar characteristics without significant loss of retrieval information.

Although theoretical calculations involving the reduction of entropy of various a priori and retrieval states are extremely illuminating, the five- channel retrieval scheme needs assessment in context of numerical 'synthetic' experiments and, more importantly, real- world measurements. In other words, the implications of relative information content will be examined in the more practical terms of retrieval performance. The results of these experiments are discussed in context of determining the feasibility of this five-channel approach at an operational level.

Synthetic retrievals are numerical experiments used to quantify retrieval performance. The basic idea of these experiments is to perform a retrieval on a system with well- defined properties, with the difference between the known and retrieved properties simply considered the retrieval bias. The use of the optimal- estimation framework in these synthetic retrievals also allows for an explicit calculation the random error for the retrieval through its set of built- in error diagnostics as explored in Chapter 2.

In the simple infrared cloud property retrieval scheme of Chapter 3, a cloud of known effective radius, optical depth, and cloud temperature was used to generate corresponding top of the atmosphere radiances through the two- layer infrared radiative transfer model. These 'synthetic' radiances were then inverted using the optimal- estimation based retrieval scheme to give our most likely estimate of cloud properties with associated errors based on our error covariance assumptions. If the relationship between the top of the atmosphere radiance and the cloud properties is very well defined and does not suffer from non- uniqueness issues, the problem is trivial as the synthetic and retrieved properties would be the same. For our split- window problem of Chapter 3, uncertainties in both cloud temperature and satellite radiances as quantified in the measurement and

forward model error covariance resulted in both appreciable retrieval bias and random error.

In this chapter, we first will explore the implications of our uncertainty estimates from the previous chapter on the performance of five channel retrieval scheme using these synthetic experiments. In other words, we will quantify how well we can determine ice cloud properties from satellite- based measurements given a realistic assessment of the ice problem. Retrieval performance for the five- channel scheme then will be compared to those of the more traditional split- window (Inoue (1985); Prabhakara et al. (1988)) and Nakajima and King (1990) approaches to determine the practical implications of the information content results of the previous chapter. Since information content was strongly case- dependent, we will finally alter some of our base assumptions such as forward model uncertainties and cloud radiative properties to determine their impact on retrieval performance.

Although these synthetic experiments provide an invaluable tool for testing the behavior of the algorithm under controlled conditions, unfortunately they may be somewhat biased by the fact that similar assumptions are often made in both forward and inverse calculations. These studies must, therefore, be complemented with applications involving real observations. A combination of MODIS Airborne Simulator (MAS) and cloud radar and lidar measurements taken during the The Cirrus Regional Study of Tropical Anvils and Cirrus Layers - Florida Area Cirrus Experiment (CRYSTAL-FACE) will be used to examine the performance of the five- channel retrieval scheme in real world conditions. Again, the five- channel scheme will be compared to more traditional approaches, where again it is hoped differences in retrieval results may allow practical insight into applying this retrieval scheme at an operational level.

2. Optimal- Estimation Retrieval

Before examining the results of either the synthetic or real- world studies, it if first necessary to briefly review the optimal- estimation based retrieval scheme for the MODIS channels. The retrieval scheme is that discussed and chapter 2 and then applied in Chapter 3 to the split- window problem. The interested reader may refer to those sections for the mathematical algorithm details. In the split- window retrieval of Chapter 3, the retrieval parameters as defined in the state vector, $\mathbf{x}$, were optical depth, effective radius, and cloud temperature. For the combined MODIS- CloudSat cloud retrieval, however, we will instead retrieve cloud ice water path (IWP), effective radius, and cloud temperature. The retrieval of the physical IWP should be of interest to those *in-situ* cloud validation and modeling efforts that are more likely to deal in physical than optical space. By retrieving the physical IWP, of course, it is trivial to calculate cloud optical depth for any desired wavelength through knowledge of ice particle size distribution and extinction coefficients.

The observation vector for this retrieval will include the radiances for each of the channels used in the retrieval plus an estimate of cloud temperature found by matching CloudSat cloud boundary information with the ECMWF re-analysis temperature profile. As seen in split- window problem of Chapter 3, both retrieval bias and random error are heavily influenced by a proper characterization of the covariance matrices $\mathbf{S}_y$ and $\mathbf{S}_a$. Determination of $\mathbf{S}_y$ as a function of state of the atmosphere was accomplished through the forward model uncertainty analysis of the previous chapter. Such a characterization will allow the retrieval scheme to change its error assumptions as it steps through it iterations through to its final solution. $\mathbf{S}_a$ and the related $\mathbf{x_a}$ come from climatology of cloud properties and are important not only for their influence on the final solution but also because $\mathbf{x_a}$ is used for the initial guess for each retrieval. It will be shown that a proper selection of $\mathbf{x_a}$ is critical in achieving an accurate retrieval given the relatively large range of expected conditions and large forward model errors associated with the

ice cloud problem.

3. Synthetic Studies

A series of synthetic experiments were performed to quantify bias and random errors for the five- channel retrieval scheme given the results of the uncertainty analysis of the proceeding chapter. Retrieval bias and random error here are defined in terms of the optimal- estimation based retrieval scheme, which returns a probability distribution function with our most likely estimate of cloud properties with associated uncertainties. The difference between the most likely estimate and truth for the fixed assumptions of these synthetic studies is termed the retrieval bias. The retrieval variance divided by truth is the random error, mathematically,

$$\sigma_i = \frac{(\mathbf{S}_{x,ii})^{1/2}}{x_{truth}} * 100 \tag{5.1}$$

where $\mathbf{S}_{x,ii}$ are the diagonal elements of the retrieval error covariance matrix.

Retrieval performance for the five- channel retrieval scheme was examined as a function of IWP and effective radius using the aggregates of Baran et al. (2001) for both the forward and inverse calculations. These retrieval results were then compared to the bi-spectral split- window and Nakajima and King approaches and even to a 16 channel retrieval scheme to try to quantify the results of our information content analysis of the proceeding chapter in terms of cloud retrievables. Base assumptions such as magnitude of forward model uncertainties and cloud optical properties were in turn altered in the five- channel approach to determine their influence upon retrieval results. The results of these experiments are discussed in context of determining the feasibility of this five-channel approach at an operational level. For those readers interested in bypassing the details and avoiding the discussion of 26 highly inter-related figures, a brief summary of the major conclusions from these synthetic studies is found in section 5.3.f.

An obvious difficulty for these studies is the relative importance of the *a priori* guess

in the optimal- estimation framework in determining retrieval bias for those cases when forward model error covariance is large or when sensitivity to retrieved parameters is low. These synthetic experiments were therefore divided into 'thin' and 'thick' cloud cases to allow a different set of a priori assumptions for each, based on the idea that reflectivities from the CloudSat Cloud Profiling Radar (CPR) used in conjunction with the MODIS measurements would allow for a rudimentary classification of cloud thickness, see Table 5.1. IWP ranged from 15 to 75 g/m^2 with an initial guess of 50 g/m^2 for the thin cloud cases and from 105 to 165 g/m^2 with an initial guess of 150 g/m^2 for the thick cases. Although it may be possible to devise a methodology for a more accurate *a priori* guess through either an empirical radar reflectivity- IWP relationship or a Nakajima and King (1990) retrieval scheme, use of a constant *a priori* guess has the additional benefit in that it allows an examination of the importance of the initial guess on retrieval performance. The synthetic retrievals were run at each of the 25 combinations of IWP and effective radius of Table 5.1 for each of the thin and thick clouds. For these base cases, the cirrus clouds were placed at 12 km over an ocean surface assuming a McClatchey Tropical atmosphere with solar zenith and observation angle at nadir. Cloud temperature uncertainty was 1.5 K, consistent with matching CloudSat cloud boundary information to an ECMWF re-analysis temperature profile (Eyre et al. (1993)).

a. Five- Channel Retrieval Base Results

Figure 5.1 shows the normalized retrieval bias for each IWP, effective radius, and cloud temperature for the thick-cloud synthetic experiments of Table 5.1 for our five- channel retrieval scheme based on our best assumptions of forward model uncertainties from the previous chapter and the *a priori* uncertainties listed in Table 5.1. Retrieval bias is less than 15 percent for nearly all states of the atmosphere for each IWP, effective radius, and cloud temperature. Cloud temperature bias is extremely small simply because CloudSat cloud boundary information has been used to constrain the problem; cloud temperature will be neglected for the remaining cases simply because in this retrieval framework

	Thin Cloud Cases	Thick Cloud Cases
R_e truth (μm)	12, 18, 24, 30, 36	12, 18, 24, 30, 36
R_e (μm) initial guess	20	20
R_e σ (μm)	25	25
IWP truth (g/m^2)	15, 30, 45, 60, 75	105, 120, 135, 150, 165
IWP initial guess (g/m^2)	50	150
IWP σ (g/m^2)	100	200

Table 5.1: List of effective radius and IWP combinations used for the synthetic studies with associated *a priori* guess and uncertainties.

it is more a well- defined input than an independent retrieval parameter. (For those readers interested in a more thorough understanding of the impacts of cloud temperature uncertainties on retrieval performance, please see Chapter 3 for an in- depth exploration of the subject.)

Although these retrieval biases are quite small, it does not necessarily imply that the retrieval performance is acceptable. Retrieval bias is somewhat complicated because the *a priori* guess will partially determine the final solution when forward model error is significant, with the obvious example being that for infinitely large forward model error, the retrieved properties will simply be the *a priori* guess. Although retrieval bias is therefore dependent on the mechanics of the estimation- based retrieval, it is still a useful diagnostic in a synthetic framework in comparing different retrieval techniques when the same initial guesses and error assumptions are employed.

To gain a better appreciation of overall retrieval performance, however, we must examine retrieval random error as defined in our retrieval error covariance matrix. Figure 5.2 shows the normalized random error for retrieved IWP and effective radius for the five- channel retrieval scheme thick cloud base case. Retrieval random error for both

IWP and effective radius are generally much larger then the relatively small biases with normalized errors ranging from 30 to 60 percent. Again, these values represent one standard deviation of a probability distribution function about our most probable estimate, indicating potentially large retrieval biases if retrieved and assumed cloud properties do not match. These relatively large retrieval random errors and potential biases for the advanced five- channel scheme suggest a note of caution in putting too much faith in current cloud retrieval products based on much simpler retrieval techniques.

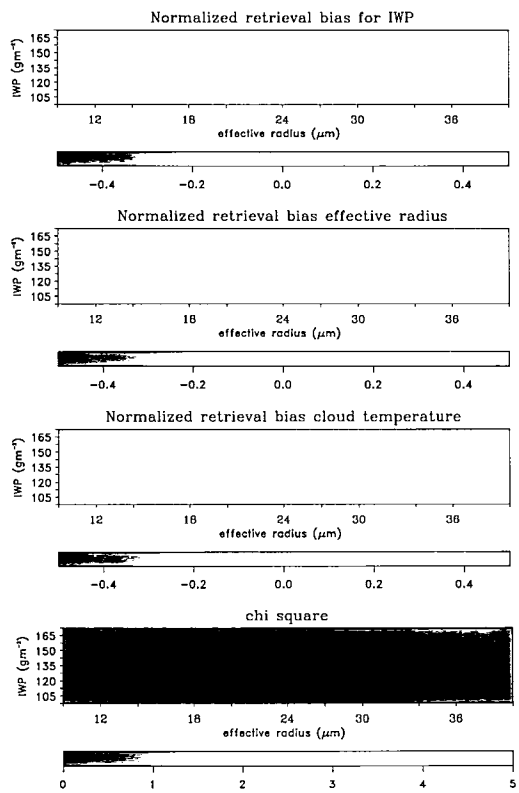

Figure 5.1: Retrieval bias for IWP, effective radius, and cloud temperature are shown in the top three panels, respectively, for the five- channel retrieval scheme for the thick cloud synthetic cases of Table 5.1. Small chi- square diagnostic values as shown in the bottom panel indicate an adequate degree of fit between observations and retrieved cloud properties.

Other than the magnitude of the uncertainties, several other trends of importance are observed in Figures 5.1 and 5.2. Retrieval bias between IWP and effective radius is clearly correlated for these synthetic studies, meaning an error in one retrieved parame-

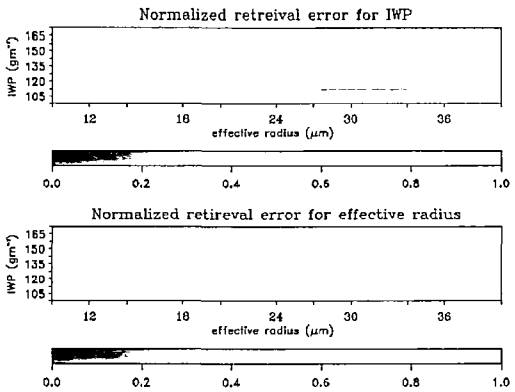

Figure 5.2: Normalized retrieval uncertainty for IWP and effective radius are shown in the top two panels, respectively, for the five- channel retrieval scheme for the thick cirrus cloud cases of Table 5.1

ter induce a corresponding error in the other. This trend is easy to understand in terms of both our estimation- based retrieval scheme and the set-up of our forward model. In our retrieval scheme, we essentially are trying to minimize the difference between our observations and the forward model simulated radiances as mapped from retrieval space. The forward model uses optical depth, which is a function of IWP and effective radius, as direct input to calculate radiance. When the *a priori* assumptions become important to the final solution and the retrieval begins to deviate from truth, the model can allow compensating errors that still allow simulated radiances to somewhat match observations. Figure 5.3 shows both the retrieved and true 0.66 μm optical depths for the thick cloud base case of Figure 5.1. Even though the retrieval returned the wrong IWP and effective radius as in Figure 5.1, most notably for the largest effective radius cases, these biases compensated to produce the correct optical depth. For example, in the 36 μm effective radius cases, retrieved IWP was too small (decreased optical depth) but was compensated by a retrieved effective radius that was also too small (increased optical depth). For an extreme case with very large compensating errors that still yield a reasonable optical depth, it is good to think in terms of the information content analysis of the previous chapter. Such cases should indicate that only one piece of information, in this case optical depth, can actually be retrieved from the measurements.

These results also have important implication for traditional look- up table schemes that retrieve cloud optical depth and effective radius, such as the Nakajima and King approach shown in Figure 5.4. This scheme relies on the idea that reflectance at the 0.66 μm channel is independent of particle size, meaning that the backscattered radiation is only dependent upon optical depth. Theoretically, once optical depth is determined, effective radius is uniquely determined through the 3.80 μm radiance. The problem with this approach, however, as illustrated by the above discussion of compensating errors is that measured 3.80 μm radiance is a function of both effective radius and IWP. The curves generated in Figure 5.4 necessarily assume some droplet size distribution and number concentration (IWP) for each effective radius that combine to yield the correct optical depth as indicated by the 0.66 measurement. As long as the relationship between IWP and effective radius is consistent for all effective radius, the unique monotonic increase in 3.80 μm radiance with decreasing effective radius is observed. The difficulty here is that the IWP- effective radius- optical depth relationship is not unique. If the assumptions in IWP used to generate the look-up tables fail to match real cloud properties for a given retrieval, then retrieved effective radius may be rather dubious. In essence, these schemes have assumed a built- in relationship between IWP and effective radius that cannot be verified through the retrieval of just optical depth and effective radius. It is only through the additional degree of freedom resulting from the inclusion of both IWP and effective radius in the retrieval vector that allows a more meaningful retrieval of effective radius.

The effects of these correlated errors in IWP and effective radius also has implications for determination of overall uncertainty in our indirectly retrieved cloud optical depths. Since optical depth is a function of both IWP and effective radius, it is necessary to consider our $\mathbf{S}_x$ calculations to determine total uncertainty. In general, the uncertainty in

$$y = f(x_1, x_2, x_3, ..., x_n) \tag{5.2}$$

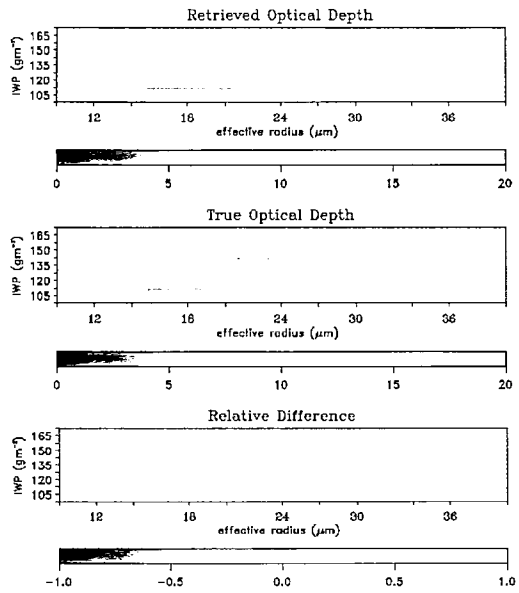

Figure 5.3: Indirectly retrieved optical depth, true optical depth, and the fractional difference (truth - retrieved) are shown in the top three panels, respectively, for the five channel retrieval scheme for the thick cloud synthetic cases of Table 5.1.

is given by (NIST, 94)

$$\delta y = + \left[\sum_{i=1}^{n} \left(\frac{\partial f}{\partial x_i} \right)^2 (\delta x_i)^2 + 2 \sum_{i=1}^{n-1} \sum_{j=i+1}^{n} \left(\frac{\partial f}{\partial x_i} \right) \left(\frac{\partial f}{\partial x_j} \right) \delta x_{ij} \right]^{1/2} \tag{5.3}$$

We find the partial derivative terms through the following expression relating optical depth to IWP and effective radius,

$$\tau = \frac{3}{2} \frac{IWP}{\rho \; r_{eff}} \tag{5.4}$$

and the uncertainties, δx_i, δx_j, and δx_{ij}, from our retrieval covariance matrix, $\mathbf{S}_x$. Figure 5.5 shows that the fractional uncertainty in retrieved optical depth is usually under 20 percent for most of the thick cloud cases. random errors of up to 50 percent are found for the smallest effective radius- large IWP combinations but it is not entirely certain such extreme combinations could actually exist in nature. The correlation in errors between IWP and effective radius in our forward model calculations, as introduced through the

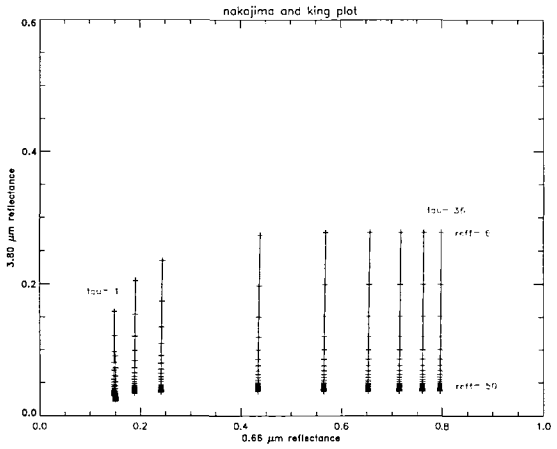

Figure 5.4: Reflectance functions for 0.66 μm and 3.80 μm for ice clouds with effective radius between 6 μm and 50 μm and optical depths between 1 and 50.

K matrix, reduce the optical depth random errors to fractional values generally less than either IWP or effective radius.

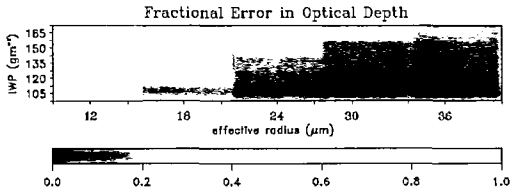

Figure 5.5: Fractional uncertainty in optical depth for the five channel retrieval scheme for the thick cloud synthetic cases of Table 5.1

Figures 5.1 and 5.2 also illustrate the importance of the *a priori* assumptions on our retrieval scheme. This idea is most easily seen in examining retrieval bias as a function of distance from the *a priori* guess of 150 g/m^2 and 20 μm. A clear minimum in IWP bias is seen at the *a priori* guess of 150 g/m^2 as indicated by the greenish line. Since errors are correlated, a good *a priori* guess in one variable will ultimately improve the retrieval of the other variable, e.g. the bias in effective radius shows a clear minimum at the IWP guess of 150 g/m^2. Similarly, bias for both effective radius and IWP is generally worst for those cases furthest from the initial guess of 20 μm and best for those cases closest. Instead of bogging down into a detailed mathematical description

of the A matrix in relation to retrieval uncertainties here, it will simply be re-stated that these trends indicate the importance of making the best *a priori* guess possible for this retrieval solution. Use of either an empirically driven radar reflectivity- IWP relationship or a bi- spectral passive approach are obvious possibilities for making a reasonable first guess for the five- channel retrieval scheme. Assessment of the operational utility of such an approach will be the focus of future research.

Figures 5.6 - 5.8 show synthetic retrieval results for our five- channel retrieval scheme for the thin cloud properties and *a priori* assumptions as listed in Table 5.1. Many of the major trends and observations from the thick cloud cases described above are also seen in these thin cloud cases, albeit with slightly different numbers. It is important to present these results, however, to later facilitate comparisons between different retrieval approaches and assumptions as a function of state of the atmosphere. Figure 5.6 shows retrieval bias for the five- channel retrieval approach for the thick cloud cases is again small with discrepancies up to around 15 percent for both IWP and effective radius. Compensating errors in either effective radius or IWP are made such that the correct optical depth is found, see Figure 5.7. The importance of the *a priori* guess is again important as trends in bias are seen relative to both the guesses of effective radius of 20 μm and IWP of 150 g/m^2. Retrieval random errors for the thin cloud cases as in Figure 5.8 are slightly smaller than for the thick cloud cases, with errors generally under 30 percent but up to a maximum of about 50 percent.

b. Effects of Retrieval Channel Selection

In this sub-section, we will examine the influence of channel selection for retrieval bias and random error. We performed synthetic tests using the traditional bi- spectral split-window and Nakajima and King approaches for the test cloud cases from Table 5.1 to determine relative retrieval performance as compared to our five- channel scheme. Table 5.2 lists the MODIS bands used for each scheme. Figure 5.9 and 5.10 show retrieval bias for IWP and effective radius, respectively, for the five- channel, Nakajima and King, and

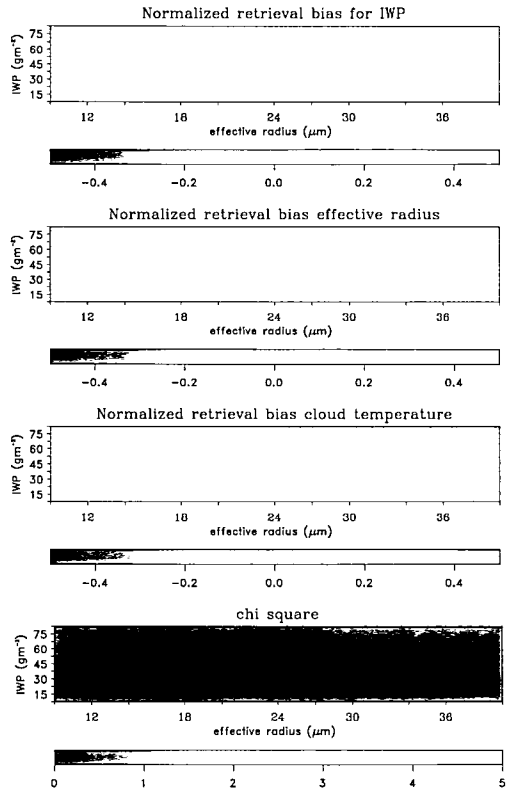

Figure 5.6: Retrieval bias for IWP, effective radius, and cloud temperature are shown in the top three panels, respectively, for the five- channel retrieval scheme for the thin cloud synthetic cases of Table 5.1. Small chi- square diagnostic values as shown in the bottom panel indicate an adequate degree of fit between observations and retrieved cloud properties.

split- window retrievals for the thick clouds. Retrieval bias for the five- channel scheme is always better for both IWP and effective radius than for either the Nakajima and King or split- window schemes but is generally much closer in magnitude to the Nakajima and King than the split- window approach. Similarly, Figure 5.11 and 5.12 show that retrieval random error is best for the five- channel retrieval scheme but again retrieval errors are much closer to the Nakajima and King than the split- window approach.

These result are expected as the five- channel retrieval scheme is supposed to use information from those channels with the greatest utility dependent upon state of the atmosphere. For these thick cloud cases, we would expect little sensitivity for the emission-based split- window channels, meaning information for these retrievals must come from

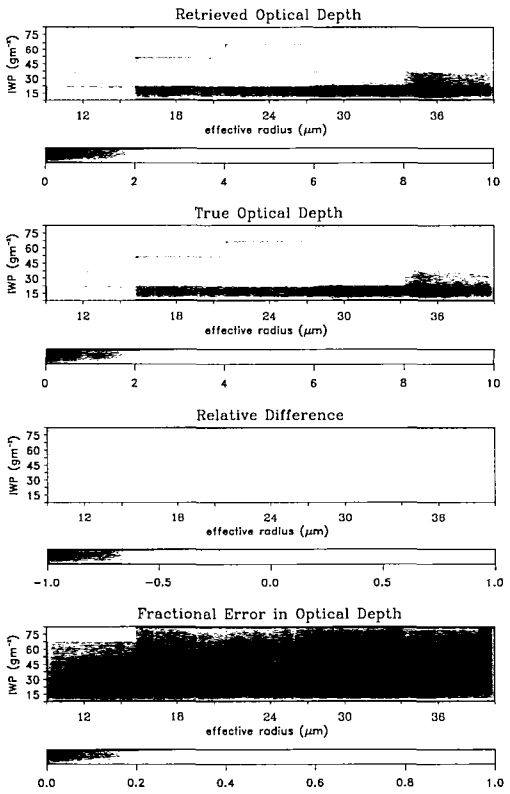

Figure 5.7: Indirectly retrieved optical depth, true optical depth, and the fractional difference (truth - retrieved) are shown in the top three panels, respectively, for the five channel retrieval scheme for the thin cloud synthetic cases of Table 5.1. Normalized uncertainty in optical depth is presented in the bottom panel.

the shortwave scattering Nakajima and King bands. Indeed, retrieval bias and random error agree quite well for the five- channel and Nakajima and King schemes. The slightly better five- channel retrievals result from the inclusion of the shortwave- infrared 4.05 μm channel which helps better constrain the solution. Figure 5.13 shows that the biases seen in Figures 5.9 and 5.10 act in such a way to yield the correct optical depth for both the five- channel and Nakajima and King approaches. As expected for these thick cloud cases, the split- window technique essentially fails, resulting in substantial uncertainties. Although the retrieval biases seem to still produce the correct optical depth, it really only works for many of the thick cloud cases because the solution converges to the relatively high optical depth associated with our *a priori* guess of 20 μm and 150 g/m^2. Figure 5.14 shows very small values for the A-matrix for both IWP and effective radius for the

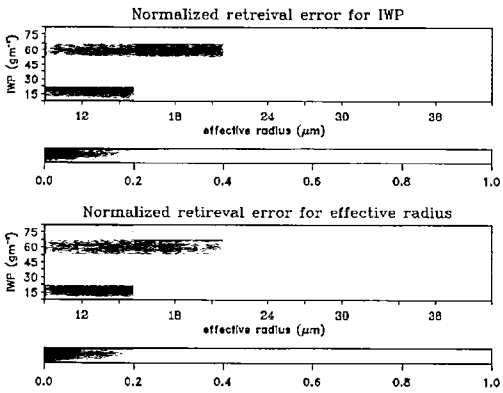

Figure 5.8: Normalized retrieval uncertainty for IWP and effective radius are shown in the top two panels, respectively, for the five- channel retrieval scheme for the thick cirrus cloud cases of Table 5.1. Absolute retrieval uncertainty again for IWP and effective radius are shown in the bottom two panels.

split- window scheme indicating heavy retrieval reliance on the *a priori* assumptions.

Figures 5.15 - 5.18 show that retrieval bias and random error for the thin cloud cases are significantly better for the five- channel retrieval approach than for either the Nakajima and King or split- window approaches. Retrieval bias of up to 50 percent and retrieval random errors of up to 100 percent are found for both the two- channel retrieval techniques. Although large, these numbers agree well with the previous work from Chapter 3 where errors of 35 to 95 percent in effective radius were found using the split- window approach constrained with CloudSat cloud boundary information. Our information content analysis of the proceeding chapter suggested that the emission- based split- window approach should be more useful than Nakajima and King due to the large uncertainties associated with single- scattering effects for these relatively low optical depth clouds. We therefore would expect retrieval performance for the split- window technique to be very much like the retrieval performance for the five- channel technique for optically thick clouds.

Split- window bias and random errors, however, are actually much closer in magnitude to the Nakajima and King approach than the five- channel. This unexpected deviation has several possible causes. First, the inclusion of the 4.05 μm channel in the

Schemes	MODIS Channels	Wavelength (μm)
Five- Channel	01	0.64
	07	2.13
	23	4.05
	31	11.0
	33	13.3
Nakajima and King	01	0.64
	07	2.13
Split- Window	31	11.0
	32	12.0

Table 5.2: List of MODIS channels and wavelengths used for each of the multi- channel retrieval schemes.

five- channel approach will benefit the retrieval and may result in better performance than just the infrared channels alone. Second, it is possible that the retrieval schemes with just two channels are inherently more susceptible to the compensating errors in retrieved IWP and effective radius than the five- channel scheme, simply because they have more play in retrieved parameters in matching a smaller number of observations. Figure 5.19 shows the difference in retrieved versus true optical depth for these synthetic studies for each of the retrieval schemes. These retrieval results re-cast in optical depth form now match expectations, as the split- window approach matches the correct optical depth for all cases while the Nakajima and King technique occasionally fails.

The synthetic studies from this section indicate the five- channel retrieval approach consistently performed better in terms of bias and random error for both the thick and thin cloud cases than either of the two- channel approaches. The error- weighted, five-channel scheme consistently outperforms the other techniques as it automatically places retrieval emphasis on those channels with the greatest information content as a function of the state of the atmosphere. In addition, the inclusion of the 4.05 μm channel provides additional information into the retrieval format that is lacking in either of the two-

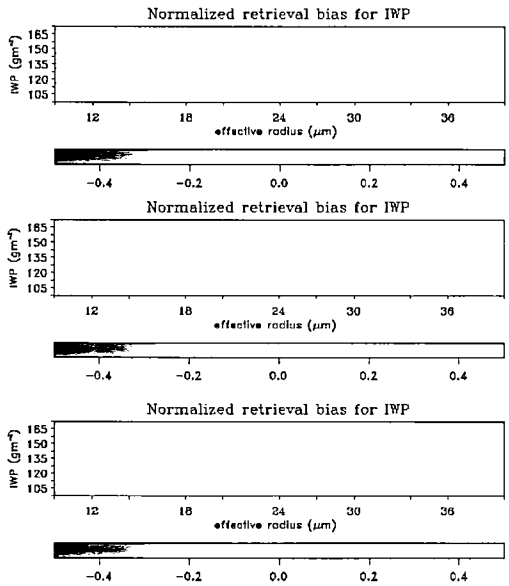

Figure 5.9: Normalized retrieval bias for IWP for each the five channel (top), Nakajima and King (middle), and split- window (bottom) approaches for the thick cloud synthetic cases of Table 5.1.

channel schemes. The obvious question becomes, if five- channels works significantly better than two channels, why not just use ten channels or, even better, all the channels to improve retrieval performance? Figures 5.20 and 5.21 show retrieval bias and random error, respectively for the five- channel and 16 channel retrieval schemes. The 16 channel scheme performed slightly better than our proposed five- channel scheme with biases close to zero and random error generally under 25 percent.

A 16 channel retrieval scheme, however, is impractical causing a huge increase in computational cost for a relatively small gain in retrieval performance. A further complication to such a large number of channels for an operational retrieval is the difficulties in achieving convergence for the optimal- estimation based algorithm. These synthetic studies were ideally controlled numerical experiments with well defined optical properties linked in a precise manner across channels. In the real- world, cloud optical properties may behave in a spectrally un-predicted manner that makes minimization of our cost function unlikely. Perhaps, even more importantly, each channel has its

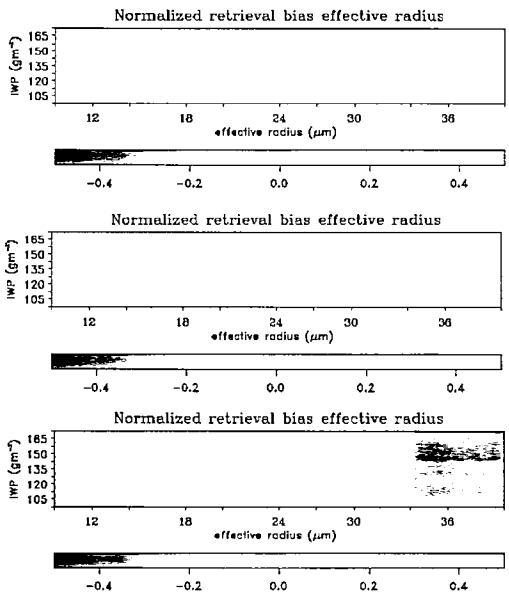

Figure 5.10: Normalized retrieval bias for effective radius for each the five channel (top), Nakajima and King (middle), and split- window (bottom) approaches for the thick cloud synthetic cases of Table 5.1.

own sources of uncertainty, e.g. ice crystal habit or temperature profile assumptions, that will not be correlated between channels. Random deviations about our expectations as a function of wavelength could cause convergence difficulties even if we have luckily guessed cloud radiative properties accurately. We therefore have picked a relatively tractable five- channel approach. The practical implications resulting from our assumptions of cloud radiative properties, and real- world operational considerations for this five- channel scheme will be examined in both the remaining synthetic studies and CRYSTAL-FACE MAS retrievals.

c. *Effects of Error Assumptions*

The synthetic retrievals described above depended on our best estimate of the state dependent measurement and forward model error as described in Chapter 4. As we did in the information content analysis of the proceeding chapter, we will assume a combined forward model and measurement error of 10 percent for all MODIS channels and

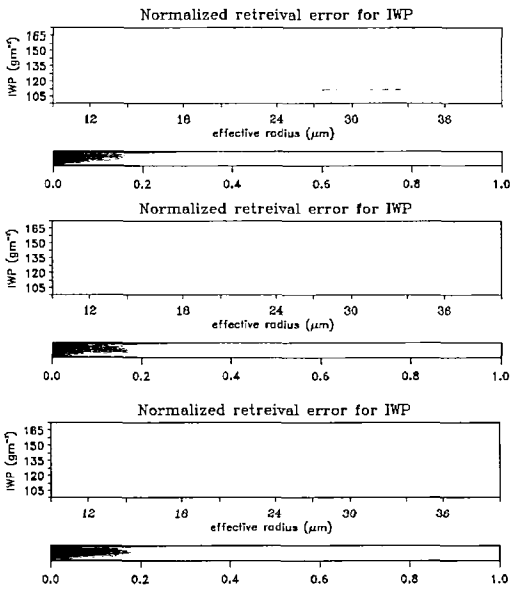

Figure 5.11: Normalized retrieval uncertainty for IWP for each the five channel (top), Nakajima and King (middle), and split- window (bottom) approaches for the thick cloud synthetic cases of Table 5.1.

states of the atmosphere. Figures 5.22 and 5.23 show retrieval bias and random error, respectively, for both IWP and effective radius for thin clouds for both state dependent error and for flat 10 percent errors. The flat 10 percent error case reduces the uncertainties in the scattering channels and allows the retrieval scheme to take advantage of the large sensitivities found at these wavelengths. As a result, both bias and random error dramatically decrease, except for the very thin optical depth clouds in the bottom right corner whose forward model uncertainties actually increased by switching to a flat 10 percent error. Retrieval random errors are generally under 20 percent for both IWP and effective radius except again for the very thin clouds. Although not shown, optical depths are matched perfectly for all these cloud cases. These figures essentially quantify the importance of our uncertainty analysis of the proceeding chapter.

If forward model and measurement uncertainties could be reduced to 10 percent, we could ensure much more accurate retrievals for almost all states of the atmosphere. The obvious difficulty is to determine a way to reduce these uncertainties. Advancements

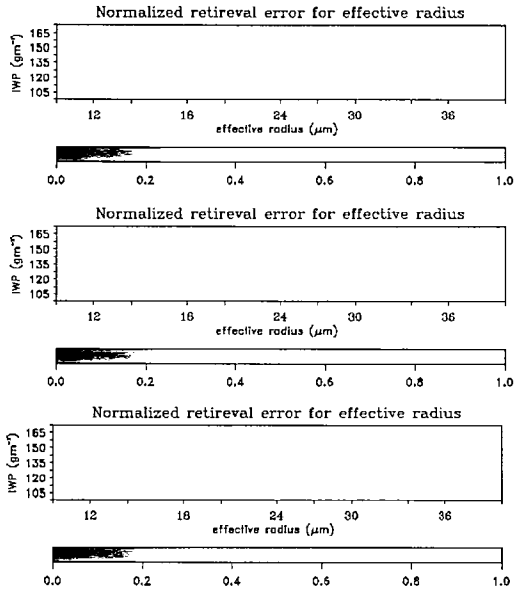

Figure 5.12: Normalized retrieval uncertainty for effective radius for each the five channel (top), Nakajima and King (middle), and split- window (bottom) approaches for the thick cloud synthetic cases of Table 5.1.

in the determination of real- world cloud properties through a combination of *in-situ* measurements and theoretical modeling along the lines of Yang et al. (2000); Baran et al. (2001) would reduce the range of expected radiative properties thus decreasing the magnitude of forward and measurement error covariances. It may also be possible to use multiple observations from several viewing angles to gain some *a priori* knowledge of the crystal type for a given radiance measurement thereby allowing a means to justify reducing the magnitude of the covariance assumptions.

d. Effects of Single Scatter Properties

The synthetic retrievals described above depended on the use of Baran's randomly oriented randomized hexagonal ice aggregates for both the forward and inverse calculations. In this sub-section, we will alter these assumptions to examine their implications for retrieval performance. For the cases above where Baran's cloud properties were used in both forward and inverse calculations, biases were the result of the relative magni-

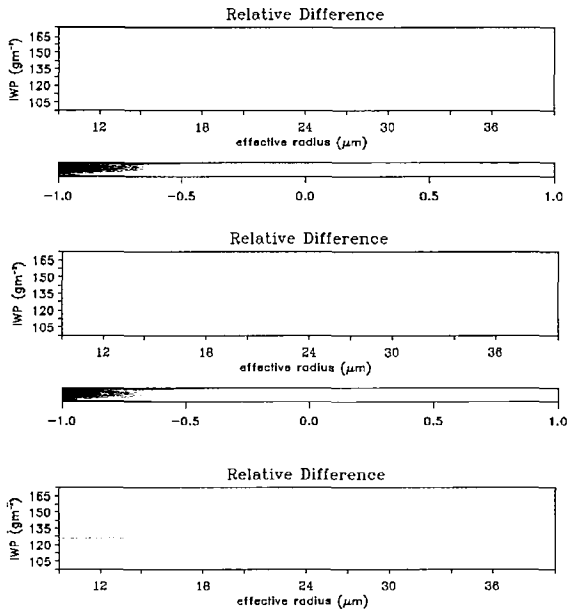

Figure 5.13: Normalized difference between retrieved and true optical depth for each the five channel (top), Nakajima and King (middle), and split- window (bottom) approaches for the thick cloud synthetic cases of Table 5.1.

tudes of the sensitivity- weighted forward model and *a priori* uncertainties. Retrieval biases go to zero as forward model uncertainties go to zero. If, however, we were to use different sets of radiative properties in the forward and inverse calculations, we could get some idea of retrieval bias resulting from bad assumptions of cloud radiative properties in our forward model. These experiments will essentially model the real- world retrieval scenario from a given set of satellite observations where cloud radiative properties cannot be known *a priori* and do not match our forward model assumptions. Technically, these biases already have been characterized by our retrieval scheme as quantified in our retrieval error covariances based on our best estimates of forward model and *a priori* uncertainties. The biases resulting from using different assumptions of cloud radiative properties in the forward and inverse problems should really fall somewhere in the range of random error estimates for the original cases where the same radiative properties were used forward and back. It is important, however, to examine the results from these synthetic tests not only to show that these biases indeed agree with our random

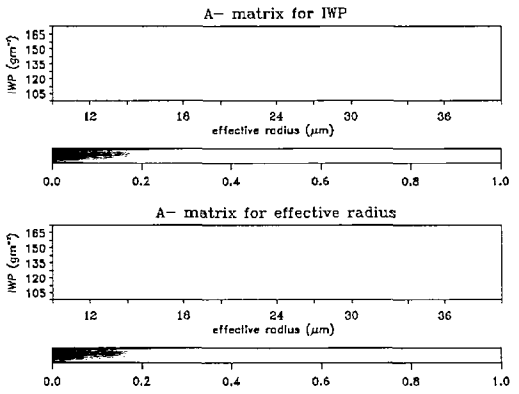

Figure 5.14: Diagonal elements of the A-matrix for IWP and effective radius for the split-window retrieval scheme for the thick cloud synthetic cases of Table 5.1.

error estimates but also to re- emphasize the idea that these biases are the only piece of information available from retrieval schemes that do not explicitly account for retrieval uncertainties.

Figure 5.24 shows synthetic retrieval bias for the five- channel retrieval scheme for thick clouds using columns to generate the synthetic radiances and then inverting using Baran's aggregates. Biases for both IWP and effective radius are now very large with values often near 50 percent but still fall within the uncertainty estimates found for the original base case. Examination of the sample case with true IWP of 120 g/m^2 and effective radius of 24 μm will show that while biases are large they are not statistically different. For the retrieval scheme using Baran's aggregates to generate synthetic radiances, retrieved IWP was 118 g/m^2 with one standard deviation of 51 g/m^2 and retrieved effective radius was 23.7 μm with one standard deviation of 10.4 μm. When columns are used to generate synthetic radiances, retrieved IWP and effective radius become 69 g/m^2 and 12.0 μm, respectively, which although quite different still fall within about one standard deviation from our best guess. It should be noted that the optical properties of the pristine columns are very different than those of the randomly oriented randomized hexagonal aggregates, meaning that large differences in retrieval results for these two habits would be expected. This idea shows the fundamental importance of making a

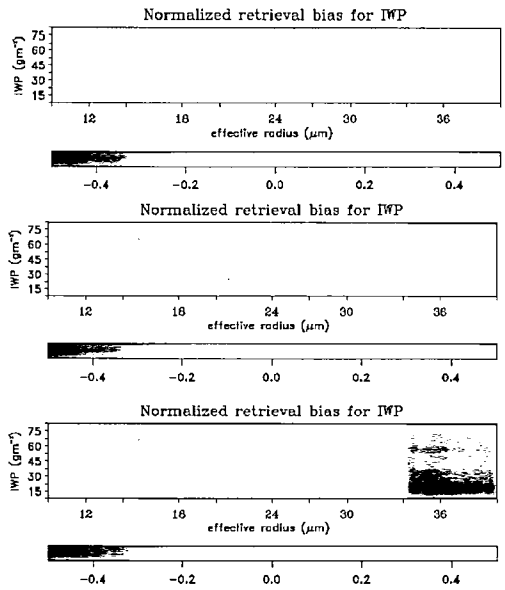

Figure 5.15: Normalized retrieval bias for IWP for each the five channel (top), Nakajima and King (middle), and split- window (bottom) approaches for the thin cloud synthetic cases of Table 5.1.

representative guess of cloud optical properties in the forward model; the choice of outlying cloud properties as the base assumptions of the model will result in heavy biases and possibly retrieval convergence issues. Figure 5.25 shows that for these cases, the biases cannot compensate to create the correct optical depth, simply because the IWP - effective radius combination for columns has a different optical depth than that for the aggregates. Relative differences in retrieved and true optical depth can be as high as 60 percent for those cloud cases with small effective radius, agreeing somewhat with the random errors for optical depth presented in Figure 5.5 for the thick cloud base cases.

Additional calculations were run for other crystal types with the same basic conclusions. Figure 5.26 shows biases and chi- square values found from inverting radiances generated with Baran's aggregates with a Henyey- Greenstein phase function. Although the biases are large, the very large chi- square values indicate that the retrieval scheme simply could not match observed and simulated radiances, again stressing the the proper selection of representative cloud properties for the retrievals.

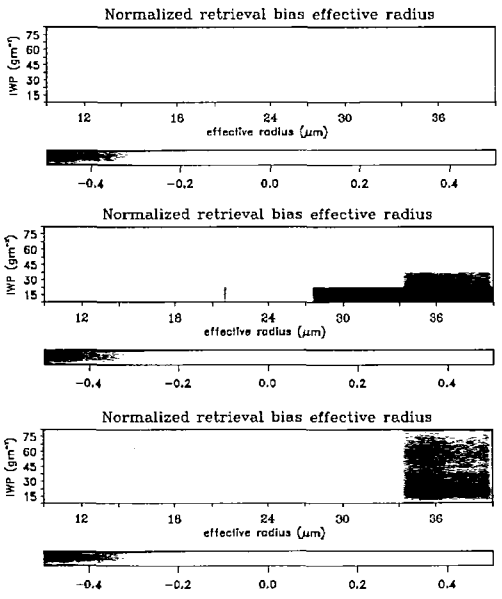

Figure 5.16: Normalized retrieval bias for effective radius for each the five channel (top), Nakajima and King (middle), and split- window (bottom) approaches for the thin cloud synthetic cases of Table 5.1

e. Other Considerations

Additional synthetic tests were run to evaluate retrieval performance for different cloud heights, atmosphere types, solar zenith angles, and even daytime- nighttime conditions. Since these results were very similar to the base assumptions described above and therefore add little to the discussion, the specific details of these cases will be neglected to spare the readers to any more figures.

f. Summary of Synthetic Results

A series of synthetic experiments were performed to quantify bias and random errors for the five- channel retrieval scheme given the results of the forward model uncertainty analysis of the proceeding chapter. Retrieval performance for our five- channel retrieval scheme was examined as a function of IWP and effective radius using the aggregates of Baran et al. (2001) for both the forward and inverse calculations. These retrieval

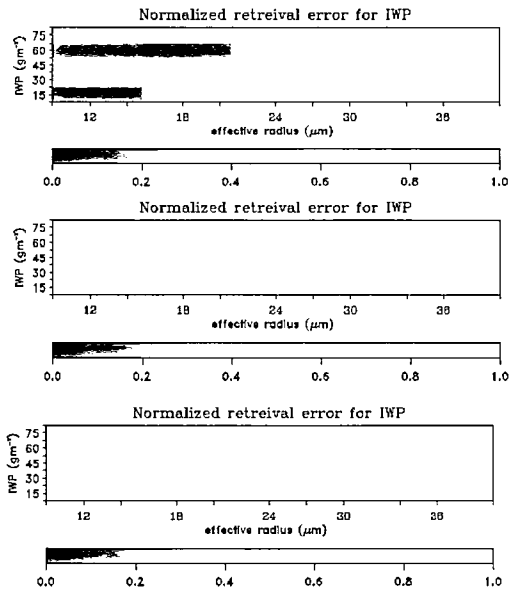

Figure 5.17: Normalized retrieval uncertainty for IWP for each the five channel (top), Nakajima and King (middle), and split- window (bottom) approaches for the thin cloud synthetic cases of Table 5.1.

results were then compared to the bi- spectral split- window and Nakajima and King approaches and even to a 16 channel retrieval scheme to try to quantify the results of our information content analysis of the proceeding chapter in terms of cloud retrievables. Base assumptions such as magnitude of forward model uncertainties and cloud optical properties were in turn altered in the five- channel approach to determine their influence upon retrieval results. The major points from these experiments:

- Uncertainties in retrieved ice cloud properties for the five- channel retrieval scheme based upon the rigorous uncertainty analyses of the proceeding chapter are large and state dependent, with typical random errors near 40 to 50 percent for both IWP and effective radius. The large uncertainties found for this relatively complex retrieval scheme need consideration when examining the utility of absolute numbers or trends found in existing cloud products which are often based on much simpler techniques that overlook all significant error sources.

- The five- channel retrieval scheme had smaller retrieval bias and random error than

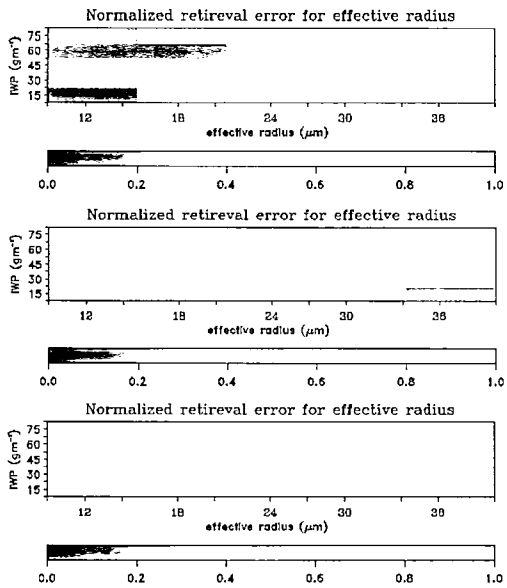

Figure 5.18: Normalized retrieval uncertainty for effective radius for each the five channel (top), Nakajima and King (middle), and split- window (bottom) approaches for the thin cloud synthetic cases of Table 5.1.

the optimal- estimation versions of the split- window and Nakajima and King approaches for all states of the atmosphere. Although the use of additional channels, as in the 16 channel scheme outlined above, does improve retrieval performance slightly, the additional computational expense associated with using more channels probably does not offset the small gains. A possible drawback to using a five-channel scheme (and to a much greater extent in using a 16 channel scheme) is retrieval convergence issues related to matching multiple real- world observation to simulated radiances based on forward model assumptions, an idea that will be re- visited in Section 5.4 describing the CRYSTAL-FACE MAS retrievals.

- Uncertainties in retrieved IWP and effective radius are highly correlated. Since both act to determine cloud optical depth, a bias in one field induces a corresponding bias in the other in such a manner as to allow the optimal- estimation based retrieval scheme to match observed radiances. As such, random errors in indirectly retrieved optical depth are generally low, with values generally under 30 %.

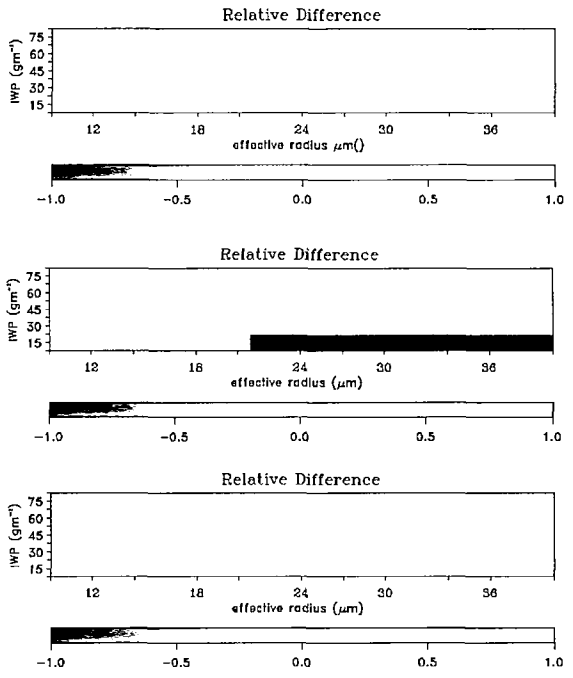

Figure 5.19: Normalized difference between retrieved and true optical depth for each the five channel (top), Nakajima and King (middle), and split- window (bottom) approaches for the thin cloud synthetic cases of Table 5.1.

These compensating retrieval biases, however, suggest that traditional look-up table schemes which retrieve optical depth and effective radius (as opposed to IWP and effective radius) require a fixed effective radius- IWP constraint that leaves the veracity of the retrieved effective radius somewhat in doubt. The additional degree of freedom provided by the retrieval of both IWP and effective radius results in a better formulated problem with a wider range of possible retrieval solutions.

- Since both forward model uncertainties and the climatological range of ice cloud properties are large, the proper selection of *a priori* assumptions is critical for reducing retrieval bias. The relative advantages of an initial guess based upon either an empirical radar reflectivity- IWP relationship or a bi- spectral passive retrieval scheme need determination for the design of an operational retrieval.

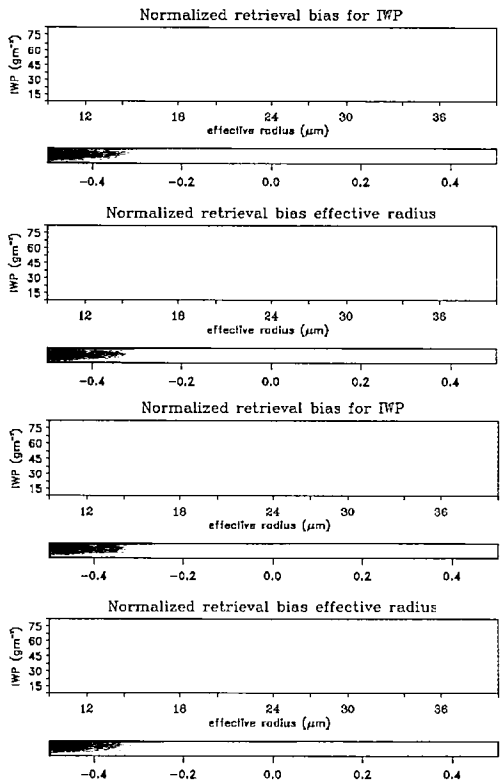

Figure 5.20: Normalized retrieval bias for IWP and effective radius for the five channel scheme are shown in the top two panels. These same two fields for the 16 channel scheme are shown in the bottom two panels.

- The use of a flat 10 percent forward model error covariance for all MODIS channels and states of the atmosphere reduces random errors in IWP and effective radius to values generally under 20 percent for most states of the atmosphere. Since our best estimates of forward model uncertainties based on the base physics of the ice problem suggest values near 100 percent for some channels and states of the atmosphere, such small retrieval random errors are not currently possible. Improvements in the understanding of real- world cloud radiative properties, *in- situ* measurement techniques, and satellite- observations of the angular dependence of the radiance field could reduce the magnitude of these uncertainties.

- Selection of representative cloud radiative properties for a retrieval scheme is important as the use of non- representative properties in either the forward model or

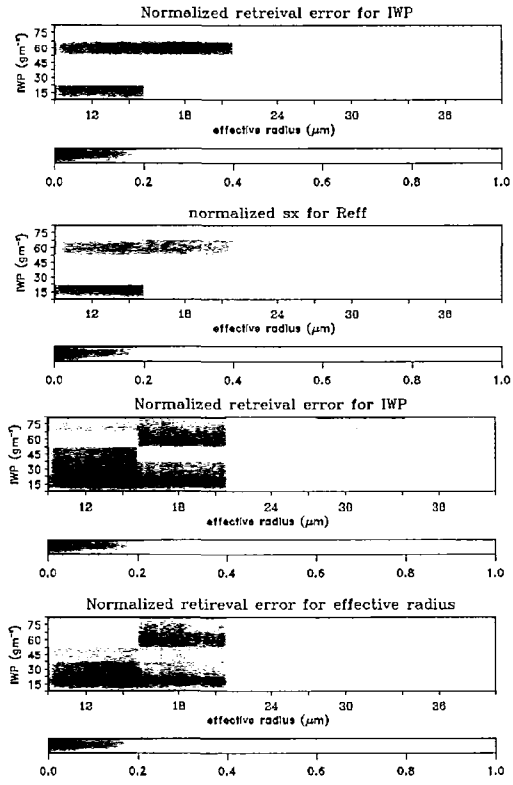

Figure 5.21: Normalized retrieval uncertainty for IWP and effective radius for the five channel scheme are shown in the top two panels. These same two fields for the 16 channel scheme are shown in the bottom two panels.

the development of a look- up table will result in heavy retrieval biases. These biases cannot be considered random errors and will not average out even for an operational retrieval on the global scale.

4. CRYSTAL-FACE Retrievals

The five- channel retrieval approach suggested from the information content analysis of the proceeding chapter was examined in context of the synthetic retrieval studies described in Section 5.3. Retrieval performance in terms of both bias and random error was quantified and found nearly always better for the five- channel approach than for either the optimal -estimation versions of the Nakajima and King and split- window ap-

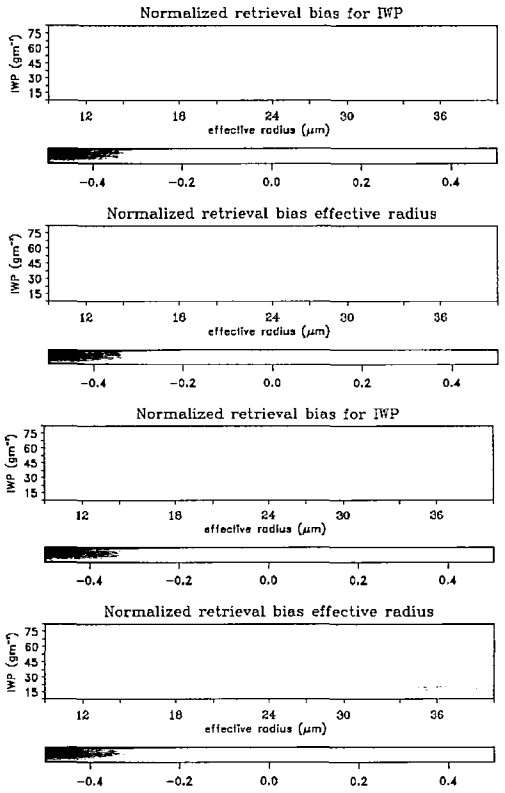

Figure 5.22: Normalized retrieval bias for IWP and effective radius for the five channel scheme using our best estimate of forward model uncertainties are shown in the top two panels. These same two fields for the five channel scheme using a flat 10 percent forward model error for all channels and states for the atmosphere scheme are shown in the bottom two panels.

proaches. Although these analyses show that the five- channel retrieval approach has significant advantages over the other schemes in both information and performance, it is important to remember that the information content analysis and the synthetic retrievals depend upon the same cloud microphysical properties and thus the same radiance sensitivities and uncertainty estimates. It is therefore necessary to use real- world data to further evaluate the retrieval. As mentioned above, the use of a five- channel retrieval scheme may suffer difficulties that the two- channel retrieval schemes may not experiences simply in trying to match more real- world observations. In this section, the five channel retrieval scheme will be applied to MODIS Airborne Simulator (MAS) data from the CRYSTAL-FACE experiment and then compared to the bi- spectral retrieval

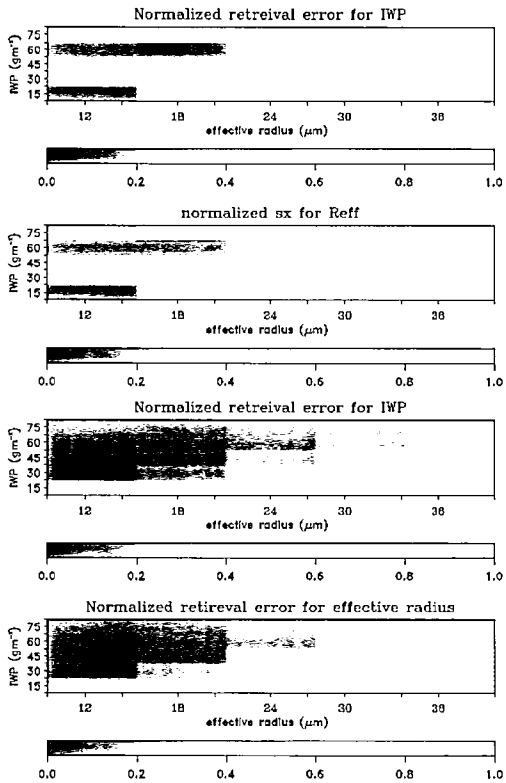

Figure 5.23: Normalized retrieval uncertainties for IWP and effective radius for the five channel scheme using our best estimate of forward model uncertainties are shown in the top two panels. These same two fields for the five channel scheme using a flat 10 percent forward model error for all channels and states of the atmosphere are shown in the bottom two panels.

schemes to determine if these real- world results meet expectations from both the information content and synthetic retrieval approaches.

a. Cirrus Cloud Case Results

The Cirrus Regional Study of Tropical Anvils and Cirrus Layers - Florida Area Cirrus Experiment (CRYSTAL-FACE) which took place in summer 2002 provides the ideal real- world data set to test the five- channel retrieval scheme. A large number of coincident airplane, ground- based, and satellite- based observations were taken during CRYSTAL-FACE to meet the ultimate project goal of gaining a better characterization

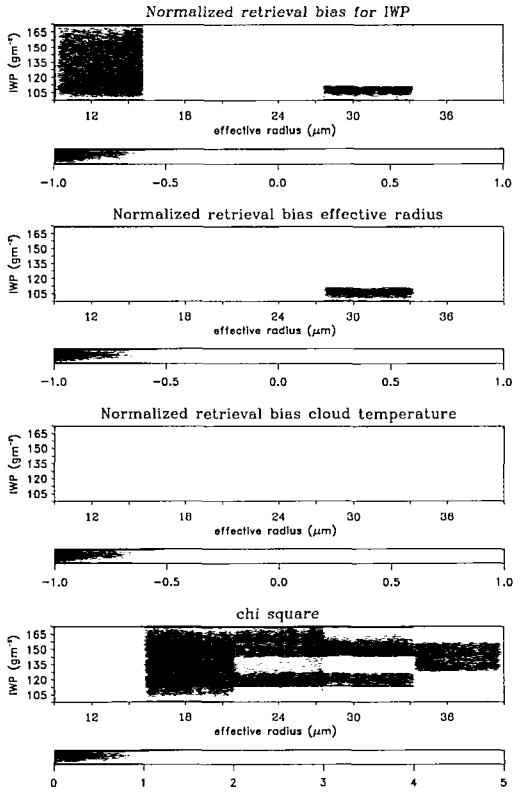

Figure 5.24: Retrieval bias for IWP, effective radius, and cloud temperature are shown in the top three panels, respectively, for the five- channel retrieval scheme assuming columns to generate synthetic radiances. Large chi- square diagnostic values as shown in the bottom panel for the the smallest effective radius indicate a poor fit of observations with retrieved parameters. The gray chi- square values indicate failure in retrieval convergence.

of the role of tropical cirrus clouds in climate processes. For the five- channel retrieval scheme designed for use with MODIS and CloudSat satellite- observations, the relevant measurements to assess the retrieval scheme from CRYSTAL- FACE measurements are the MODIS Airborne Simulator (MAS) measurements used in conjunction with the either the Cloud Radar System (CRS) or the Cloud Physics Lidar (CPL), all which were flown aboard the ER-2 research aircraft. Even though a tremendous number of measurements were taken during the campaign, the actual number of test cases available for assessment of our retrieval scheme is limited to a relatively few cases which did not grossly violate our error covariance assumptions of single- layer clouds, ocean surface,

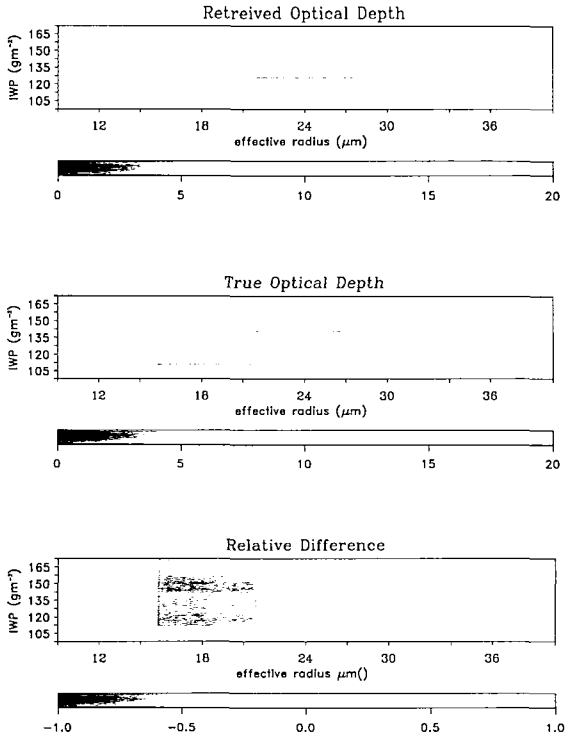

Figure 5.25: Indirectly retrieved optical depth, true optical depth, and the fractional difference (truth - retrieved) are shown in the top three panels, respectively, for the five channel retrieval scheme using columns to generate synthetic radiances and Baran's aggregates to invert them.

and near overhead sun. Figure 5.27 shows the ER-2 flight leg from July 23, 2002 for just such an ideal validation case. At approximately 18:30 Z, the ER-2 over flew a progressively thickening cirrus cloud shield off the east coast of Florida as indicated by the combined CRS- CPL overlap shown in Figure 5.28. The increasing 0.66 μm and decreasing 10.8 μm MAS radiances of Figure 5.29 clearly indicate the presence of an optically variant cloud with a clear jump in visible reflectance corresponding to the lowering of cloud base as indicated by the CRS. This assessment scenario is nearly perfect for testing the relative merits of the five- channel retrieval scheme as compared to the two- channel schemes simply because the range of the observed cloud properties should span the theoretical strengths and weaknesses of each of the bi- spectral approaches.

Figures 5.30 and 5.31 show retrieved IWP and effective radius, respectively, for each

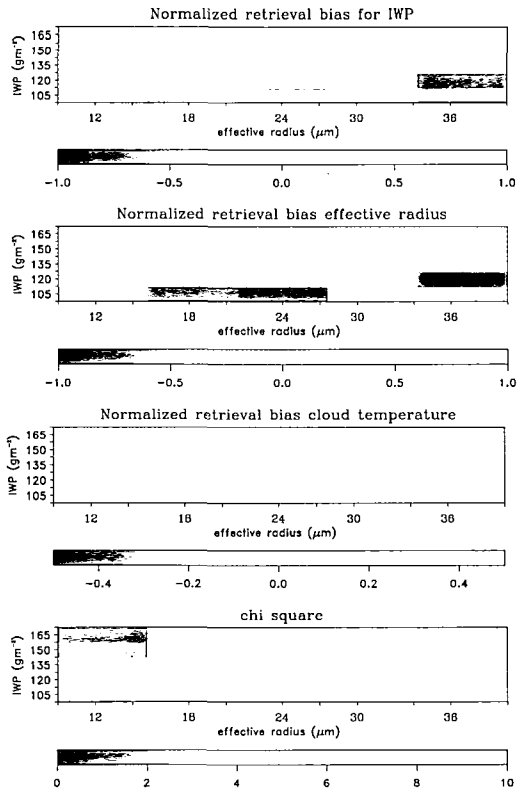

Figure 5.26: Retrieval bias for IWP, effective radius, and cloud temperature are shown in the top three panels, respectively, for the five- channel retrieval scheme assuming Baran's aggregates to generate synthetic radiances and Henyey- Greenstein phase function to invert them. Large chi- square diagnostic values as shown in the bottom panel indicate that the retrieval scheme failed for many of the cloud cases. The gray chi-square values indicate failure in retrieval convergence.

the five- channel, Nakajima and King, and split- window retrievals from the combined MAS and CRS measurements for the cirrus cloud case shown in Figure 5.28. The same *a priori* guess of 20 μm for effective radius and 100 g/m^2 for IWP was used for each of these retrievals for continuity. Retrieval results are clearly different for each of these approaches, with large differences between the bi- spectral retrievals for all cloud states. The five- channel retrieval, however, tends to agree with the split- window approach for thin clouds and with the Nakajima and King approach for thick clouds. These results agree with expectations from both the information content analysis and the synthetic retrievals. For thin clouds, the five- channel retrieval is similar to the split- window

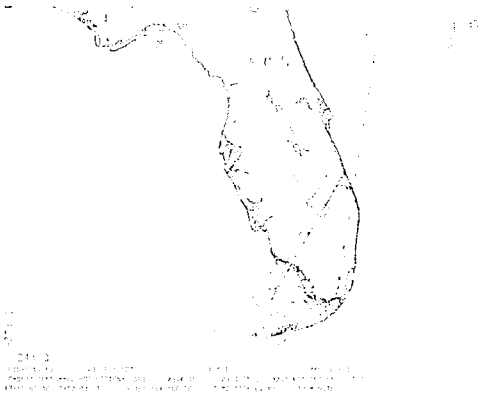

Figure 5.27: ER-2 aircraft flight pattern for CRYSTAL-FACE July 23, 2002. The cirrus test case described in this section occurred near 18:30 Z as the ER-2 was over the Atlantic Ocean off Cape Canaveral.

simply because large forward model uncertainties in the shortwave channels due to habit effects forces the retrieval to emphasize the information in the emission- based channels. The Nakajima and King technique is susceptible to large retrieval uncertainties for thin clouds when real- world cloud assumptions differ from forward model assumptions and therefore its solution is not entirely trusted. Once the clouds become thick, however, the lack of sensitivity in the emission- based channels forces the five- channel solution to rely on the information from the Nakajima and King bands. Use of the split- window channels for the thick clouds is relatively useless as retrieval properties converge very near the *a priori* guess of 20 μm and 100 g/m^2.

Another interesting feature is the relatively smooth transition of the five- channel results between thin and thick clouds as it essentially shifts from a split- window to a Nakaijma and King type approach. These results imply that neither of the two- channel approaches perform decently in these moderate optical depth conditions. In terms of optical depth, Figure 5.32 also suggests that the five- channel retrieval scheme agrees best with the split-window for thin clouds and with the Nakajima and King for thick clouds, as expected. It should be noted that the five- channel scheme should not be expected to behave exactly like the Nakajima and King approach even for very thick

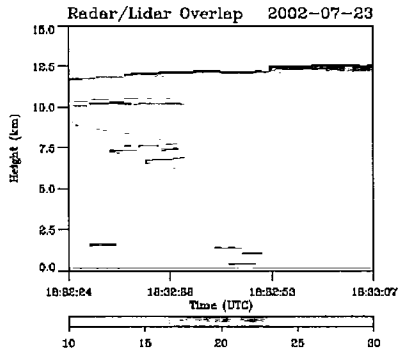

Figure 5.28: Radar (CRS) and lidar (CPL) reflectivities for CRYSTAL-FACE cirrus test case of July 23. Areas of blue indicate only lidar signal; areas of red indicate only radar signal, areas of green indicate lidar and radar overlap.

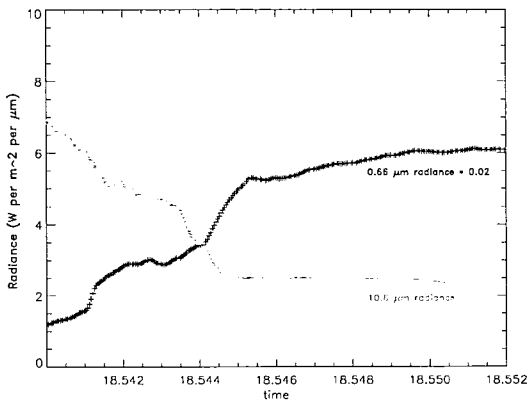

Figure 5.29: MODIS Airborne Simulator radiances for 0.66 μm and 10.8 μm bands for CRYSTAL-FACE cirrus test case of July 23.

clouds simply because of he influence of the 4.05 μm channel. Likewise, the five-channel should not behave exactly as the split- window for thin clouds not only because of the influence of the scattering and SWIR channels but also because it has replaced the 12.0 μm split- window channel with the 13.3 CO_2 slicing band. Regardless, these encouraging real- world results suggest the five- channel retrieval scheme may have utility for real- world data at an operational level.

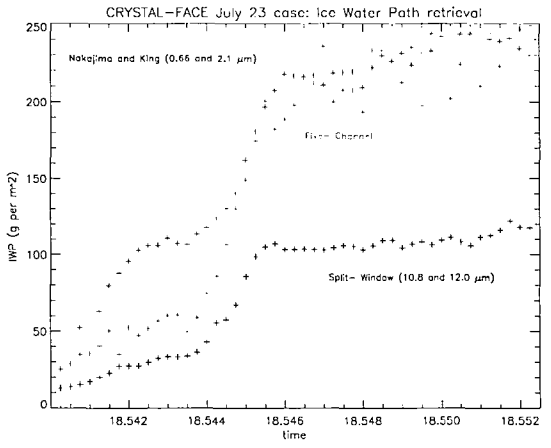

Figure 5.30: Retrieved IWP for CRYSTAL-FACE cirrus cloud case using each the five-channel, Nakajima and King, and split- window approaches.

b. Retrieval Difficulties for Cirrus Case

Although the final results from the CRYSTAL-FACE MAS- CRS retrievals seem nearly idyllic in matching expectations from the information content analysis and synthetic studies, it should be noted that the both the five- channel and Nakajima and King retrievals required an initial relaxation of forward model error covariance assumptions to achieve convergence for some of the thin cloud measurements. When using our best assumptions of forward model uncertainties from the previous chapter, the five- channel retrieval scheme did not achieve convergence for any of the thin clouds up to optical depth of about five, whereas the Nakajima and King failed for a few of the thinnest cloud cases. To achieve convergence, the error covariance assumptions for the visible channels were relaxed to 30 percent for the scattering channels and 15 percent for the infrared channels whenever state- dependent error assumptions fell below these levels. In fact, even this relaxation does not always ensure convergence for the Nakajima and King scheme as indicated by the missing values for four of the thin cloud retrievals as shown in Figures 5.30 - 5.32.

The implication of these failed retrievals is that the real- world does not entirely match the quantification of potential sources of error as outlined in the proceeding chap-

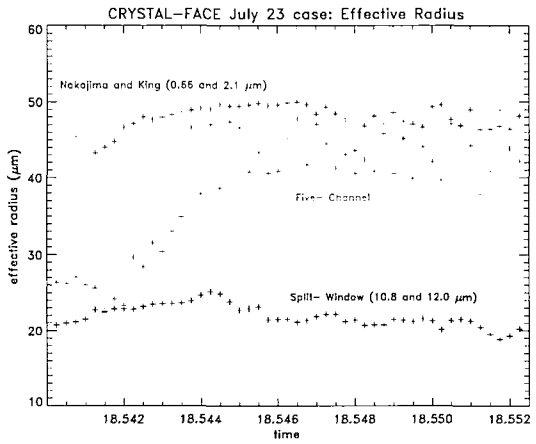

Figure 5.31: Retrieved effective radius for CRYSTAL-FACE cirrus cloud case using each the five- channel, Nakajima and King, and split- window approaches.

ter. One likely cause of these discrepancies is the use of a very well- defined ocean surface albedo of 10 percent for the visible channels and 1 percent for the SWIR and infrared channels in our forward model uncertainty analysis of Chapter 4. Deviations of the real- world albedo from this guess would cause the most difficulties for the thin cloud cases where convergence sometimes failed. Although unlikely, it is entirely possible that the relatively small 50 m field of view of the MAS instrument flying at 20 km could be contaminated, say by a large fish. Other possible sources of difficulty in matching observations with expectations are solar and cloud geometry. Estimation of forward model error covariance matrices for the synthetic studies above were based on an overhead sun, a condition which is technically violated for the CRYSTAL-FACE case with a zenith angle of 15 °C. The total neglect of real- world 3-D effects may cause difficulties in matching visible band observations as these channels would be most susceptible to variations in cloud geometry. Regardless of specific sources of error, more channels used in a retrieval necessarily means more chances for the real- world to deviate from the idealized assumptions of the inversion scheme, as represented by the original failure of the five- scheme approach for almost all cases under optical depth of 5.

This failure of convergence for the multi- band retrieval schemes does bring up the possibility that the use of observations may provide an empirical means to estimate

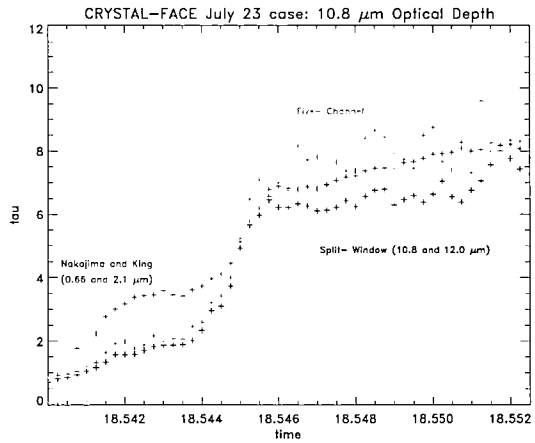

Figure 5.32: Retrieved optical depth for CRYSTAL-FACE cirrus cloud case using each the five- channel, Nakajima and King, and split- window approaches.

measurement and forward model error. A series of retrievals could be run with different base forward model and error covariance assumptions to determine when the retrieval converges as a function of state of the atmosphere. These results , however, would need independent validation of the state of the atmosphere to make the results of use operationally and should be considered as a possibility for future research.

5. Conclusions

In the proceeding chapter, a formal information content analysis suggested that the ideal combination of MODIS measurements for an ice cloud property retrieval constrained by CloudSat cloud boundary information was highly dependent upon the state of the atmosphere. Each of the scattering, non- conservative scattering, SWIR, and infrared bands has the potential to be the most useful depending upon exact cloud and atmospheric properties. The use of traditional bi- spectral schemes that only employ one or two of these spectral regions, such as the Nakajima and King and split- window approaches, therefore cannot always ensure an accurate estimate of cloud properties for all retrievals. A five- channel retrieval scheme was therefore proposed that would incorporate measurements from each of these spectral regions and would hopefully allow an

accurate retrieval regardless of state. The use of the flexible optimal- estimation based retrieval framework provides the ideal means to properly weight those channels with the most information given atmospheric state through a rigorous accounting of the forward model and measurement error covariance matrix. In this chapter, we quantified the implications of retrieval information content in the more practical terms of retrieval performance for the five- channel scheme as opposed to the more traditional approaches.

The various retrieval approaches were applied to both a series of numerical synthetic experiments and to real- world CRYSTAL-FACE data. The five- channel retrieval approach consistently performed better than either of the bi- spectral schemes in terms of both bias and random error for retrieved IWP and effective radius in these synthetic studies. Even though the five- channel retrieval approach did an excellent job in maximizing possible information for any given retrieval, the large fundamental uncertainties in the physics of the ice cloud problem result in substantial retrieval random error typically near 30 to 40 percent for both IWP and effective radius. In addition, uncertainties in the representative cloud radiative properties used for global retrieval schemes imply the possibilities that substantial biases exist in these data sets which cannot average out regardless of the number of retrievals. These large uncertainties surely inject a note of caution on a literal interpretation of exact values or small trends found in existing cloud climate products. Although the use of all MODIS channels would improve theoretical retrieval performance, the increased computational cost for minor retrieval gains and the increased risk of retrieval failure when applied to real- world data make such an option intractable.

For application to CRYSTAL-FACE data, the five- channel retrieval behaved somewhat as expected, agreeing with the Nakajima and King type approach for thick clouds when emission- based channels have little sensitivity and with the split- window approach for thin clouds when the scattering- based channels may produce large biases. A practical difficulty in application to CRYSTAL-FACE data, however, was that the forward model error covariance assumptions had to be relaxed to achieve retrieval con-

vergence for thin clouds. This difficulty can only mean that our rigorous forward model error covariance analysis of the proceeding chapter was not quite correct, where either improper characterization of surface albedo or lack of inclusion of cloud 3-D scattering effects were the most likely cause of the discrepancies.

Despite minor differences, the results of the five- channel retrieval scheme as applied to real- world CRYSTAL-FACE data supported the conclusions drawn from the theoretical information content analysis and the numerical synthetic studies, giving hope that the five- channel approach has the potential as an operational retrieval on a global scale. An initial concern would be the huge computational cost associated with the use of five channels in the iterative optimal- estimation retrieval framework. The near constant increase in computer power combined with recent advances in the efficiency of forward model radiative transfer calculations (Christi and Gabriel (2003)), however, should allow this scheme to be implemented at an operational level in the very near future. The potentially more damaging problem for the five- channel scheme, however, is that of retrieval convergence for real- world measurements. In the relatively well- defined CRYSTAL-FACE retrieval for a single- layer cloud over an ocean surface, the forward model and measurement retrieval error covariance still had to be relaxed to gain convergence. More channels in a retrieval necessarily means more chances for the forward model variance assumptions to be violated, possibly resulting in an inability to match observations with our estimated cloud properties. In addition, improper selection of forward model cloud radiative properties for this retrieval will not only lead to substantial biases but may also lead to convergence failure for the reactively inaccurate ball-park estimates used for the forward model error covariances. Much further work on classification of the ideal cloud radiative properties with associated uncertainties for the wide- range of scenes expected for an operational global retrieval is needed to determine the utility of this approach.

Chapter 6

Conclusions

The purpose of this dissertation was a re-examination of the ice cloud retrieval problem based upon a realistic assessment of the fundamental physics of the ice clouds themselves. Although seemingly narrow in scope, the idea was to take a step backward to our core knowledge in attempt to assess our confidence in retrieved ice cloud properties given the practical constraints of our current observational platforms. It is hoped that a more realistic understanding of the retrieval problem may allow insights that will ultimately result in a better characterization of the distribution and microphysical properties of these clouds and their impacts on climate. These works were made possible only by the recent development of optical properties at the MODIS channel wavelength for a number of realistic crystal habits, allowing a means to quantify expected variability in both forward and inverse calculations as a function of ice crystal habit. Implementation of the optimal- estimation based retrieval technique for these studies was also critical, not only in facilitating the direct inclusion of uncertainties from habit as well as other potential sources of error in quantifying overall retrieval performance but also in providing a flexible framework capable of incorporating measurements from complementary sensors.

1. Summary of Results

The split- window study presented in Chapter 3 provided the overall motivation and general methodology for the entire dissertation. The split-window cirrus cloud retrieval technique was cast in an optimal estimation framework to examine uncertainties in the retrieval of cloud properties as a function of uncertainty in cloud emitting temperature. This retrieval technique relies on differences in radiative properties for cloud particles at 10.8 μm and 12.0 μm to estimate cloud optical depth and effective radius from satellite observed brightness temperatures. Small errors in assumed cloud temperature, however, can lead to large errors in retrieved cloud properties. The incorporation of cloud boundary information from either the CloudSat Cloud Profiling Radar or the CALIPSO lidar to constrain the window- region measurements is found to substantially reduce the errors inherent to this approach. Uncertainties in optical depth and effective radius are found to diminish from $\sim$45 and $\sim$80 %, respectively, in the absence of explicit cloud boundary information to $\sim$15 and $\sim$60 % when accurate radar- or lidar-based estimates are included. Retrieval performance, however, was found to be strongly dependent upon the uncertainties arising from forward model assumptions such as ice crystal habit and particle size distribution.

In Chapter 4, the ideas and methodology developed for the split- window channels were applied at a more general level. Instead of just examining the effects of uncertainties on retrieval performance for a well- known bi- spectral technique, rigorous sensitivity and uncertainty analyses were performed across the expected climatological range of ice cloud conditions for seventeen MODIS channels commonly used in ice cloud retrieval schemes. The results of these studies were incorporated into a formal information content analysis to select objectively those MODIS channels with the most information for a cloud retrieval scheme constrained by co- incident CloudSat cloud boundary information. We found that the combination of measurements that maximizes information content is state dependent, meaning that no combination of two or three channels will

always ensure an accurate retrieval for all states of the atmosphere. We therefore suggested a five channel retrieval scheme that would consist of a combination of error-weighted visible, near- infrared, and infrared channels chosen to use the inherent sensitivities in each of these regions to ensure high information content regardless of the state of the atmosphere. Application of such a unified approach at an operational level for the global retrieval of ice cloud properties would have the additional advantage of ensuring consistency in retrieved cloud products across different remote sensing campaigns.

In Chapter 5, we quantified the implications of retrieval information content in the more practical terms of retrieval performance. Both the five- channel and the traditional bi- spectral retrieval schemes were applied to a series of numerical synthetic experiments and to real- world CRYSTAL-FACE data. In the synthetic studies, the five- channel retrieval approach consistently performed better than either of the two channel schemes in terms of both bias and random error for retrieved IWP and effective radius. Even though the five- channel retrieval approach did an excellent job in maximizing relative information for any given retrieval, the large fundamental uncertainties in the physics of the ice cloud problem result in substantial retrieval uncertainties typically near 30 to 40 percent for both IWP and effective radius. Uncertainties in the selection of representative cloud optical properties used for global retrieval schemes also imply the possibilities that substantial biases exist in these data sets which cannot average out regardless of the number of retrievals. This potential combination of large uncertainties and large biases surely inject a note of caution on a literal interpretation of exact values or small trends found in existing cloud climate products. For application to CRYSTAL-FACE data, the five-channel retrieval behaved somewhat as expected, agreeing with the Nakajima and King type approach for thick clouds when emission- based channels have little sensitivity and with the split- window approach for thin clouds when the scattering- based channels may produce large biases. A practical problem in application to CRYSTAL-FACE data, however, was that the forward model error covariance assumptions had to be relaxed to achieve retrieval convergence for thin clouds. This difficulty can only mean that our rig-

orous forward model error covariance analysis of the proceeding chapter was not quite correct, where either improper characterization of surface albedo or lack of inclusion of cloud 3-D scattering effects were the most likely cause of the discrepancies.

2. Future Work

The results and implications of this dissertation need thoughtful consideration in context of future research possibilities. Much of the work presented here, such as the sensitivity and uncertainty analyses, were based on relatively simplistic physical assumptions such as a well- defined ocean surface underlying a single- layer ice cloud. The ocean surface was selected for these studies because it has a relatively well- defined albedo for the MODIS wavelengths and because water covers nearly three- fourths of the surface of the globe. Changing this assumption to a more problematic land surface with both a larger magnitude and variability in visible and near- infrared albedo may alter the results and conclusions of our studies for optically thin clouds. A larger albedo would reduce the dynamic range and thus the sensitivity of most of these channels but may actually decrease relative uncertainty simply because a larger reflected signal may somewhat mask the fractional uncertainties associated with the forward model assumption of crystal shape. Rigorous quantification of these competing effects for many different surface types would be critical for the development of an operational algorithm. Similarly, even a casual perusal of real- world measurements suggest that multi- layer cloud systems are common. The methodologies developed in these studies could easily be extrapolated to the much more difficult problem of multiple- layer clouds, which are often ignored or neglected in many retrieval schemes. Indeed, with the expected increase in knowledge of the vertical profile of the atmosphere gained with the launch of CloudSat, it may be possible to develop an operational algorithm for these multi- layer clouds.

The next step in this research, however, is simply to determine the feasibility of the five- channel retrieval scheme for single layer clouds using a combination of measure-

ments from both MODIS and CloudSat. Although theoretical results based on a realistic examination of our current understanding of ice cloud physics suggest the wisdom of this approach, its application to real- world data may be more problematic. Indeed, use of this retrieval on MAS data from CRYSTAL- FACE was somewhat promising but suffered from the fact that our rigorous forward model covariances did not facilitate a match to real- world observations. It is possible that these real- world deviations from idealized assumptions may cause retrieval convergence difficulties when trying to match five distinct observations. In such a case, the only way to achieve convergence would be to inflate the forward model error covariances such as to cause heavy reliance on the *a priori* guess and very large retrieval uncertainties. These issues will be examined in depth with the launch of CloudSat when the combination of active and passive measurements needed for this retrieval become available on the global scale. It should be noted a more practical concern for this retrieval scheme is the large computational cost associated with the iterative retrieval approach and the complicated ice crystal phase functions. Although the retrieval scheme as outlined in this dissertation could certainly not be implemented at a global level, it is hoped recent advances in both the efficiency of radiative transfer calculations and computational power will allow a variation this technique to be applied to the global scale in the near future.

Finally, another equally interesting option for future research would be to use the results of the forward model error analysis work in a data assimilation context. Most work in the atmospheric sciences tend to ignore errors for various reasons, but the data assimilation community not only considers errors but relies on a proper error characterization to get realistic results. The results of the error analysis could be incorporated into the RAMDAS 4-D VAR data assimilation scheme developed at the Cooperative Institute for Research in the Atmosphere (CIRA) at Colorado State University. The preliminary work would examine how errors in satellite- based radiances affect the estimation of mesoscale cloud state from visible and infrared GOES imager measurements, based on Vukivecic (in press). A more advanced application would be to use the state depen-

dence nature of the uncertainty analysis in the data assimilation framework to estimate the effects of scale on 4D-VAR results.

Bibliography

Ackerman, S., W. Smith, J. Spinhirne, and H. Revercombe: 1990, The 27-28 october 1986 fire ifo cirrus case study: spectral properties of cirrus clouds in the 8-12 μm window. *Monthly Weather Review*, **118**, 2377–2388.

Austin, R. and G. Stephens: 2001, Retrieval of stratus cloud microphysical parameters using millimeter-wave radar and visible optical depth in preparation for CloudSat. *J. Geophys. Res.*, **106**, 28233–28242.

Baran, A., P. Francis, L. Labonnote, and M. Doutriax-Boucher: 2001, A scattering phase function for ice cloud: tests of applicability using aircraft and satellite multi-angle multi-wavelength radiance measurements. *J. Quant. Spectrosc. Radiat. Transfer*, **127**, 2395–2416.

Baran, A., S. Havemann, P. Francis, and P. Watts: 2003, A consistent set of single-scattering properties for cirrus cloud: tests using radiance measurements from a dual-viewing multi- wavelength satellite-based instrument. *J. Quant. Spectrosc. Radiat. Transfer*, **79**, 549–567.

Baum, B. and B. Wielicki: 1994, Cirrus cloud retrieval using infrared sounding data: multilevel cloud layers. *J. Appl. Meteor.*, **33**, 107–117.

Chandrasekhar, S.: 1960, *Radiative transfer*. Dover, New York, NY.

Christi, M. and P. Gabriel: 2003, *Radiant 2.0: a user's guide*. Colorado State University, 39 pp., Fort Collins, CO.

Cooper, S., T. L'Ecuyer, and G. Stephens: 2003, The impact of explicit cloud boundary information on ice cloud microphysical property retrievals from infrared radiances. *J. Geophys. Res.*, **108**, 2002JD002611.

Dave, J. and B. Armstrong: 1970, Computations of high-order associated legendre polynomials. *J. Quant. Spectrosc. Radiat. Transfer*, **10**, 557–562.

Deeter, M. and K. Evans: 1998, A hybrid Eddington-single scattering radiative transfer model for computing radiances from thermally emitting atmospheres. *J. Quant. Spectrosc. Radiat. Transfer*, **60**, 635–648.

Dowling, D. and L. Radke: 1990, A summary of the physical properties of cirrus clouds. *J. Appl. Meteor.*, **29**, 970–978.

Engelen, R. and G. Stephens: 1997, Infrared radiative transfer in the 9.6 μm band: application to TOVS ozone retrieval. *J. Geophys. Res.*, **92**, 6929–6940.

— 1999, Characterization of water vapour retrievals from TOVS/HIRS and SSM/T-2 measurements. *Quart. J. Roy. Meteorol. Soc.*, **125**, 331–351.

Eyre, J., G. Kelly, A. McNally, E. Anderson, and A. Persson: 1993, Assimilation of TOVS radiance information through one- dimensional variational analysis. *Quart. J. Roy. Meteorol. Soc.*, **119**, 1427–1463.

Flatau, P.: 1992, *Scattering by Irregular Particles in Anomalous Diffraction and Discrete Dipole Approximations*. Ph.D. thesis, Colorado State University.

Francis, P., A. Jones, R. Saunders, K. Shine, A. Slingo, and Z. Sun: 1994, An observational and theoretical study of the radiative properties of cirrus: some results from ICE'89. *Quart. J. Roy. Meteorol. Soc.*, **120**, 809–848.

Fu, Q., M. Baker, and D. Hartmann: 2002, Tropical cirrus and water vapor: an effective Earth infrared iris feedback? *Atmos. Chem. Phys.*, **2**, 31–37.

Fu, Q. and K.-N. Liou: 1992, On the correlated k-distribution for radiative transfer in nonhomogeneous atmospheres. *J. Atmos. Sci*, **49**, 2139–2156.

Gao, B. and Y. Kaufman: 1995, Selection of the 1.375-μm modis channel for the remote sensing of cirrus clouds and stratospheric aerosols from space. *J. Atmos. Sci*, **52**, 4231–4237.

Grenfell, T. and S. Warren: 1999, Representation of a nonspherical ice particle by a collection of independent spheres for scattering and absorption of radiation. *J. Geophys. Res.*, **104**, 31697–31709.

Guenther, B., W. Barnes, E. Knight, J. Barker, J. Harnden, R. Weber, M. Roberto, G. Godden, H. Montgomery, and P. Abel: 1996, Modis calibration: A brief review of the strategy for the at-launch calibration approach. *J. Atmos. Oceanic Technol.*, **13**, 274–285.

Hartmann, D. L., H. H. Hendon, and J. R. A. Houze: 1984, Some implications of the mesoscale circulation in tropical cloud clusters for large-scale dynamics and climate. *J. Atmos. Sci*, **41**, 113–121.

Inoue, T.: 1985, On the temperature and effective emissivity determination of semi-transparent cirrus clouds by bi-spectral measurements in the 10 μm window region. *J. Meteor. Soc. Japan*, **63**, 88–89.

IPCC: 1995. Intergovernmental Panel on Climate Change (IPCC) (1995) World Meteorological Office, United Nations Environmental Programme, *Radiative Forcing of Climate Change. The 1994 Report of the Scientific Assessment Working Group of IPCC. Summary for Policymakers.*

King, M., Y. Kaufman, W. Menzel, and D. Tanre: 1992, Remote sensing of cloud, aerosol, and water vapor properties from the Moderate Resolution Imaging Spectrometer (MODIS. *IEEE Trans. Geosci. Remote Sens.*, **30**, 2–27.

Kratz, D.: 1995, The correlated- k distribution technique as applied to the AVHRR channels. *J. Quant. Spectrosc. Radiat. Transfer*, **64**, 501–517.

Kummerow, C. and L. Giglio: 1994, A passive microwave technique for estimating rainfall and vertical structure information from space. Part I: algorithm development. *J. Appl. Meteor.*, **33**, 3–18.

Lau, K.-M. and L. Peng: 1987, Origin of low-frequency (intraseasonal) oscillations in the tropical atmosphere Part I: Basic theory. *J. Atmos. Sci*, **44**, 950–972.

L'Ecuyer, T., P. Gabriel, K. Leesman, S. Cooper, and G. Stephens: 2004, Objective assessment of the information content of visible and infrared radiance measurements for cloud microphysical property retrievals over the global oceans. Part 1: Lquid clouds. *J. Appl. Meteor.*, **43**, submitted.

L'Ecuyer, T. and G. Stephens: 2002, An estimation-based precipitation retrieval algorithm for attenuating radars. *J. Appl. Meteor.*, **41**, 272–285.

Lindzen, R., M. Chou, and A. Hou: 2001, Does the Earth have an adaptive infrared iris? *Bull. Amer. Meteor. Soc.*, **82**, 417–432.

Liou, K. N.: 1986, Influence of cirrus clouds on weather and climate processes: A global perspective. *Monthly Weather Review*, **114**, 1167–1199.

Liou, K. N., S. Ou, Y. Takano, F. Valero, and T. Ackerman: 1990, Remote sounding of the tropical cirrus cloud temperatures and optical depth using 6.5 and 10.5 μm radiometers during STEP. *J. Appl. Meteor.*, **29**, 716–726.

Liou, K. N. and Y. Takano: 1994, Light scattering by nonspherical particles: remote sensing and climatic applications. *Atmos. Res.*, **31**, 271–298.

Lyu, C., W. Barnes, and R. Barnes: 2000, First results from the on-orbit calibration of the Visible and Infrared Scanner for the Tropical Rainfall Measuring Mission. *J. Atmos. Oceanic Technol.*, **17**, 385–394.

Marks, C. and C. Rodgers: 1993, A retrieval method for atmospheric composition from limb emission measurements. *J. Geophys. Res.*, **98**, 14939–14953.

McClatchey, F. A., R. W. Fenn, J. E. Selby, F. E. Volz, and J. S. Goring: 1972, *Optical Properties of the Atmosphere, 3rd ed.*. AFCRL-72-0497, 102 pp., Air Force Cambridge Res. Lab., L. G. Hanscom Field, Mass.

Menzel, W., D. Wylie, and K. Strabala: 1992, Seasonal and diurnal changes in cirrus clouds as seen in four years of observations with the VAS. *J. Appl. Meteor.*, **31**, 370–385.

Miller, S.: 2000, *A multi-sensor approach to the retrieval and model validation of global cloudiness*. Ph.D. thesis, Colorado State University.

Miller, S., G. Stephens, C. Drummond, A. Heidinger, and P. Partain: 2000, A multisensor diagnostic satellite cloud property retrieval scheme. *J. Geophys. Res.*, **105**, 19955–19971.

Minnis, P., K.-N. Liou, and Y. Takano: 1993, Inference of cirrus cloud properties using satellite- observed visible and infrared radiances: Part I, Parameterization of radiance fields. *J. Atmos. Sci*, **50**, 1279–1304.

Mitchell, D. and W. Arnott: 1994, A model predicting the evolution of ice particle size spectra and radiative properties of cirrus clouds: Part II: Dependence of absorption and extinction on ice crystal morphology. *J. Atmos. Sci*, **51**, 817–832.

Mitrescu, C. and G. Stephens: 2004, On similarity and scaling of the radiative transfer equation. *J. Quant. Spectrosc. Radiat. Transfer*, **86**, 387–394.

Nakajima, T. and M. King: 1990, Determination of the optical thickness and effective particle radius of clouds from reflected solar radiation measurements. Part I: Theory. *J. Atmos. Sci*, **47**, 1878–1893.

Ou, S., K. Liou, W. Gooch, and Y. Takano: 1993, Remote sensing of cirrus cloud parameters using Advanced Very- High- Resolution Radiometer 3.7- and 10.9 μm channels. *Applied Optics*, **32**, 2171–2180.

Parol, F., J. Buriez, G. Brogniez, and Y. Fouquart: 1991, Information content of AVHRR channels 4 and 5 with respect to the effective radius of cirrus cloud particles. *J. Appl. Meteor.*, **30**, 973–984.

Pierrehumbert, R.: 1995, Thermostats, radiator fins, and the local runaway greenhouse. *J. Atmos. Sci*, **52**, 1784–1806.

Prabhakara, C., R. Fraser, M. Wu, and R. Curran: 1988, Thin cirrus clouds: seasonal distributions over oceans deduced from NIMBUS-4 IRIS. *J. Appl. Meteor.*, **27**, 379–399.

Reist, P.: 1994, *Aerosol Science and Technology*. Oxford University Press, New York, NY.

Ritter, B. and J.-F. Geleyn: 1992, A comprehensive radiation scheme for numerical weather prediction models with potential applications in climate simulations. *Monthly Weather Review*, **120**, 303–325.

Rodgers, C.: 1976, Retrieval of atmospheric temperature and composition from remote measurements of thermal radiation. *Rev. Geophys. and Space Phys.*, **14**, 609–624.

— 1990, Characterization and error analysis of profiles retrieved from remote sounding measurements. *J. Geophys. Res.*, **95**, 5587–5595.

— 2000, *Inverse Methods for Atmospheric Sounding*. World Scientific Publishing, River Edge, NJ.

Sassen, K.: 2002, Cirrus: A modern perspective. *In: Cirrus*, D. K. Lynch, K. Sassen, D. O. Starr, and G. L. Stephens, eds., Oxford University Press, 11–40.

Shannon, C. and W. Weaver: 1949, *The mathematical theory of communication*. University of Illinois Press, Urbana, IL.

Stephens, G. L.: 1980, Radiative properties of cirrus clouds in the infrared region. *J. Atmos. Sci*, **37**, 435–446.

— 1994, *Remote Sensing of the Lower Atmosphere*. Oxford University Press, New York, NY.

Stephens, G. L., P. M. Gabriel, and P. T. Partain: 2001a, Parameterization of atmospheric radiative transfer I: Validity of simple models. *J. Atmos. Sci*, **58**, 3391–3409.

Stephens, G. L., S.-C. Tsay, J. P. W. Stackhouse, and P. J. Flatau: 1990, The relevance of the microphysical and radiative properties of cirrus clouds to climate and climatic feedback. *J. Atmos. Sci*, **47**, 1742–1753.

Stephens, G. L., M. Vaughn, R. Engelen, and T. Anderson: 2001b, Toward retrieving properties of the tenuous atmosphere using space-based lidar measurements. *J. Geophys. Res.*, **106**, 28143–28157.

Stephens, G. L. and P. Webster: 1981, Clouds and climate: sensitivity of simple systems. *J. Atmos. Sci*, **38**, 235–247.

Stephens, G. L. and P. J. Webster: 1979, Sensitivity of radiative forcing to variable cloud and moisture. *J. Atmos. Sci*, **36**, 1542–1556.

Stone, R., G. Stephens, C. Platt, and S. Banks: 1990, The remote sensing of thin cirrus clouds using satellites, lidar, and radiative transfer theory. *J. Appl. Meteor.*, **29**, 353–366.

van de Hulst, H.: 1980, *Multiple light scattering : tables, formulas, and applications, Vol. 1*. Academic Press, New York, NY.

Wielicki, B., B. Barkstrom, E. Harrison, R. L. III, G. Smith, and J. Cooper: 1996, Clouds and the Earth's Radiant Energy System (CERES): An earth observing system experiment. *Bull. Amer. Meteor. Soc.*, **77**, 853–868.

Wielicki, B., J. Suttles, A. Heymsfield, R. Welch, J. Spinhirne, M.-L. C. Wu, D. Starr, L. Parker, and R. Arduini: 1990, The 27-28 October 1986 FIRE IFO cirrus case study: comparison of radiative transfer theory with observations by satellite and aircraft. *Monthly Weather Review*, **118**, 2356–2376.

Wiscombe, W.: 1977, The delta-m method: rapid yet accurate radiative flux calculations for strongly asymmetric phase functions. *J. Atmos. Sci*, **34**, 1408–1422.

Yang, P., B. Baum, A. Heymsfield, Y. Hu, H. Huang, S. Tsay, and S. Ackerman: 2003, Single- scattering properties of droxtals. *J. Quant. Spectrosc. Radiat. Transfer*, **79**, 1159–1169.

Yang, P., B. Gao, B. Baum, Y. Hu, W. Wiscombe, S. Tsay, D. Winker, and S. Nasiri: 2001, Radiative properties of cirrus clouds in the infrared (8-13μm) spectral region. *J. Quant. Spectrosc. Radiat. Transfer*, **70**, 473–504.

Yang, P., K. Liou, K. Wyser, and D. Mitchell: 2000, Parameterization of the scattering and absorption properties of individual ice crystals. *J. Geophys. Res.*, **105**, 4699–4718.